

Invitation

It is my pleasure to invite you to the public defense of my PhD thesis entitled:

“Chameleon” Macromolecules: Synthesis, Structures and Applications of Stimulus Responsive Polymers

on Friday 29th June
at 14:45h
in the
Prof. dr. G. Berkhoff Zaal
Waaier building
at the University of Twente

I will give a short
introduction to my thesis
at 14:30

A reception will follow
immediately after
the ceremony

Xiaofeng Sui
x.sui@utwente.nl

Paranimfen

Bart Kieviet
b.d.kieviet@utwente.nl

Xueling Feng
x.feng-1@utwente.nl

"Chameleon" Macromolecules: Synthesis, Structures and Applications of Stimulus Responsive Polymers

Xiaofeng Sui

"Chameleon" Macromolecules: Synthesis, Structures and Applications of Stimulus Responsive Polymers Xiaofeng Sui 2012



ISBN 978-90-365-3361-4

GR 2012

**“CHAMELEON” MACROMOLECULES:
SYNTHESIS, STRUCTURES AND APPLICATIONS OF
STIMULUS RESPONSIVE POLYMERS**

Xiaofeng Sui

Thesis committee members

Chairman:	Prof. Dr. H. J. M. ter Brake	University of Twente, The Netherlands
Promotor:	Prof. Dr. G. J. Vancso	University of Twente, The Netherlands
Assistant promotor:	Dr. M. A. Hempenius	University of Twente, The Netherlands
Members:	Prof. Dr. J. F. J. Engbersen	University of Twente, The Netherlands
	Prof. Dr. J. G. E. Gardeniers	University of Twente, The Netherlands
	Prof. Dr. R. G. H. Lammertink	University of Twente, The Netherlands
	Prof. Dr. I. Manners	University of Bristol, UK
	Prof. Dr. N. D. Spencer	ETH Zürich, Switzerland

The work described in this thesis was performed at the Materials Science and Technology of Polymers (MTP) group, MESA⁺ Institute for Nanotechnology, Faculty of Science and Technology, University of Twente, PO Box 217, 7500 AE Enschede, The Netherlands.

This research was financially supported by the MESA⁺ Institute for Nanotechnology of the University of Twente and the Netherlands Organization for Scientific Research (NWO, TOP Grant 700.56.322, Macromolecular Nanotechnology with Stimulus Responsive Polymers).

“Chameleon” Macromolecules: Synthesis, Structures and Applications of Stimulus Responsive Polymers

X. Sui

PhD Thesis

University of Twente, Enschede, The Netherlands

© Xiaofeng Sui 2012

ISBN : 978-90-365-3361-4

DOI: 10.3990/1.9789036533614

**“CHAMELEON” MACROMOLECULES:
SYNTHESIS, STRUCTURES AND APPLICATIONS OF
STIMULUS RESPONSIVE POLYMERS**

DISSERTATION

to obtain
the degree of doctor at the University of Twente,
on the authority of the rector magnificus,
Prof. Dr. H. Brinksma,
on account of the decision of the graduation committee,
to be publicly defended
on Friday, 29 June 2012, at 14:45

by

Xiaofeng Sui

Born on 19 november 1983
in Shandong, China

This dissertation has been approved by:

Promotor: Prof. Dr. G. J. Vancso

Assistant-promotor: Dr. M. A. Hempenius

Table of Contents

Chapter 1 General Introduction	1
1.1 Introduction	1
1.2 Concept of this Thesis	1
1.3 References	4
Chapter 2 Addressable Stimuli-Responsive Polymer Architectures	5
2.1 Introduction	5
2.2 Polymer grafts on surfaces	6
2.3 Polymer networks in bulk	12
2.3.1 Macroscopic hydrogels	13
2.3.2 Microgels/nanogels	16
2.4 Conclusions	20
2.5 References	21
Chapter 3 Engineering of Surface Grafted Poly(<i>N</i>-isopropylacrylamide) Layers Across the Length Scales: Swelling, Collapse and Cell Culture Applications	27
3.1 Introduction	28
3.2 Results and discussion	32
3.2.1 Synthesis and characterization of PNIPAM grafts	32
3.2.2 <i>In-situ</i> ellipsometric studies on MB PNIPAM grafts	34
3.2.3 AFM force measurements on MB PNIPAM grafts	42
3.2.4 Stability of PNIPAM grafts	51
3.2.5 Cell adhesion and detachment	53
3.3 Conclusions	55
3.4 Experimental	56
3.5 References and notes	59
Chapter 4 Grafting Mixed Responsive Layers of Poly(<i>N</i>-isopropylacrylamide) and Poly(methacrylic acid) from Gold by Selective Initiation	65
4.1 Introduction	66
4.2 Results and discussion	68
4.2.1 Preparation of mixed PNIPAM-PMAA grafts	68
4.2.2 pH responsive behavior of mixed PNIPAM-PMAA grafts	70

4.3 Conclusions	72
4.4 Experimental	73
4.5 References	75
Chapter 5 Electrochemical Sensing by Surface-immobilized Poly(ferrocenylsilane) Grafts	79
5.1 Introduction	80
5.2 Results and discussion	81
5.2.1 Preparation of PFS grafts	81
5.2.2 Electrochemical properties of PFS grafts	84
5.2.3 Electrochemical sensing of ascorbic acid	88
5.3 Conclusions	89
5.4 Experimental	90
5.5 References and notes	92
Chapter 6 Preparation of a Rapidly Forming Poly(ferrocenylsilane)-Poly(ethylene glycol)-based Hydrogel via Thiol-Michael Addition Click Reaction	95
6.1 Introduction	96
6.2 Results and discussion	97
6.2.1 Synthesis and characterization of PFS-acryl	97
6.2.2 Formation of PFS-PEG hydrogel	98
6.2.3 Redox responsive properties of PFS-PEG hydrogel	100
6.3 Conclusions	102
6.4 Experimental	102
6.5 References	103
Chapter 7 Poly(<i>N</i>-isopropylacrylamide)-Poly(ferrocenylsilane) Dual-responsive Hydrogels: Synthesis, Characterization and Antimicrobial Applications	105
7.1 Introduction	106
7.2 Results and discussion	107
7.2.1 Synthesis and characterization of PNIPAM-PFS hydrogel	107
7.2.2 <i>In-situ</i> formation of PNIPAM-PFS silver composites	112
7.3 Conclusions	114
7.4 Experimental	114
7.5 References	117

Chapter 8 Poly(ferrocenylsilane)-based Redox-active Nanogels/Microgels	119
8.1 Introduction	120
8.2 Results and discussion	121
8.2.1 Preparation and characterization of PFS-PIL	121
8.2.2 PFS-PIL based nanogels	124
8.2.3 PFS-PIL based microgels obtained by microfluidics	127
8.2.4 PFS-acryl based microgels obtained by microfluidics	130
8.3 Conclusions	132
8.4 Experimental	132
8.5 References	135
Outlook	139
Summary	141
Samenvatting	145
Acknowledgements	149
List of Publications	151
Curriculum Vitae	155

Chapter 1

General Introduction

1.1 Introduction

Response to stimuli is a basic process in living systems.¹ To sustain life and maintain biological function, nature requires selectively tailored molecular assemblies and interfaces that provide a specific chemical function and structure which can change in their environment.² Stimuli responsiveness is crucial for maintaining normal function as well as fighting disease. For example, the human body releases insulin to initiate glycogen formation in response to raised glucose levels in the blood.³ Another well-known example are chameleons, which can change color often and quickly according to light, temperature, and mood.^{4,5}

At their most fundamental level, many of the most important substances in living systems are macromolecules such as nucleic acids, proteins that can adapt to varying conditions in their surrounding environment.⁶ Based on the lessons from nature, synthetic polymer systems with “chameleon like” attributes that respond to external stimuli such as light, pH, temperature, mechanical force, electric field, or solvent composition have been prepared. Stimuli-responsive polymers can dynamically alter their structure and properties like shape, surface characteristics, color, solubility or sol-to-gel transition on demand or in response to changes in their environment. Some systems can respond to a combination of two or more stimuli and therefore represent multi-responsive structures. The changes are also reversible, the system returning to its initial state when the trigger is removed. These materials have been widely applied to fabricate sensors and actuators, to regulate cell culture, to control wetting and adhesion, to tune drug-delivery and release and in many other areas.^{2,7-12}

Stimuli-responsive polymers can be classified by their physical form, that is, free chains in solutions, chains grafted on a surface¹³, cross-linked networks in bulk and polymeric solids.^{14,15} Kinetic control of the stimuli-responses is crucial in all applications, therefore understanding the structure-property relationship is essential for further development and rational design of new functional smart materials.

1.2 Concept of this Thesis

The research described in this Thesis is centered around preparing responsive polymer materials as building blocks for addressable structures, their characterization, and their applications. Stimuli-responsive polymer chains including temperature

responsive poly(*N*-isopropylacrylamide) (PNIPAM),^{16,17} pH responsive poly(methacrylic acid) (PMAA)¹⁸ and redox responsive poly(ferrocenylsilane) (PFS)¹⁹⁻²³ can be assembled into various functional polymer architectures such as polymer grafts on surface and polymer networks in bulk.

Polymer grafts on surface: Surface structure and chemistry are very important properties of solid materials, because they exert disproportionately large effects on surface characteristics such as adhesiveness, wettability, bioactivity and many other areas.²⁴ With the development of polymer science, the choice of polymerizable compounds and the control over grafting chemistry have seen tremendous advancement. Uniform, gradient and patterned responsive polymer grafts on surfaces have been successfully developed.²⁵

Polymer networks in bulk: A flexible cross-linked polymer network with a solvent filling the interstitial space of the network forms a polymer gel. Such solvent-insoluble networks are capable of accommodating a large amount of corresponding solvent, whose volume is determined by a balance between thermodynamic forces of mixing and the elastic restoring forces of the network. Polymer networks can be in the form of macroscopic networks or be confined to smaller dimensions such as microgels that range from hundreds of nm to several hundred microns. Those with sizes smaller than ca. 100 nm are sometimes referred as nanogels.

The systems covered are summarized in Figure 1.1.

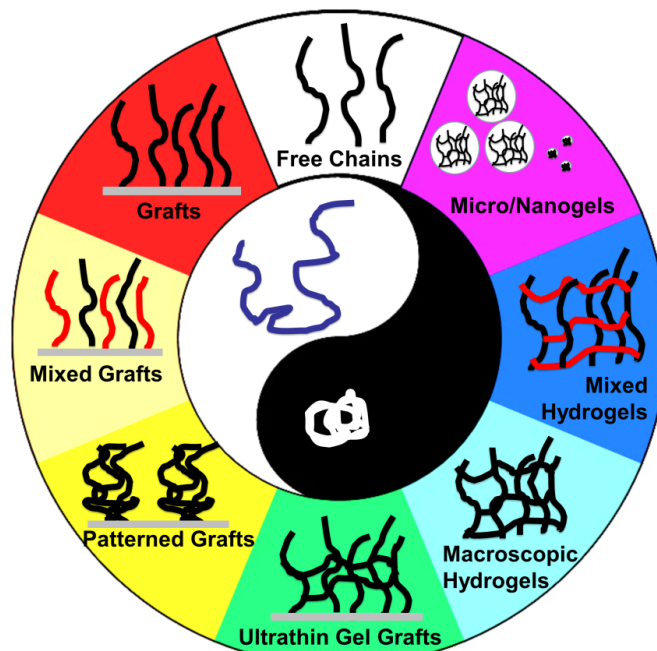


Figure 1.1 Addressable polymer architectures based on stimuli-responsive polymers.

In **Chapter 2**, a comprehensive literature background is provided, covering polymer grafts, macroscopic hydrogels and microgels/nanogels. For each section, the discussion starts by introducing the approaches used to obtain the structures, followed by some examples from literature.

In **Chapter 3**, the properties of PNIPAM layers with different grafting densities under variable solvent and temperature conditions are described. The grafts are prepared by surface-initiated atom transfer radical polymerization (SI-ATRP). *In-situ* ellipsometry and lateral force microscopy are used to study the swelling and collapse behavior across the LCST. These polymer grafts are further evaluated as supporting substrates for cell cultures.

In **Chapter 4**, mixed polymer grafts consisting of PNIPAM and PMAA are prepared by a sequential combination of SI-ATRP and iniferter-mediated photopolymerization (SI-IMP). The responsive behavior as a function of pH is investigated.

In **Chapter 5**, PFS chains are tethered onto silicon or gold substrates by a "grafting to" approach, employing amine alkylation reactions. The electrochemical properties are studied both in water and organic media. An ascorbic acid electrochemical sensor based on these surface-anchored PFS chains is fabricated.

In **Chapter 6**, a rapidly forming redox responsive PFS-poly(ethylene glycol) (PFS-PEG)-based hydrogel is generated *via* thiol-Michael addition click reaction. PFS bearing acrylate side groups (PFS-acryl) is synthesized as the precursor for the network. The equilibrium swelling ratio, morphology, rheology and redox responsive properties of the PFS-PEG-based hydrogel are reported.

In **Chapter 7**, multi-responsive hydrogels composed of PNIPAM and PFS are formed by photopolymerization of NIPAM and PFS-acryl. The *in-situ* fabrication of silver nanoparticles inside the hydrogel network *via* reduction of silver nitrate is discussed. These composites show strong antimicrobial activity while maintaining a high biocompatibility with cells.

In **Chapter 8**, two different types of crosslinkable PFS, PFS-acryl and PFS with vinyl imidazole groups (PFS polyionic liquids, PFS-PIL) are chosen as precursors for gel formation. PFS nanogels are formed by self-crosslinking of PFS-PIL at low concentrations. PFS microgels based on PFS-PIL and PFS-acryl are prepared using a microfluidic system coupled with UV photopolymerization. These techniques enable us to generate and precisely control the size of the redox responsive spheres. These PFS nanogels/microgels produced show redox responsive properties and have promising applications as catalyst support and in molecular release.

Overall, responsive polymer materials are among the most exciting focal points in materials science. Here, various responsive polymer systems with different dimensions (polymer grafts, macroscopic hydrogels and microgels/nanogels) capable

of responses to external or internal stimuli are developed and potential applications are demonstrated.

1.3 References

- 1 B. Jeong and A. Gutowska, *Trends Biotechnol.*, 2002, **20**, 305-311.
- 2 M. A. C. Stuart, W. T. S. Huck, J. Genzer, M. Müller, C. Ober, M. Stamm, G. B. Sukhorukov, I. Szleifer, V. V. Tsukruk, M. Urban, F. Winnik, S. Zauscher, I. Luzinov and S. Minko, *Nat. Mater.*, 2010, **9**, 101-113.
- 3 A. Nelson, *Nat. Mater.*, 2008, **7**, 523-525.
- 4 S. K. Cooper, *National Geographic Explorer*, 2002, **10**, 4-7.
- 5 J. P. Kennedy, *J. Macromol. Sci. Part A-Pure Appl. Chem.*, 1994, **A31**, 1771-1790.
- 6 D. Roy, J. N. Cambre and B. S. Sumerlin, *Prog. Polym. Sci.*, 2010, **35**, 278-301.
- 7 P. Bawa, V. Pillay, Y. E. Choonara and L. C. du Toit, *Biomed. Mater.*, 2009, **4**, 022001.
- 8 D. Schmaljohann, *Adv. Drug Deliv. Rev.*, 2006, **58**, 1655-1670.
- 9 J. Kost and R. Langer, *Adv. Drug Deliv. Rev.*, 2001, **46**, 125-148.
- 10 A. Kumar, A. Srivastava, I. Y. Galaev and B. Mattiasson, *Prog. Polym. Sci.*, 2007, **32**, 1205-1237.
- 11 I. Y. Galaev and B. Mattiasson, *Trends Biotechnol.*, 1999, **17**, 335-340.
- 12 F. Liu and M. W. Urban, *Prog. Polym. Sci.*, 2010, **35**, 3-23.
- 13 R. Barbey, L. Lavanant, D. Paripovic, N. Schüwer, C. Sugnaux, S. Tugulu and H. A. Klok, *Chem. Rev.*, 2009, **109**, 5437-5527.
- 14 S. K. Ahn, R. M. Kasi, S. C. Kim, N. Sharma and Y. X. Zhou, *Soft Matter*, 2008, **4**, 1151-1157.
- 15 J. K. Oh, R. Drumright, D. J. Siegwart and K. Matyjaszewski, *Prog. Polym. Sci.*, 2008, **33**, 448-477.
- 16 O. Smidsrød and J. E. Guillet, *Macromolecules*, 1969, **2**, 272-277.
- 17 H. G. Schild, *Prog. Polym. Sci.*, 1992, **17**, 163-249.
- 18 S. Tugulu, R. Barbey, M. Harms, M. Fricke, D. Volkmer, A. Rossi and H. A. Klok, *Macromolecules*, 2007, **40**, 168-177.
- 19 G. R. Whittell, M. D. Hager, U. S. Schubert and I. Manners, *Nat. Mater.*, 2011, **10**, 176-188.
- 20 V. Bellas and M. Rehahn, *Angew. Chem. -Int. Edit.*, 2007, **46**, 5082-5104.
- 21 Y. J. Ma, W. F. Dong, M. A. Hempenius, H. Möhwald and G. J. Vancso, *Nat. Mater.*, 2006, **5**, 724-729.
- 22 M. A. Hempenius, C. Cirmi, F. Lo Savio, J. Song and G. J. Vancso, *Macromol. Rapid Commun.*, 2010, **31**, 772-783.
- 23 D. A. Foucher, B. Z. Tang and I. Manners, *J. Am. Chem. Soc.*, 1992, **114**, 6246-6248.
- 24 J. L. Zhang and Y. C. Han, *Chem. Soc. Rev.*, 2010, **39**, 676-693.
- 25 X. F. Sui, J. Y. Yuan, W. Z. Yuan and M. Zhou, *Prog. Chem.*, 2008, **20**, 1122-1127.

Chapter 2

Addressable Stimuli-Responsive Polymer Architectures

2.1 Introduction

The term stimuli-responsive polymer materials refers to materials that can adapt to variations in their surrounding environments, regulate transport of ions and molecules, change wettability and adhesion of different species in response to temperature, mechanical, electro-magnetic irradiation, electrochemical, pH, and ionic strength stimuli, or respond to the presence of bioactive species. These materials are playing an increasingly important part in a diverse range of application areas, such as biocatalysis, separation, drug delivery, diagnostics, tissue engineering as well as sensors and actuators.¹⁻⁷

Stimuli-responsive polymers can be classified by their physical form, that is, free chains in solutions, chains grafted on a surface,⁸ cross-linked networks in bulk,^{9,10} and polymeric solids. These significant diversities in spatial constraints lead to different restrictions in mobility within variable dimensions, therefore stimuli-responsiveness is clearly influenced by confinement.¹¹ To illustrate spatial restrictions of segmental mobility of polymer chains in x , y , and z directions in solutions, at surfaces and interfaces, in gels, and in solids, Figure 2.1 depicts a schematic diagram of the four states and relative dimensional restrictions within each state. The examples of responses are classified into physical and chemical categories, where multiple stimuli may result in one or more responses, or one stimuli may result in more than one response.

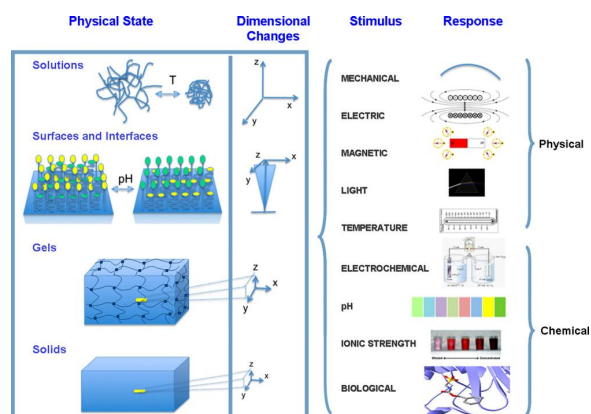


Figure 2.1 Schematic representation of dimensional changes in polymeric solutions, at surfaces and interfaces, in polymeric gels, and polymer solids resulting from physical or chemical stimuli.¹¹

In our studies, stimuli-responsive polymers were used as building blocks for the creation of various functional polymer architectures such as polymer grafts on surface by “grafting from” and “grafting to” approaches and polymer networks in bulk including macroscopic hydrogels and microgels/nanogels. In this chapter, the stimuli-responsive systems: polymer grafts, macroscopic hydrogels and microgels/nanogels are reviewed. For each section, the discussion starts by introducing the approaches used to obtain the structures, followed by some examples from the literature.

2.2 Polymer grafts on surfaces

Surface structure and chemistry are very important properties of solid materials, because they exert disproportionately large effects on surface properties such as adhesiveness, wettability, bioactivity and many other areas.¹²

Generally, there are two standard methods to fabricate responsive polymer surfaces.¹³⁻²³ The first method, physical modification, is to deposit functional surface structures on surfaces *via* spin casting, precipitation, Langmuir–Blodgett technique or polymer adsorption. This method is simple, efficient, and well controlled, but the resulting surface structures suffer from instability and a short lifetime. The second method, chemical modification, is to modify the target surface *via* grafting functional polymer chains. It is necessary to highlight that grafting techniques have advantages over others for several reasons. They enable an easy and controllable introduction of polymer chains with a high surface density, precise localization of the chain at the surface, and the grafted layers possess a high stability. The tethered chains also open avenues to specific applications. Among others, the grafts can be used to efficiently stabilize colloids, to significantly reduce friction between the sliding surfaces, and to control and switch surface wetting.¹³⁻²³

Numerous structures on stimuli-responsive surfaces were developed by chemical grafting of polymer chains.²⁴ The conformation of those polymers in a solvent can dramatically change with grafting density.²⁵ For example, for polymer brushes,^{8,26-28} the density of the anchoring sites should be high enough to ensure an extended conformation of the crowded chains with end-to-end distances larger than for the free chains in the same solvent. At lower grafting densities of the tethered chains, they adopt conformations with reduced macromolecular stretching, exhibiting so-called “pancake” or “mushroom” shapes (Figure 2.2), while for higher grafting densities a polymer brush layer is formed.

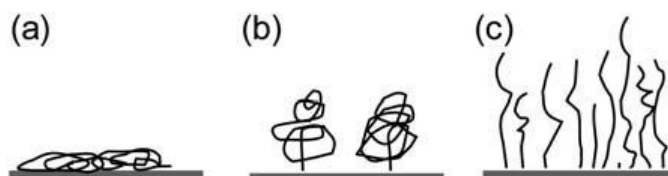


Figure 2.2 Scheme of the conformations of the surface tethered polymer chains: (a) “pancake”, (b) “mushroom” and (c) “brush”.²⁴

Polymer grafts can be formed on a variety of solid substrates including metals, semiconductors and polymeric supports, and have thicknesses typically ranging from a few to several hundred nanometers.²⁹ Chemical functionality can be incorporated in specific positions, allowing a precise embedding of desired molecules in the layer. Polymer grafts can usually be prepared by either of two main approaches: “grafting to” and “grafting from”.^{21,30-32}

In the “grafting to” technique, macromolecules are attached to a surface using one functional end group or using functional side groups. In the latter case, the grafted chains form loops or tails on the surface. Due to steric hindrance (slow diffusion of the macromolecules through the already grafted chains to the surface), only low grafting densities can be achieved. “Grafting from” utilizes surface-tethered initiating sites from which polymeric chains may be grown. This method renders it possible to control the surface concentration of the active sites (e.g. by using mixed, self-assembled monolayers (SAMs) of surface active initiators mixed with inactive molecules) and can yield high grafting densities.

Recent advances in controlled free radical polymerizations (CRP) enable the use of a wide variety of monomers to obtain precisely tailored, grafted surfaces with near-molecular control.³²⁻³⁵ The frequently used CRP techniques include Atom Transfer Radical Polymerization (ATRP), INItiators-tansFER-terminaTER agent (INIFERTER) based polymerization, Reversible Addition-Fragmentation chain Transfer radical polymerization (RAFT), and Nitroxide-Mediated Polymerization (NMP).^{36,37} The basic concept of CRP is a reversible activation process. CRP methods include activation and deactivation steps (with rate constants k_{act} and k_{deact}), for RAFT the exchange process apparent rate constant k_{exch} . If the living chain experiences the activation-deactivation cycles frequently enough over a period corresponding to the polymerization time, all chains may have a nearly equal chance to grow, yielding a low-polydispersity product. Free radicals may be generated *via* a catalyzed reaction (ATRP), by UV (iniferter-based), by a spontaneous thermal process (NMP) or reversibly *via* the degenerative exchange process with dormant species (RAFT).

By appropriate choice of initiating system, temperature, monomer nature and concentration, it is quite possible to find conditions for the synthesis of layers possessing a targeted morphology, thickness and composition.^{33,38} Uniform, gradient and patterned responsive polymer grafts on planar and curved surfaces have been successfully developed by surface initiated (SI) polymerization.

In case of single-component homopolymer brushes, various responsive grafts such as temperature responsive ones,^{39,40} pH responsive ones⁴¹⁻⁴⁴ etc. were prepared. For example, poly(*N*-isopropylacrylamide) (PNIPAM) has been widely studied as a thermally responsive polymer since its lower critical solution temperature (LCST, $\sim 32^\circ\text{C}$) in water is in the range of the physiologically relevant temperatures.⁴⁵⁻⁴⁷ Apparently, below the LCST, water molecules form hydrogen bonds with the polar amide groups attached to the polymer backbone and organize around hydrophobic groups as iceberg water. Above the LCST, bound water molecules are released to the bulk with a large gain in entropy resulting in collapse of the polymer. The influence of the temperature on the polymer structure and hydration of PNIPAM grafts is well documented in the literature.^{39,48-60}

PNIPAM grafts can be readily prepared in aqueous solution at room temperature with high thickness by SI-ATRP.⁶¹ Figure 2.3 shows that PNIPAM can be polymerized in aqueous solution at a low methanol concentration at room temperature to maintain the growing PNIPAM chains in a hydrophilic and an extended conformational state.⁶¹ Under these conditions, thick polymer layers (up to 500 nm in the swollen state) are produced after 1 h of polymerization.

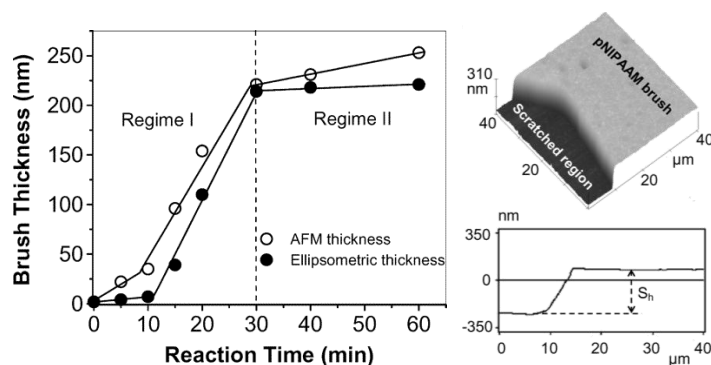


Figure 2.3 Surface-initiated ATRP of NIPAM on gold surfaces to yield PNIPAM polymer grafts and average PNIPAM dry thickness in air plotted as a function of polymerization time, measured by AFM (open circles) and ellipsometry (filled circles). Adapted from reference.⁶¹

Gradient polymer grafts possess a continuous, directional variation in physicochemical properties on a surface, resulting from a corresponding gradient in

composition or grafting density.⁶²⁻⁶⁶ PNIPAM layers with a surface gradient in grafting densities can be prepared by varying the initiator coverage across the grafted substrate.⁶⁷ This “high throughput” approach allowed the imaging of the morphology variation at one substrate in the different grafting regimes. The images demonstrated that variation in chain density is accompanied by a concomitant change in surface morphology, gradually evolving from discontinuous mushroom structures at low grafting densities to heterogeneous patchy structures at intermediate grafting densities. The size of the patch structures gradually increased with increasing initiator coverage, until in high grafting density regions the morphology evolved to a smoother, presumably more extended, structure encompassing more extended chains (Figure 2.4).⁶⁷

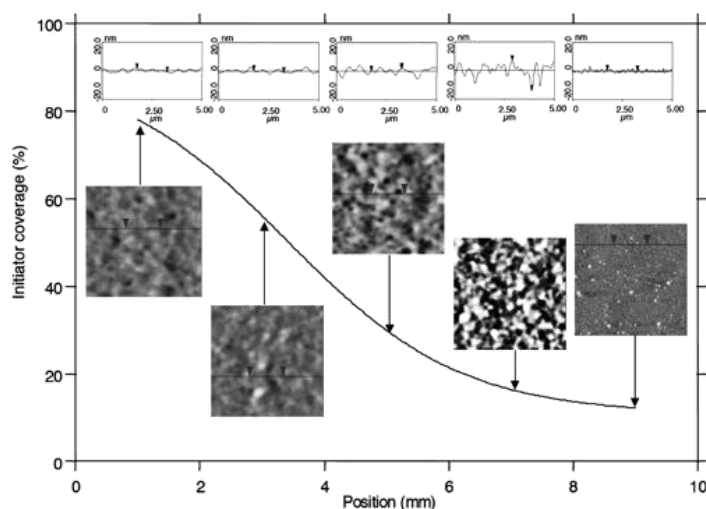


Figure 2.4 Relationship of PNIPAM grafts morphology to local grafting density as tracked through the initiator density. The solid line gives the initiator coverage as a function of position. Individual insets show $5 \times 5 \mu\text{m}^2$ tapping mode AFM topography images and section analysis line scans (above the respective images) at $x = 1, 3, 5, 7,$ and 9 mm of a 10 mm long PNIPAM density gradient.⁶⁷

Mixed polymer grafts, composed of at least two distinct polymer chains randomly immobilized at a solid substrate, were also described.^{68,69} The exposure to a selective solvent induced a clear morphological rearrangement in the architecture of the grafts by turning the soluble segments to the interface and resulting in a collapse of the non-soluble ones. Minko et al.⁷⁰ investigated binary poly(methyl methacrylate)/polystyrene (PMMA/PS) grafts and found surface features with two distinct AFM phase shifts, indicating lateral phase separation of the polymers and the presence of PS- and PMMA-rich surface regions (Figure 2.5).

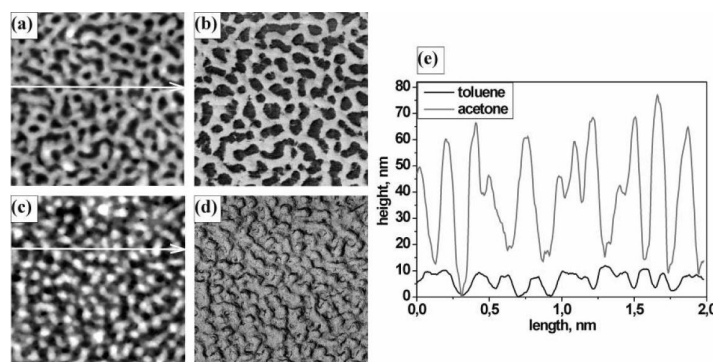


Figure 2.5 Representative morphologies for PMMA/PS mixed grafts. The ripple (a and b) and dimple (c and d) morphologies were formed after 5 min of exposure to toluene and acetone, respectively, and were recorded in the AFM repulsive tapping mode ($2 \times 2 \mu\text{m}^2$: topography (a and c), phase contrast (b and d)). Cross-sections are shown in the panel (e). White arrows in panels a and c mark the locations of the cross-sections. Z ranges are (a) 13 nm, (b) 3.2° , (c) 78.4 nm, and (d) 27.2° . Adapted from reference.⁷⁰

As mentioned in the beginning of this section, the structural control of polymer grafts is of central importance for advanced molecular surface engineering.⁷¹⁻⁷⁸ Patterned polymer nanostructures with controlled structural motifs, feature dimensions and controlled chemical functionality offer great opportunities in molecular engineering of “designer” surfaces, sensing, microfluidics, biomedical applications, as nanoreactors for particle synthesis, etc. due to the precise control of physical and chemical surface properties, and so on.⁷⁹ Nanopatterned polymer grafts with defined features become especially interesting when the pattern dimensions are close to the length of the grafted macromolecules.⁸⁰⁻⁸² AFM-based techniques, such as nanoscratching,^{83,84} dip-pen nanolithography (DPN)⁸⁵⁻⁸⁷ and scanning probe oxidation (SPO)⁸⁸⁻⁹⁰ offer versatile patterning techniques across the length scales. Advantages of AFM based methods for the nano-fabrication include high resolution, the ability to generate features with nearly arbitrary geometries, and a precise position control. For example, by using DPN to deposit tetrachloroauric acid onto the H-terminated silicon substrates, gold wires were produced upon reduction in contact with the substrate.⁸⁷ Subsequently, disulfide iniferters were immobilized on these gold wires. Poly(methacrylic acid) (PMAA) polymer brushes were then grafted from the functionalized nanopatterns by means of controlled photopolymerization. The height and width of the polymer brush nanostructures were controlled by the preparation conditions (Figure 2.6).

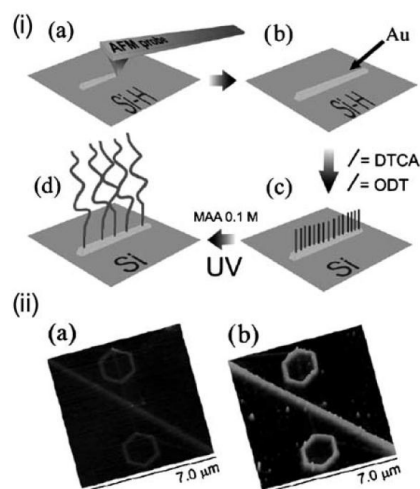


Figure 2.6 (i) The preparation of polymer grafts from immobilized precursors on gold nanowires: (a) and (b) tip-assisted deposition of gold nanowires on hydride-terminated silicon; (c) selective immobilization of functional adsorbates on the gold structures; and (d) UV-initiated grafting of PMAA using the functionalized nanowires as platforms. (ii) Height images (vertical scale from black to white 10 nm) from tapping-mode AFM measurements: (a) 240 (± 30) nm wide gold wires deposited on hydride terminated silicon and (b) the subsequently grafted PMAA. Adapted from reference.⁸⁷

However, AFM related nano-fabrication approaches are relatively slow (mostly serial) and are presently not very suitable for large-scale and high-throughput pattern formation.⁹¹ The above-mentioned drawback could be overcome by applying high-throughput processes, such as nanoimprint lithography.⁹² Nanoimprint lithography has shown great promise as it is a low-cost process that allows the patterning of large areas and simultaneously achieves high pattern resolutions. Functional polymer graft nanostructures are obtained by combining step-and-flash imprint lithography (SFIL) with controlled, surface-initiated polymerization.⁹³ Patterning is achieved at length scales such that the smallest elements have dimensions in the sub-100 nm range. The patterns exhibit different shapes, including lines and pillars, over large surface areas (Figure 2.7). The platforms obtained are used to selectively immobilize functional biomacromolecules.

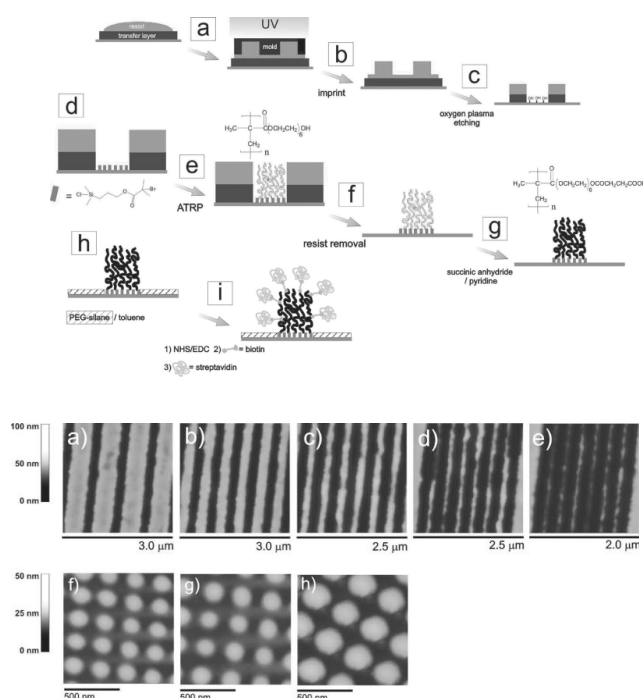


Figure 2.7 Top: Step-wise fabrication process for creating protein-immobilized poly(ethylene glycol)methacrylates (PEGMA) brush nanostructures; Down: Tapping-mode AFM images displaying PEGMA brush nanostructures fabricated by SFIL/SI-ATRP, a series of brush lines (a–e) characterized by line-width values ranging from 520 ± 7 to 80 ± 10 nm and pillars presenting average diameters of 130, 140, and 200 nm (f–h) are shown. Adapted from reference.⁹³

2.3 Polymer networks in bulk

A flexible cross-linked polymer network with a solvent filling the interstitial space of the network forms a polymer gel.⁹ Such solvent-insoluble networks are capable of accommodating a large amount of corresponding solvent, whose volume is determined by a balance between thermodynamic forces of mixing and the elastic restoring forces of polymer.⁹⁴ Polymer networks can be in the form of macroscopic networks or be confined to smaller dimensions such as microgels that range from hundreds of nm to several hundred microns. Those with sizes smaller than ca. 100 nm are sometimes referred to as nanogels.⁹⁵ The characteristic structure of responsive networks is responsible for their unique ability to undergo changes in response to environmental stimuli. The stimuli applied may include thermal, electrical, magnetic, pH, light, ionic or metallic interactions or combinations thereof. These materials have many applications, e.g. as actuators and sensors or in controlled cell adhesion and drug delivery.⁹⁶⁻⁹⁹

Polymer gels are generally prepared from polymer matrices that are crosslinked by physical crosslinking or chemical crosslinking.⁹ Physical crosslinking refers to gels which are formed by the growth of physically connected aggregates.^{100,101} Ionic interactions, hydrogen bonds, crystallized domains, hydrophobic interactions, stereocomplexation, inclusion complexation, sol–gel transition, supramolecular chemistry host–guest interaction, and self-assembly have been utilized for the synthesis of these bulk gels. These physically crosslinked gels could reversibly degrade into the corresponding precursors upon receiving external stimuli.^{100,101}

Chemical crosslinking is achieved through permanent covalent bonds.¹⁰¹ Several methods like copolymerization of monomers in the presence of either difunctional or multifunctional crosslinkers,¹⁰ thiol-ene¹⁰²⁻¹⁰⁴ and quarternization¹⁰⁵ have been explored for the preparation of gels. The crosslinked network will not dissolve in response to solvent presence due to the irreversible network structure.

2.3.1 Macroscopic hydrogels

Hydrogels are crosslinked polymeric networks which absorb and retain large amounts of water.^{99,101,106-112} The obtained networks show visco-elastic and sometimes pure elastic behavior. From a physical point of view, hydrogels resemble living tissues because they have high water content and a soft and rubbery consistency.¹¹³ Their classification may be based on the source: natural, synthetic, or hybrid hydrogels; the crosslinking: chemical or physical gels; the network: homopolymer, copolymer, interpenetrating, or double networks; physical structure: homogeneous, microporous, and macroporous hydrogels; on their fate in the organism: degradable and nondegradable hydrogels; on the nature of the incorporated functional groups: neutral, cationic, anionic amphiphilic or zwitterionic hydrogels.¹¹⁴ The design and preparation of hydrogels have attracted a great deal of interest in biomedical engineering, pharmaceutical applications, and biomaterials science because of their tunable chemical and three-dimensional (3D) physical structure, desirable mechanical properties, high water content and biocompatibility.¹¹⁵⁻¹²⁰

Temperature-sensitive hydrogels are usually based on polymers exhibiting a LCST, i.e. like PNIPAM. A novel kind of PNIPAM based hydrogel composed of NIPAM, ruthenium(II)tris(2,2'-bipyridine) ($\text{Ru}(\text{bpy})_3^{2+}$) and hydrophilic 2-acrylamide-2-methylpropane sulfonic acid (AMPS) was developed (Figure 2.8).^{121,122} It involves a built-in system of energy conversion from chemical oscillation to mechanical oscillation. The catalyst of the Belousov–Zhabotinsky (BZ) reaction,¹²³ $\text{Ru}(\text{bpy})_3^{2+}$ is covalently bound to the polymer chain of PNIPAM. The BZ reaction occurs in the gel when the hydrogel is immersed in a suitable aqueous solution. The LCST of PNIPAM in the oxidized Ru(III) state becomes higher than that in the

reduced Ru(II) state because of the charge increase of the catalyst.¹²⁴ At constant temperature, redox changes of the catalyst lead to hydrophilic changes of the polymer chains. Consequently, periodical redox changes induced by the BZ reaction produce periodical swelling–deswelling changes in the gel.^{121,125} By coupling with a ratchet mechanism, the gel walks with repeated bending and stretching motions by itself like a looper at a speed of $170 \mu\text{m min}^{-1}$. This “self-walking” gel actuator could serve as a new framework for a biomimetic robot.

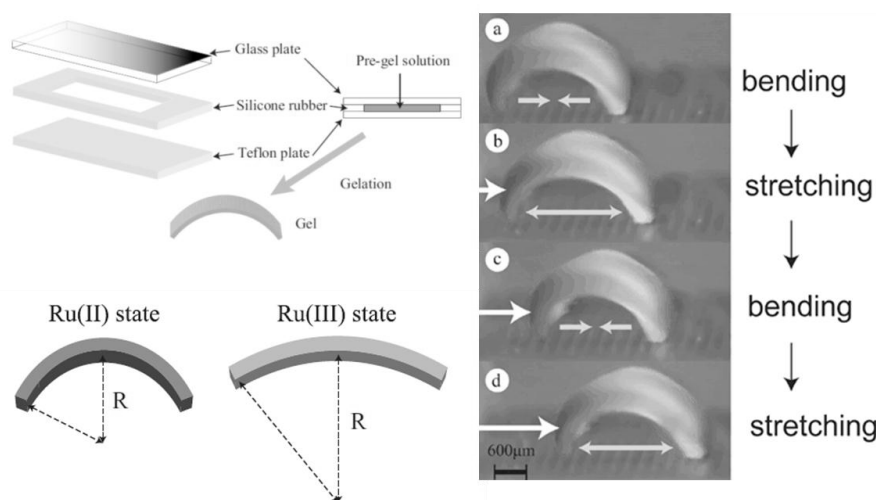


Figure 2.8 Left: Preparation of the poly(NIPAM-co-Ru(bpy)₃-co-AMPS) gel membrane undergoing anisotropic contraction; Right: Schematic illustration of anisotropic contraction of the poly(NIPAM-co-Ru(bpy)₃-co-AMPS) gel strip at the Ru(II) and Ru(III) states. In the reducing agent (Ce(III) solution), the gel keeps a tinge of orange originating from the Ru(II) state. In the oxidizing agent (Ce(IV) solution), on the other hand, the gel keeps a tinge of light green originating from the Ru(III) state. *R* is the radius of curvature. Outer solution: 62.5 mM malonic acid, 84 mM sodium bromate, 0.894 M nitric acid, 18 °C. Adapted from reference.¹²²

Redox responsive poly(ferrocenylsilane) (PFS) hydrogels¹⁰⁵ were prepared based on crosslinked PFS polyelectrolyte chains (Figure 2.9). PFS^{108,126-129} is a class of organometallic polymers which is composed of alternating ferrocene and alkylsilane units in the main chain. With the discovery of the anionic ring-opening polymerization of silicon-bridged ferrocenophanes, well-defined PFS and block copolymers featuring corresponding organometallic blocks have become accessible.¹³⁰ The ferrocene units of the PFS chains can be reversibly oxidized and reduced by chemical and by electrochemical means.

The PFS polyelectrolyte hydrogels formed by crosslinked chains possess side groups with either permanent positive or negative charges. A cationic PFS hydrogel was obtained by quaternization. First, high molar mass poly(ferrocenyl(3-

iodopropyl)methylsilane) chains¹³¹ were crosslinked with *N,N,N',N'',N''*-pentamethyldiethylenetriamine at room temperature. Subsequently, remaining iodopropyl side groups were converted into positively charged side groups using *N,N*-dimethylethylamine, resulting in a permanently charged cationic network. Finally, iodide counterions were exchanged to chloride ions to increase the water swellability. A polyanionic PFS hydrogel was also obtained by side group modification of poly(ferrocenyl(3-iodopropyl)methylsilane). Reaction with one equivalent of α -lithio isobutyl methanesulfonate led to the formation of a PFS network, likely through intermolecular alkylation after α -deprotonation of isobutylsulfonate side groups. The isobutyl protecting groups were removed by heating the network with tetrabutylammonium iodide in THF. Exchange of the tetrabutylammonium counterions with sodium ions in aqueous NaCl produced the polyanionic network.

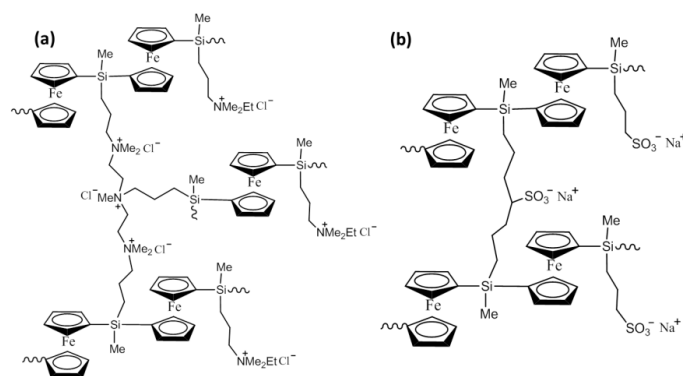


Figure 2.9 Structures of a polycationic PFS and a polyanionic PFS hydrogel. Adapted from reference.¹⁰⁵

Cyclic voltammograms obtained after swelling of PFS hydrogel network in aqueous NaClO_4 show two oxidation and reduction waves, typical of PFS.¹³² Upon electrochemical oxidation, the hydrogels changed color from amber to green–blue and turned back to amber upon reduction. Oxidation of the anionic hydrogel was accompanied by a clear change in mechanical behavior: the gel collapsed and lost its elastic nature. Upon reduction the network reswelled and regained its elasticity. The observed collapse is ascribed to electrostatic attraction between the positively charged ferrocenium units in the PFS main chain and the negatively charged sulfonate side groups of the polymer (Figure 2.10).

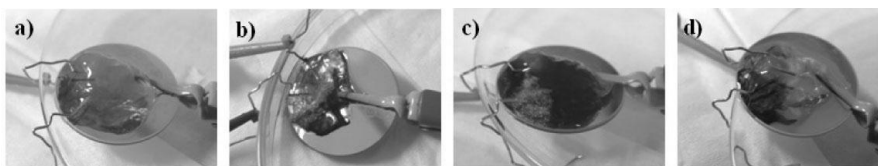


Figure 2.10 Electrochemical oxidation and reduction of polyanionic hydrogel, swollen in aqueous NaClO_4 and supported on a gold electrode. (a) Neutral amber colored PFS hydrogel; (b) Oxidation starts, accompanied by a color change from amber to blue-green; (c) Fully oxidized PFS hydrogel; (d) Electrochemical reduction of the PFS hydrogel has almost completed, the color changed back from blue-green to amber. Adapted from reference.¹⁰⁸

2.3.2 Microgels/nanogels

Stimuli-responsive microgels/nanogels represent a rapidly developing class of materials that find applications in sensing,¹³³ molecular imprinting,¹³⁴ the fabrication of photonic crystals,¹³⁵ bioseparation,¹³⁶ diagnostics¹³⁷ and especially in drug delivery systems, since they have tunable sizes from nanometers to several micrometers, a large surface area for multivalent bioconjugation and an interior network for the incorporation of bioactive molecules.^{10,138-140}

Various synthetic approaches for the preparation of microgels/nanogels were developed and reviewed.^{10,141-146} They include imprint photolithographic technique,¹⁴⁷ micromolding methods,^{148,149} crosslinking of single polymer chain,¹⁵⁰⁻¹⁵² various heterogeneous polymerization methods such as dispersion,¹⁵³ precipitation,¹⁵⁴ inverse (mini)emulsion^{155,156} and inverse microemulsion polymerization¹⁵⁷ by conventional and controlled radical polymerization,¹⁴⁵ and microfluidics.¹⁵⁸ The discussions below are limited to the following three approaches, crosslinking of a single polymer chain, heterogeneous polymerization and microfluidics.

For the radical polymerization process, decreasing the monomer concentration increases the distance between propagating chains, thus limiting intermolecular crosslinking and increasing the probability of intramolecular crosslinking. Consequently, macroscopic gelation can be prevented. Here, the size of the gels will be limited by confining the crosslinking to intraparticle rather than interparticle crosslinking (Figure 2.11).

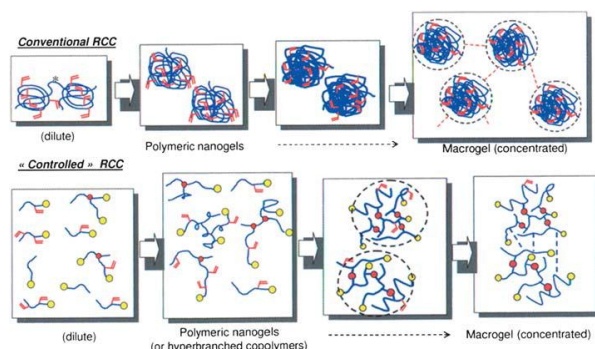


Figure 2.11 Schematic presentation of the crosslinking reactions in conventional and “controlled”/“living” radical polymerization systems.¹⁵⁹

The synthesis of polymeric nanogels through the crosslinking and collapse of single or a few polymer chains is currently being investigated as a simple and facile route.¹⁵⁰⁻¹⁵² Aliphatic polycarbonates with pendant vinyl groups were transformed into nanoparticles through intramolecular olefin cross-metathesis under dilute conditions.¹⁵¹ Formation of molecular nanogels was confirmed by AFM through visualization of individual molecules at different stages of cross-linking (Figure 2.12).

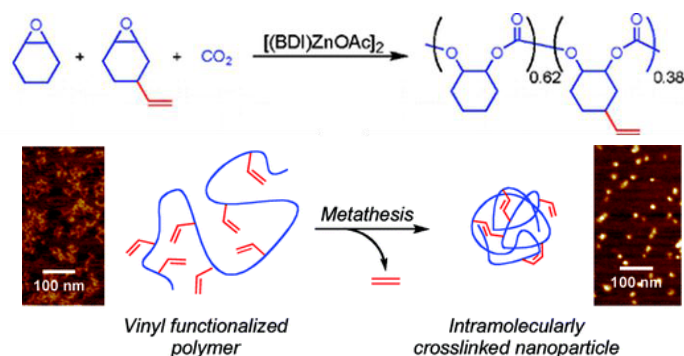


Figure 2.12 Synthesis of alkene cross-linked polycarbonate nanogels and AFM height images for the nanogels. Adapted from reference.¹⁵¹

Heterogeneous polymerization is one of the most commonly employed synthetic techniques for the formation of monodisperse polymer microspheres. Kulbaba et al.^{160,161} used a heterogeneous polymerization method for the formation of redox responsive PFS microgels. Mixtures of xylenes and decane were employed since they are miscible in all proportions and xylenes are considered to be a good solvent for PFS while decane is known to act as a precipitant. Chemical oxidation of the microgels led to positively charged particles which underwent electrostatically driven

emulsification in microfluidic devices with different geometries that were most frequently exploited to produce droplets with narrow size distribution.

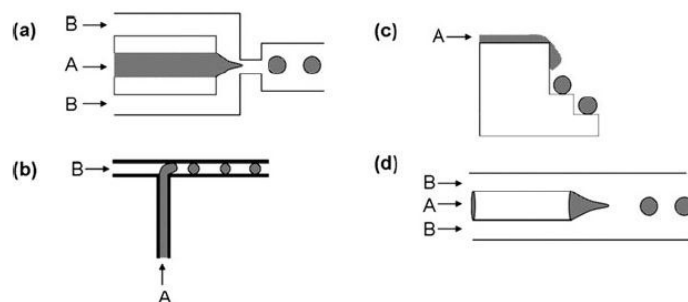


Figure 2.14 Schematic drawings of various types of microfluidic droplet generators: (a) flow-focusing, (b) T-junction, (c) terrace-like, and (d) co-flowing stream geometries. The droplet and the disperse phases are labeled as A and B, respectively.¹⁵⁸

Several approaches were examined for the microfluidic preparation *on-chip* or *off-chip* of microgels of both synthetic and biological polymers based on chemical gelation^{163,164} and physical gelation.¹⁶⁵ Chemical gelation utilizes polymerization to crosslink low-viscosity monomer droplets stably dispersed in a continuous phase with the aid of surfactants. Physical gelation is typically induced by hydrophobic interactions, hydrogen bond interactions, or ionic interactions.¹⁶²

In addition to the control over droplet sizes, the combination of hydrodynamic variables and thermodynamic factors allows the formation of droplets with interesting multiphase morphologies such as porous, core-shell or Janus morphologies.^{164,166} Variation in the composition of precursor droplets (and hence, the corresponding microgel particles) can be achieved by mixing liquid reagents in the concentration ratio pre-determined by the ratio of their flow rates.¹⁶⁷ Parallel microfluidic reactors can enable high-throughput screening of the compositions of microgel properties and the properties of the encapsulated species.¹⁶⁸

Monodisperse thermo-responsive PNIPAM microgels can be successfully prepared *on chip* by microfluidics devices.¹⁶⁹⁻¹⁷¹ The productivity of a microfluidic reactor is determined by the flow rate of the droplet phase, which in the synthesis of monodisperse polymer particles generally does not exceed a fraction of a few mL/h. This range of flow rates is sufficient for exploratory purposes, e.g., for the high-throughput screening of reaction conditions or the optimization of formulations, however in order to compete with conventional technologies for the production of high value polymer particles, the productivity of microfluidic synthesis has to be significantly increased. By using the integrated multiple modular microfluidic reactor,¹⁶⁸ PNIPAM microgel particles can be synthesized continuously. A higher

productivity of the reactor can be achieved by combining a larger number of modules (Figure 2.15). It shows that the reactors can produce polymer microgel particles with polydispersity not exceeding 5% at a productivity of approximately 50 g/h.

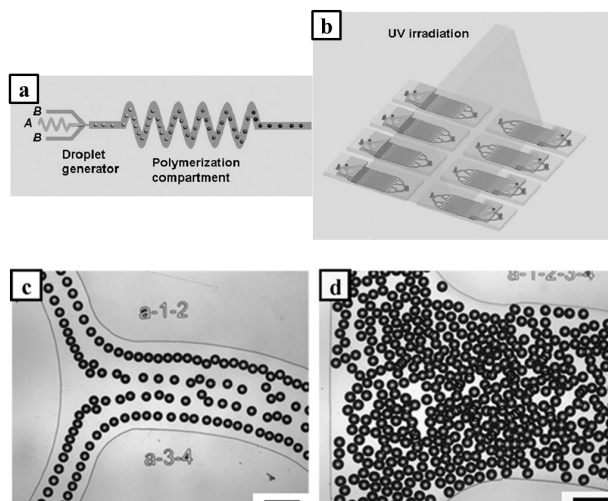


Figure 2.15 Schematics of multiple modular microfluidics reactors. (a) An individual microfluidic reactor for the synthesis of polymer particles comprising an emulsification and a polymerization compartment, (b) A reactor comprising eight modules, (c) Typical optical microscopy image of aqueous NIPAM droplets generated in an individual flow-focusing droplet generator module of reactor, and (d) Microgel particles following their on-chip polymerization. In a,b the flow rates of the monomer solution and mineral oil were 0.4 and 0.6 mL/h per generator, respectively. Adapted from reference.¹⁶⁸

2.4 Conclusions

The approaches used to obtain responsive polymer structures such as polymer grafts on surfaces and polymer networks in bulk have been discussed.

Responsive polymer systems capable of responding to external or internal stimuli represent one of the most exciting and emerging areas of scientific interest and they can be used for a variety of applications, such as switching surfaces and adhesives, protective coatings that adapt to the environment, artificial muscles, sensors and drug delivery. Kinetic control of the stimuli-responses is crucial in all applications, therefore understanding structure-property relationships is essential for further development and rational design of new functional smart materials.

Further developments will be in the area of bionic materials, such as systems that can be responsive to biochemical signals or biomarkers typically present in less than nanomolar concentrations. For all the different physical states, overcoming the

barriers of biocompatibility, biodegradability and non-toxicity are also particularly important.

2.5 References

- 1 M. A. C. Stuart, W. T. S. Huck, J. Genzer, M. Müller, C. Ober, M. Stamm, G. B. Sukhorukov, I. Szleifer, V. V. Tsukruk, M. Urban, F. Winnik, S. Zauscher, I. Luzinov and S. Minko, *Nat. Mater.*, 2010, **9**, 101-113.
- 2 P. Bawa, V. Pillay, Y. E. Choonara and L. C. du Toit, *Biomed. Mater.*, 2009, **4**, 022001.
- 3 D. Schmaljohann, *Adv. Drug Deliv. Rev.*, 2006, **58**, 1655-1670.
- 4 J. Kost and R. Langer, *Adv. Drug Deliv. Rev.*, 2001, **46**, 125-148.
- 5 A. Kumar, A. Srivastava, I. Y. Galaev and B. Mattiasson, *Prog. Polym. Sci.*, 2007, **32**, 1205-1237.
- 6 I. Y. Galaev and B. Mattiasson, *Trends Biotechnol.*, 1999, **17**, 335-340.
- 7 L. Ionov, *J. Mater. Chem.*, 2010, **20**, 3382-3390.
- 8 R. Barbey, L. Lavanant, D. Paripovic, N. Schüwer, C. Sugnaux, S. Tugulu and H. A. Klok, *Chem. Rev.*, 2009, **109**, 5437-5527.
- 9 S. K. Ahn, R. M. Kasi, S. C. Kim, N. Sharma and Y. X. Zhou, *Soft Matter*, 2008, **4**, 1151-1157.
- 10 J. K. Oh, R. Drumright, D. J. Siegwart and K. Matyjaszewski, *Prog. Polym. Sci.*, 2008, **33**, 448-477.
- 11 F. Liu and M. W. Urban, *Prog. Polym. Sci.*, 2010, **35**, 3-23.
- 12 J. L. Zhang and Y. C. Han, *Chem. Soc. Rev.*, 2010, **39**, 676-693.
- 13 J. Bunsow, T. S. Kelby and W. T. S. Huck, *Acc. Chem. Res.*, 2010, **43**, 466-474.
- 14 W. S. Choi, H. Y. Koo, J. Y. Kim and W. T. S. Huck, *Adv. Mater.*, 2008, **20**, 4504-4508.
- 15 O. Azzaroni, A. A. Brown and W. T. S. Huck, *Adv. Mater.*, 2007, **19**, 151-154.
- 16 C. Zhao, L. Y. Li and J. Zheng, *Langmuir*, 2010, **26**, 17375-17382.
- 17 Y. Q. Zou, N. A. A. Rossi, J. N. Kizhakkedathu and D. E. Brooks, *Macromolecules*, 2009, **42**, 4817-4828.
- 18 T. Chen, R. Ferris, J. M. Zhang, R. Ducker and S. Zauscher, *Prog. Polym. Sci.*, 2010, **35**, 94-112.
- 19 A. Hucknall, S. Rangarajan and A. Chilkoti, *Adv. Mater.*, 2009, **21**, 2441-2446.
- 20 N. Ayres, *Polym. Chem.*, 2010, **1**, 769-777.
- 21 S. Edmondson, V. L. Osborne and W. T. S. Huck, *Chem. Soc. Rev.*, 2004, **33**, 14-22.
- 22 P. M. Mendes, *Chem. Soc. Rev.*, 2008, **37**, 2512-2529.
- 23 I. Luzinov, S. Minko and V. V. Tsukruk, *Soft Matter*, 2008, **4**, 714-725.
- 24 X. F. Sui, S. Zapotoczny, E. M. Benetti, P. Schön and G. J. Vancso, *J. Mater. Chem.*, 2010, **20**, 4981-4993.
- 25 J. Rühe, M. Ballauff, M. Biesalski, P. Dziezok, F. Grohn, D. Johannsmann, N. Houbenov, N. Hugenberg, R. Konradi, S. Minko, M. Motorov, R. R. Netz, M. Schmidt, C. Seidel, M. Stamm, T. Stephan, D. Usov and H. N. Zhang, *Adv. Polym. Sci.*, 2004, **165**, 79-150.
- 26 S. T. Milner, *Science*, 1991, **251**, 905-914.
- 27 W. J. Brittain and S. Minko, *J. Polym. Sci. Pol. Chem.*, 2007, **45**, 3505-3512.
- 28 R. R. Shah, D. Merreces, M. Husemann, I. Rees, N. L. Abbott, C. J. Hawker and J. L. Hedrick, *Macromolecules*, 2000, **33**, 597-605.
- 29 Y. Tsujii, K. Ohno, S. Yamamoto, A. Goto and T. Fukuda, *Adv. Polym. Sci.*, 2006, **197**, 1-45.
- 30 X. F. Sui, J. Y. Yuan, W. Z. Yuan and M. Zhou, *Prog. Chem.*, 2008, **20**, 1122-1127.

Chapter 2

- 31 J. R uhe, *Macromolecular Symposia*, 1998, **126**, 215-222.
- 32 S. Minko, *Polym. Rev.*, 2006, **46**, 397-420.
- 33 K. Matyjaszewski and N. V. Tsarevsky, *Nat. Chem.*, 2009, **1**, 276-288.
- 34 J. Pyun and K. Matyjaszewski, *Chem. Mat.*, 2001, **13**, 3436-3448.
- 35 S. Tugulu, M. Harms, M. Fricke, D. Volkmer and H. A. Klok, *Angew. Chem. -Int. Edit.*, 2006, **45**, 7458-7461.
- 36 T. Fukuda, A. Goto and K. Ohno, *Macromol. Rapid Commun.*, 2000, **21**, 151-165.
- 37 K. Matyjaszewski and J. H. Xia, *Chem. Rev.*, 2001, **101**, 2921-2990.
- 38 B. Zhao and W. J. Brittain, *Prog. Polym. Sci.*, 2000, **25**, 677-710.
- 39 E. M. Benetti, S. Zapotoczny and J. Vancso, *Adv. Mater.*, 2007, **19**, 268-271.
- 40 S. Burkert, E. Bittrich, M. Kuntzsch, M. M uller, K. J. Eichhorn, C. Bellmann, P. Uhlmann and M. Stamm, *Langmuir*, 2010, **26**, 1786-1795.
- 41 G. M. Liu and G. Z. Zhang, *J. Phys. Chem. B*, 2008, **112**, 10137-10141.
- 42 S. Sanjuan, P. Perrin, N. Pantoustier and Y. Tran, *Langmuir*, 2007, **23**, 5769-5778.
- 43 N. D. Treat, N. Ayres, S. G. Boyes and W. J. Brittain, *Macromolecules*, 2006, **39**, 26-29.
- 44 A. J. Parnell, S. J. Martin, R. A. L. Jones, C. Vasilev, C. J. Crook and A. J. Ryan, *Soft Matter*, 2009, **5**, 296-299.
- 45 H. G. Schild, *Prog. Polym. Sci.*, 1992, **17**, 163-249.
- 46 O. Smidsr od and J. E. Guillet, *Macromolecules*, 1969, **2**, 272-277.
- 47 X. F. Sui, S. Zapotoczny, E. M. Benetti, M. Memesa, M. A. Hempenius and G. J. Vancso, *Polym. Chem.*, 2011, **2**, 879-884.
- 48 E. S. Alla Synytska, N. Puretskiy, G. Stoychev, S. Berger, L. Ionov, C. Bellmann, K.-J. Eichhorn and M. Stamm, *Soft Matter*, 2010, **6**, 5907.
- 49 N. Ishida and S. Biggs, *Macromolecules*, 2010, **43**, 7269-7276.
- 50 E. C. Cho, Y. D. Kim and K. Cho, *J. Colloid Interface Sci.*, 2005, **286**, 479-486.
- 51 M. A. Cole, N. H. Voelcker, H. Thissen, R. G. Horn and H. J. Griesser, *Soft Matter*, 2010, **6**, 2657-2667.
- 52 N. Ishida and S. Biggs, *Langmuir*, 2007, **23**, 11083-11088.
- 53 D. M. Jones, J. R. Smith, W. T. S. Huck and C. Alexander, *Adv. Mater.*, 2002, **14**, 1130-1134.
- 54 S. Kidoaki, S. Ohya, Y. Nakayama and T. Matsuda, *Langmuir*, 2001, **17**, 2402-2407.
- 55 G. M. Liu and G. Z. Zhang, *Langmuir*, 2005, **21**, 2086-2090.
- 56 I. B. Malham and L. Bureau, *Langmuir*, 2010, **26**, 4762-4768.
- 57 S. Mendez, B. P. Andrzejewski, H. E. Canavan, D. J. Keller, J. D. McCoy, G. P. Lopez and J. G. Curro, *Langmuir*, 2009, **25**, 10624-10632.
- 58 K. N. Plunkett, X. Zhu, J. S. Moore and D. E. Leckband, *Langmuir*, 2006, **22**, 4259-4266.
- 59 H. Yim, M. S. Kent, S. Mendez, G. P. Lopez, S. Satija and Y. Seo, *Macromolecules*, 2006, **39**, 3420-3426.
- 60 X. Zhu, C. Yan, F. M. Winnik and D. Leckband, *Langmuir*, 2007, **23**, 162-169.
- 61 M. Kaholek, W. K. Lee, S. J. Ahn, H. W. Ma, K. C. Caster, B. LaMattina and S. Zauscher, *Chem. Mat.*, 2004, **16**, 3688-3696.
- 62 D. W. Jiang, X. Y. Huang, F. Qiu, C. P. Luo and L. L. Huang, *Macromolecules*, 2010, **43**, 71-76.
- 63 T. Wu, K. Efimenko and J. Genzer, *J. Am. Chem. Soc.*, 2002, **124**, 9394-9395.
- 64 C. Xu, S. E. Barnes, T. Wu, D. A. Fischer, D. M. DeLongchamp, J. D. Batteas and K. L. Beers, *Adv. Mater.*, 2006, **18**, 1427-1430.
- 65 T. Wu, P. Gong, I. Szleifer, P. Vlcek, V. Subr and J. Genzer, *Macromolecules*, 2007, **40**, 8756-8764.

- 66 C. Xu, T. Wu, C. M. Drain, J. D. Batteas and K. L. Beers, *Macromolecules*, 2005, **38**, 6-8.
- 67 X. J. Wang, H. L. Tu, P. V. Braun and P. W. Bohn, *Langmuir*, 2006, **22**, 817-823.
- 68 P. Uhlmann, L. Ionov, N. Houbenov, M. Nitschke, K. Grundke, M. Motornov, S. Minko and M. Stamm, *Prog. Org. Coat.*, 2006, **55**, 168-174.
- 69 B. Zhao, *Langmuir*, 2004, **20**, 11748-11755.
- 70 D. Usov, V. Gruzdev, M. Nitschke, M. Stamm, O. Hoy, I. Luzinov, I. Tokarev and S. Minko, *Macromolecules*, 2007, **40**, 8774-8783.
- 71 A. M. Jonas, Z. J. Hu, K. Glinel and W. T. S. Huck, *Nano Lett.*, 2008, **8**, 3819-3824.
- 72 H. Tu, C. E. Heitzman and P. V. Braun, *Langmuir*, 2004, **20**, 8313-8320.
- 73 T. Chen, J. M. Zhong, D. P. Chang, A. Carcia and S. Zauscher, *Adv. Mater.*, 2009, **21**, 1825-1829.
- 74 M. Mathieu, A. Friebe, S. Franzka, M. Ulbricht and N. Hartmann, *Langmuir*, 2009, **25**, 12393-12398.
- 75 R. Dong, S. Krishnan, B. A. Baird, M. Lindau and C. K. Ober, *Biomacromolecules*, 2007, **8**, 3082-3092.
- 76 C. Slim, Y. Tran, M. M. Chehimi, N. Garraud, J. P. Roger, C. Combellas and F. Kanoufi, *Chem. Mat.*, 2008, **20**, 6677-6685.
- 77 S. Schilp, N. Ballav and M. Zharnikov, *Angew. Chem. -Int. Edit.*, 2008, **47**, 6786-6789.
- 78 U. Schmelmer, A. Paul, A. Kuller, M. Steenackers, A. Ulman, M. Grunze, A. Golzhäuser and R. Jordan, *Small*, 2007, **3**, 459-465.
- 79 C. Schuh, S. Santer, O. Prucker and J. Rühle, *Adv. Mater.*, 2009, **21**, 4706-4710.
- 80 R. Ducker, A. Garcia, J. M. Zhang, T. Chen and S. Zauscher, *Soft Matter*, 2008, **4**, 1774-1786.
- 81 B. Zdyrko, O. Hoy, M. K. Kinnan, G. Chumanov and I. Luzinov, *Soft Matter*, 2008, **4**, 2213-2219.
- 82 M. Patra and P. Linse, *Nano Lett.*, 2006, **6**, 133-137.
- 83 M. Kaholek, W. K. Lee, B. LaMattina, K. C. Caster and S. Zauscher, *Nano Lett.*, 2004, **4**, 373-376.
- 84 M. Hirtz, M. K. Brinks, S. Miele, A. Studer, H. Fuchs and L. F. Chi, *Small*, 2009, **5**, 919-923.
- 85 H. W. Ma, J. H. Hyun, P. Stiller and A. Chilkoti, *Adv. Mater.*, 2004, **16**, 338-341.
- 86 X. G. Liu, S. W. Guo and C. A. Mirkin, *Angew. Chem. -Int. Edit.*, 2003, **42**, 4785-4789.
- 87 S. Zapotoczny, E. M. Benetti and G. J. Vancso, *J. Mater. Chem.*, 2007, **17**, 3293-3296.
- 88 C. R. Becer, C. Haensch, S. Hoepfner and U. S. Schubert, *Small*, 2007, **3**, 220-225.
- 89 W. K. Lee, K. C. Caster, J. Kim and S. Zauscher, *Small*, 2006, **2**, 848-853.
- 90 E. M. Benetti, H. J. Chung and G. J. Vancso, *Macromol. Rapid Commun.*, 2009, **30**, 411-417.
- 91 C. A. Mirkin, *ACS Nano*, 2007, **1**, 79-83.
- 92 S. Y. Chou, P. R. Krauss and P. J. Renstrom, *Science*, 1996, **272**, 85-87.
- 93 E. M. Benetti, C. Acikgoz, X. F. Sui, B. Vratzov, M. A. Hempenius, J. Huskens and G. J. Vancso, *Adv. Funct. Mater.*, 2011, **21**, 2088-2095.
- 94 Y. Osada, J. P. Gong and Y. Tanaka, *J. Macromol. Sci., Rev. Macromol. Chem. Phys.*, 2004, **44**, 87-112.
- 95 S. Nayak and L. A. Lyon, *Angew. Chem. -Int. Edit.*, 2005, **44**, 7686-7708.
- 96 D. Kuckling, *Colloid Polym. Sci.*, 2009, **287**, 881-891.
- 97 A. M. Kloxin, C. J. Kloxin, C. N. Bowman and K. S. Anseth, *Adv. Mater.*, 2010, **22**, 3484-3494.
- 98 L. Dong and H. Jiang, *Soft Matter*, 2007, **3**, 1223-1230.
- 99 P. Calvert, *Adv. Mater.*, 2009, **21**, 743-756.

Chapter 2

- 100 Y. Q. Tang, C. L. Heaysman, S. Willis and A. L. Lewis, *Expert Opin. Drug Deliv.*, 2011, **8**, 1141-1159.
- 101 T. R. Hoare and D. S. Kohane, *Polymer*, 2008, **49**, 1993-2007.
- 102 C. E. Hoyle and C. N. Bowman, *Angew. Chem. -Int. Edit.*, 2010, **49**, 1540-1573.
- 103 A. Dondoni, *Angew. Chem. -Int. Edit.*, 2008, **47**, 8995-8997.
- 104 K. L. Killops, L. M. Campos and C. J. Hawker, *J. Am. Chem. Soc.*, 2008, **130**, 5062-5064.
- 105 M. A. Hempenius, C. Cirmi, J. Song and G. J. Vancso, *Macromolecules*, 2009, **42**, 2324-2326.
- 106 B. V. Slaughter, S. S. Khurshid, O. Z. Fisher, A. Khademhosseini and N. A. Peppas, *Adv. Mater.*, 2009, **21**, 3307-3329.
- 107 J. K. H. Hui, Z. Yu and M. J. MacLachlan, *Angew. Chem. -Int. Edit.*, 2007, **46**, 7980-7983.
- 108 M. A. Hempenius, C. Cirmi, F. Lo Savio, J. Song and G. J. Vancso, *Macromol. Rapid Commun.*, 2010, **31**, 772-783.
- 109 J. Kopeček and J. Y. Yang, *Polym. Int.*, 2007, **56**, 1078-1098.
- 110 J. M. G. Swann and A. J. Ryan, *Polym. Int.*, 2009, **58**, 285-289.
- 111 K. Deligkaris, T. S. Tadele, W. Olthuis and A. van den Berg, *Sens. Actuator B-Chem.*, 2010, **147**, 765-774.
- 112 I. Tokarev and S. Minko, *Soft Matter*, 2009, **5**, 511-524.
- 113 J. F. Mano, *Adv. Eng. Mater.*, 2008, **10**, 515-527.
- 114 J. Kopecek, *J. Polym. Sci. Pol. Chem.*, 2009, **47**, 5929-5946.
- 115 K. Peng, I. Tomatsu and A. Kros, *Chem. Commun.*, 2010, **46**, 4094-4096.
- 116 S. Chaterji, I. K. Kwon and K. Park, *Prog. Polym. Sci.*, 2007, **32**, 1083-1122.
- 117 P. Li, Y. F. Poon, W. Li, H. Y. Zhu, S. H. Yeap, Y. Cao, X. Qi, C. Zhou, M. Lamrani, R. W. Beuerman, E. T. Kang, Y. Mu, C. M. Li, M. W. Chang, S. S. Leong and M. B. Chan-Park, *Nat. Mater.*, 2011, **10**, 149-156.
- 118 N. S. Satarkar, D. Biswal and J. Z. Hilt, *Soft Matter*, 2010, **6**, 2364-2371.
- 119 T. Potta, C. Chun and S. C. Song, *Biomacromolecules*, 2010, **11**, 1741-1753.
- 120 C. W. Zhao, X. L. Zhuang, P. He, C. S. Xiao, C. L. He, J. R. Sun, X. S. Chen and X. B. Jing, *Polymer*, 2009, **50**, 4308-4316.
- 121 R. Yoshida, T. Takahashi, T. Yamaguchi and H. Ichijo, *J. Am. Chem. Soc.*, 1996, **118**, 5134-5135.
- 122 S. Maeda, Y. Hara, T. Sakai, R. Yoshida and S. Hashimoto, *Adv. Mater.*, 2007, **19**, 3480-3484.
- 123 A. N. Zaikin and A. M. Zhabotinsky, *Nature*, 1970, **225**, 535-537.
- 124 R. Yoshida, T. Sakai, S. Ito and T. Yamaguchi, *J. Am. Chem. Soc.*, 2002, **124**, 8095-8098.
- 125 R. Yoshida, K. Takei and T. Yamaguchi, *Macromolecules*, 2003, **36**, 1759-1761.
- 126 G. R. Whittell, M. D. Hager, U. S. Schubert and I. Manners, *Nat. Mater.*, 2011, **10**, 176-188.
- 127 V. Bellas and M. Rehahn, *Angew. Chem. -Int. Edit.*, 2007, **46**, 5082-5104.
- 128 Y. J. Ma, W. F. Dong, M. A. Hempenius, H. Möhwald and G. J. Vancso, *Nat. Mater.*, 2006, **5**, 724-729.
- 129 D. A. Foucher, B. Z. Tang and I. Manners, *J. Am. Chem. Soc.*, 1992, **114**, 6246-6248.
- 130 Y. Z. Ni, R. Rulken and I. Manners, *J. Am. Chem. Soc.*, 1996, **118**, 4102-4114.
- 131 M. A. Hempenius, F. F. Brito and G. J. Vancso, *Macromolecules*, 2003, **36**, 6683-6688.
- 132 R. Rulken, A. J. Lough, I. Manners, S. R. Lovelace, C. Grant and W. E. Geiger, *J. Am. Chem. Soc.*, 1996, **118**, 12683-12695.
- 133 J. S. Kim, N. Singh and L. A. Lyon, *Angew. Chem. -Int. Edit.*, 2006, **45**, 1446-1449.
- 134 G. Wulff, B. O. Chong and U. Kolb, *Angew. Chem. -Int. Edit.*, 2006, **45**, 2955-2958.
- 135 A. C. Arsenault, D. P. Puzzo, I. Manners and G. A. Ozin, *Nat. Photonics*, 2007, **1**, 468-472.

- 136 F. Arai, C. Ng, H. Maruyama, A. Ichikawa, H. El-Shimy and T. Fukuda, *Lab Chip*, 2005, **5**, 1399-1403.
- 137 T. Miyata, M. Jige, T. Nakaminami and T. Uragami, *Proc. Natl. Acad. Sci. U. S. A.*, 2006, **103**, 1190-1193.
- 138 B. R. Saunders, N. Laajam, E. Daly, S. Teow, X. H. Hu and R. Stepto, *Adv. Colloid Interface Sci.*, 2009, **147-48**, 251-262.
- 139 A. V. Kabanov and S. V. Vinogradov, *Angew. Chem. -Int. Edit.*, 2009, **48**, 5418-5429.
- 140 L. Y. Chu, J. W. Kim, R. K. Shah and D. A. Weitz, *Adv. Funct. Mater.*, 2007, **17**, 3499-3504.
- 141 K. Albrecht, M. Moeller and J. Groll, *Adv. Polym. Sci.*, 2010, **234**, 65-93.
- 142 A. Pich and W. Richtering, *Adv. Polym. Sci.*, 2010, **234**, 1-37.
- 143 K. Landfester and A. Musyanovych, *Adv. Polym. Sci.*, 2010, **234**, 39-63.
- 144 F. Krahl and K. F. Arndt, *Adv. Polym. Sci.*, 2010, **234**, 95-128.
- 145 N. Sanson and J. Rieger, *Polym. Chem.*, 2010, **1**, 965-977.
- 146 G. R. Hendrickson, M. H. Smith, A. B. South and L. A. Lyon, *Adv. Funct. Mater.*, 2010, **20**, 1697-1712.
- 147 J. P. Rolland, B. W. Maynor, L. E. Euliss, A. E. Exner, G. M. Denison and J. M. DeSimone, *J. Am. Chem. Soc.*, 2005, **127**, 10096-10100.
- 148 M. D. Tang, A. P. Golden and J. Tien, *J. Am. Chem. Soc.*, 2003, **125**, 12988-12989.
- 149 H. Tekin, T. Tsinman, J. G. Sanchez, B. J. Jones, G. Camci-Unal, J. W. Nichol, R. Langer and A. Khademhosseini, *J. Am. Chem. Soc.*, 2011, **133**, 12944-12947.
- 150 E. J. Foster, E. B. Berda and E. W. Meijer, *J. Am. Chem. Soc.*, 2009, **131**, 6964-6966.
- 151 A. E. Cherian, F. C. Sun, S. S. Sheiko and G. W. Coates, *J. Am. Chem. Soc.*, 2007, **129**, 11350-11351.
- 152 M. E. Mackay, T. T. Dao, A. Tuteja, D. L. Ho, B. Van Horn, H. C. Kim and C. J. Hawker, *Nat. Mater.*, 2003, **2**, 762-766.
- 153 J. S. Song, F. Tronc and M. A. Winnik, *J. Am. Chem. Soc.*, 2004, **126**, 6562-6563.
- 154 O. Tagit, N. Tomczak and G. J. Vancso, *Small*, 2008, **4**, 119-126.
- 155 M. Antonietti and K. Landfester, *Prog. Polym. Sci.*, 2002, **27**, 689-757.
- 156 K. Landfester, *Macromol. Rapid Commun.*, 2001, **22**, 896-936.
- 157 O. Braun, J. Selb and F. Candau, *Polymer*, 2001, **42**, 8499-8510.
- 158 E. Tumarkin and E. Kumacheva, *Chem. Soc. Rev.*, 2009, **38**, 2161-2168.
- 159 K. Matyjaszewski, Y. Gnanou and L. Leibler, *Macromolecular Engineering: precise synthesis, materials properties, applications*, 2007, **2**, 1007-1056.
- 160 K. Kulbaba, A. Cheng, A. Bartole, S. Greenberg, R. Resendes, N. Coombs, A. Safa-Sefat, J. E. Greedan, H. D. H. Stöver, G. A. Ozin and I. Manners, *J. Am. Chem. Soc.*, 2002, **124**, 12522-12534.
- 161 K. Kulbaba, R. Resendes, A. Cheng, A. Bartole, A. Safa-Sefat, N. Coombs, H. D. H. Stover, J. E. Greedan, G. A. Ozin and I. Manners, *Adv. Mater.*, 2001, **13**, 732-736.
- 162 H. Zhang, E. Tumarkin, R. M. A. Sullan, G. C. Walker and E. Kumacheva, *Macromol. Rapid Commun.*, 2007, **28**, 527-538.
- 163 M. Seo, Z. H. Nie, S. Q. Xu, M. Mok, P. C. Lewis, R. Graham and E. Kumacheva, *Langmuir*, 2005, **21**, 11614-11622.
- 164 S. Xu, Z. Nie, M. Seo, P. Lewis, E. Kumacheva, H. A. Stone, P. Garstecki, D. B. Weibel, I. Gitlin and G. M. Whitesides, *Angew. Chem. -Int. Edit.*, 2005, **44**, 3799-3799.
- 165 D. N. Breslauer, S. J. Muller and L. P. Lee, *Biomacromolecules*, 2010, **11**, 643-647.

Chapter 2

- 166 Z. H. Nie, W. Li, M. Seo, S. Q. Xu and E. Kumacheva, *J. Am. Chem. Soc.*, 2006, **128**, 9408-9412.
- 167 W. Li, H. H. Pham, Z. Nie, B. MacDonald, A. Guenther and E. Kumacheva, *J. Am. Chem. Soc.*, 2008, **130**, 9935-9941.
- 168 W. Li, J. Greener, D. Voicu and E. Kumacheva, *Lab Chip*, 2009, **9**, 2715-2721.
- 169 T. Kanai, D. Lee, H. C. Shum and D. A. Weitz, *Small*, 2010, **6**, 807-810.
- 170 R. K. Shah, J. W. Kim, J. J. Agresti, D. A. Weitz and L. Y. Chu, *Soft Matter*, 2008, **4**, 2303-2309.
- 171 J. W. Kim, A. S. Utada, A. Fernandez-Nieves, Z. B. Hu and D. A. Weitz, *Angew. Chem. -Int. Edit.*, 2007, **46**, 1819-1822.

Chapter 3

Engineering of Surface Grafted Poly(*N*-isopropylacrylamide)

Layers Across the Length Scales: Swelling, Collapse and Cell

Culture Applications

In this chapter, poly(*N*-isopropylacrylamide) PNIPAM layers with three different grafting densities and similar chain lengths were synthesized *via* surface-initiated atom transfer radical polymerization (SI-ATRP) with monochlorosilane-based (MB) or trimethoxysilane-based (TB) ATRP initiators. We investigated changes of the chain conformation during the temperature-induced collapse transition of MB PNIPAM grafts with *in-situ* ellipsometry. The density and thickness variation accompanying the collapse transition across the lower critical solution temperature (LCST) was characterized. By changing the solvent from water to a water/methanol (50% v/v, co-nonsolvent) mixture, the polymer grafts switched from a swollen to a collapsed state at room temperature. This process was recorded by AFM force measurements. A silica colloidal probe attached to the tip was employed to obtain the Young's moduli of the polymer grafts in different solvation states. The collapse dynamics of the grafts was followed by monitoring the pull-off force (adherence) *in-situ*, as well. AFM based friction force microscopy, utilized to investigate the stimulus-induced tribological behavior, showed that the friction coefficient of PNIPAM grafts in water and in the co-nonsolvent differed. For cell culture studies, it was shown that the TB PNIPAM grafts were much more stable than the MB ones under cell-culture medium conditions. The TB polymer grafts were then evaluated as supporting substrates for MC-3T3 cell cultures. At 37 °C ($T > \text{LCST}$), the seeded cells adhered, spread, and proliferated, whereas at 25 °C ($T < \text{LCST}$), the cells detached from the surface.

* Parts of this chapter have been published in: Sui, X.; Di Luca, A.; Klein Gunnewiek, M.; Kooij, E. S.; van Blitterswijk, C. A.; Moroni, L.; Hempenius, M. A. and Vancso, G. J. *Aust. J. Chem.*, **2011**, 64, 1261-1268; Sui, X.; Chen, Q. (co-first author); Hempenius, M. A. and Vancso, G. J. *Small*, **2011**, 7, 1440-1447.

3.1 Introduction

Stimuli-responsive polymer grafts made of surface tethered macromolecules have been widely applied to prepare sensors, to regulate cell culture, to control wetting and adhesion, and in many other areas.¹⁻⁷ Small changes in the external environment (e.g., temperature, pH, or ionic strength) can generally trigger a sharp and large response in the structure and properties of these grafted polymer layers. Various polymer grafts have been synthesized *via* the surface-initiated atom-transfer radical polymerization (SI-ATRP) approach from different substrates using surface-attached initiators. This method allows one to accurately control the structure and properties of the polymer grafts.¹

Poly(*N*-isopropylacrylamide) (PNIPAM) has been widely studied due to the presence of a lower critical solution temperature (LCST).⁸⁻¹⁰ PNIPAM chains show strong hydration behavior below the LCST, while above the LCST they adopt a dehydrated and compact form. By utilizing the hydration/dehydration effect, PNIPAM grafts are expected to have applications in, for example, permeation-controlled filters, tissue engineering, and actuators.¹¹⁻¹⁴

In this chapter, PNIPAM grafts with variable grafting densities were synthesized by two approaches including: (i) monochlorosilane-based (MB), and (ii) trimethoxysilane-based (TB) ATRP methods (Figure 3.1). The responsive behaviors of these grafts under different temperature and solvent conditions were thoroughly studied by *in-situ* spectroscopic ellipsometry and AFM, further applications on cell cultures were also explored.

The influence of temperature on the polymer structure and hydration of PNIPAM grafts is well documented in the literature. Several methods, including atomic force microscopy (AFM),¹⁵⁻²³ surface force measurements,^{24,25} neutron reflectivity,^{26,27} quartz-crystal microbalance,^{16,28-30} optical micromanipulation technique,³¹ ellipsometry,³²⁻³⁶ and surface plasmon resonance^{37,38} have been used to monitor the reversibly changed properties for PNIPAM films in solution with different densities and molar masses. Theoretical work has indicated that the collapse of the surface-grafted polymer grafts are accompanied by a continuous solubility transition.³⁹ However, owing to the relatively small amount of polymer chains tethered to the substrate surface, the elucidation of a detailed mechanism for the collapse transition of PNIPAM grafts remains an experimental challenge.

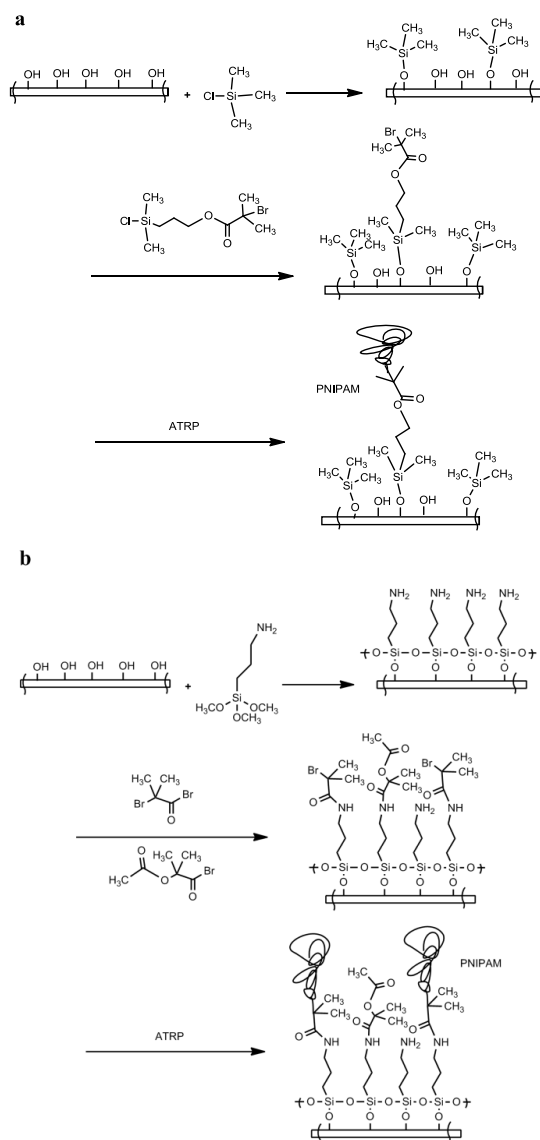


Figure 3.1 Schematic representation of grafting PNIPAM on silicon or glass substrates: (a) monochlorosilane-based (MB) grafts, and (b) trimethoxysilane-based (TB) grafts.

Balamurgan et al.³⁷ used the surface plasmon resonance technique to characterize PNIPAM grafts and observed a gradual change of the polymer grafts thickness with temperature. In contrast, their contact angle measurements exhibited an abrupt change around 32 °C. A bilayer profile was proposed, where the outermost region of the grafts remains highly solvated until the LCST, while the densely packed, less solvated segments within the grafts undergo dehydration

over a much broader temperature range. In a recent study, the collapse transition of temperature responsive poly(di(ethyleneglycol) methyl ether methacrylate) (PMEO₂MA) grafts was monitored using a combination of quartz crystal microbalance and contact angle measurements.⁴⁰ Essentially, the same results were obtained: the *bulk* collapsed over a broad temperature range and the end of the transition was signaled by a sharp first order transition of the *outer surface*.

Here, we used *in-situ* spectroscopic ellipsometry⁴¹ to study the thermally induced collapse of MB PNIPAM entities as a function of phase state across the LCST in real time. Ellipsometry comprises a powerful, non-invasive surface/interface probe enabling characterization of thin films by optical means of a number of (structural) material properties on solid surfaces. It has been widely used for studies of polymer grafts under different conditions.^{35,42-44} However, in the vast majority of studies single wavelength ellipsometry is used,^{33,34} rendering it difficult to unambiguously analyze the data in terms of a detailed model incorporating (optical) density profiles. Recently, Edmondson et al.⁴² performed *in-situ* spectroscopic ellipsometric measurements (from 300 to 700 nm) to study the co-nonsolvency effect of poly(2-(methacryloyloxy) ethyl phosphorylcholine) (PMPC) grafts. The results showed that the judicious selection of the model was essential for extracting meaningful information. It was found that the best data fits were obtained using an exponential decay of polymer density away from the surface. Our ellipsometry measurements were analyzed in terms of a model involving a bi-layer graded density profile, which adequately fits the data, therewith enabling a quantitative discussion of the reversible thickness change with varying temperature. As such, our experiments complement frequently used, but considerably more complex neutron reflectivity measurements.⁴⁵⁻⁴⁷

PNIPAM is also known to exhibit co-nonsolvency behavior, that is, solvation responsiveness to the variation in the composition of mixed solvents consisting of water and certain water-miscible organic solvents such as alcohols.^{48,49} At a temperature below its LCST, PNIPAM can be dissolved in pure water as well as in these organic solvents, but it will precipitate in some solvent mixtures at certain volume ratios. This so-called co-nonsolvency effect is of substantial technological relevance in applications such as actuators and microfluidics. However, the co-nonsolvency effect for well-defined PNIPAM polymer grafts has received very limited attention.^{23,29}

AFM and nanoindentation⁵⁰ allow one to measure the local hardness and the elastic properties of polymer films with thicknesses in the range from a few tens to hundreds of nanometers. AFM has also been used with success to image the surface morphology of polymer grafts, measure their height, and determine their surface adhesion as well as modulus.⁵¹ For instance, the pull-off force of an AFM silicon

nitride tip from a PNIPAM surface was recorded when the grafts were swollen (below LCST) or collapsed (above LCST) and a difference in the adhesion was observed.¹⁷ In another example,^{51,52} topography and microtribological properties of Y-shaped binary polymer grafts made of polystyrene and polyacrylic acid were studied by AFM. It was found that these polymer grafts exhibited a dramatic variation in topography as well as adhesive, elastic and frictional properties under different solvents.^{52,53} Another important aspect in AFM-related studies is the study of time-dependent processes. Research showed that the dynamic response of polymer grafts to environmental changes could be followed using AFM. In a recent case, Ryan et al. directly visualized the swelling and collapse of poly(methacrylic acid) grafts by monitoring the change in the height of a patterned layer under different pH values.⁵⁴ In the above-mentioned examples, the dynamic responses of polymer grafts were studied primarily by monitoring the change in thickness. Herein, we measured the adherence of MB PNIPAM grafts to an AFM colloidal probe. Adherence is an important parameter for the utilization of stimulus-responsive grafts in various applications, such as wetting and adhesion control.⁵⁵ Adherence was monitored by recording AFM force curves during the collapse of the swollen grafts induced by the addition of co-nonsolvent. To our knowledge, this is the first time that the dynamics of adherence variation associated with molecular rearrangements during a phase transition of responsive polymer grafts was directly monitored using AFM. The values of Young's moduli of PNIPAM grafts under different solvent conditions were estimated based on the Hertz model using AFM force–distance curves.

Measurements by friction force microscopy (FFM) can yield quantitative insights into various polymer grafts properties.⁵⁶⁻⁵⁸ For instance, greatly enhanced lubrication for poly(2-(dimethylamino)ethyl methacrylate) grafts was observed at low pH, which was attributed to the formation of a repulsive, highly charged, hydrated cushion.⁵⁹ In another case,⁶⁰ the frictional properties of poly(2-(methacryloyloxy) ethyl phosphorylcholine) grafts under co-nonsolvency conditions were studied in detail and substantially increased friction coefficients were observed in ethanol/water (90% v/v) mixtures. Here, the friction properties of MB PNIPAM grafts as a function of phase state were also investigated.

Convenient adjustment of cell adhesion on surfaces is an important topic in the field of biomedical and biomaterials research.⁶¹ Owing to the change of PNIPAM hydrophilicity across the LCST, surfaces featuring this polymer can be switched from a hydrophilic, biologically inert form, to a more hydrophobic form exhibiting cell-adhesive properties.^{62,63} An important issue with respect to possible biomedical applications is the long-term stability of grafts grown from these initiators.⁶⁴ The degradation and possible cleavage of polymer grafts may have detrimental

consequences for the properties.^{65,66} For instance, the stability and non-fouling properties of poly(poly(ethylene glycol) methacrylate) grafts prepared using trimethoxysilane-based anchoring under cell-culture conditions were discussed by Tugulu et al.⁶⁶ It was shown that at high chain densities, these grafts rapidly detached from the modified surface. However, the stability of well-defined PNIPAM polymer grafts with variable grafting densities for cell-culture applications has received little attention. Our results showed that TB PNIPAM grafts were much more stable than the MB grafts in cell-culture media. Cell-culture studies on TB PNIPAM grafts demonstrated that MC-3T3 cells adhered and proliferated on PNIPAM grafts at 37 °C, whereas they detached from the substrates at 25 °C.

3.2 Results and discussion

3.2.1 Synthesis and characterization of PNIPAM grafts

Two approaches, outlined in Figure 3.1, were used to prepare samples exhibiting different grafting densities. MB grafts were fabricated using chlorosilane-terminated initiators, which were deposited into the defect sites of previously prepared inert alkylchlorosilane monolayers on silicon. TB grafts were made by the reaction of a (3-aminopropyl) trimethoxysilane monolayer with mixtures of ATRP-active (2-bromo-2-methylpropionyl bromide) and inert (1-bromocarbonyl-1-methylethyl acetate) chemicals. For each approach, we studied three different grafts with various grafting densities, which we refer to as high-, middle-, and low-density (hereafter HD, MD, and LD) surfaces. The polymerization time was 30 min for each sample. AFM cross-sectional profiles yielded thickness values (for dry thicknesses). (Figure 3.2 displays tapping mode AFM height images of MB grafts, For TB grafts, similar thickness were found, Table 3.1, *Thickness before*) The formation of PNIPAM grafts was also confirmed by FTIR, ellipsometry and contact angle measurements. These values by ellipsometry are in good agreement with the AFM data. Static contact angle measurements using MilliQ water showed values of $56 \pm 2^\circ$ for all samples regardless of the height, which is typical for PNIPAM films.⁶⁷ This indicates that the wetting is mainly sensitive to the chemical composition of the outermost region of the layers.²⁴

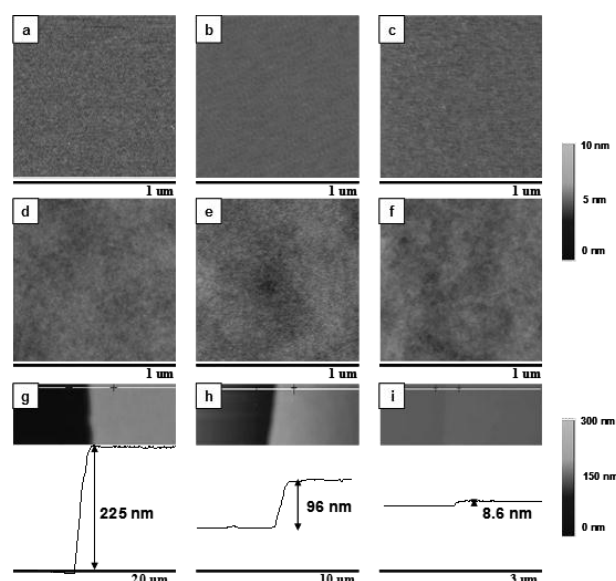


Figure 3.2 Tapping mode AFM height images of MB samples in air of the a) 3-(chlorodimethylsilyl)propyl 2-bromo-2-methylpropionate (CDB) deposited (HD) surface, b) chlorotrimethylsilane (CTS)/CDB deposited (MD) surface, c) CTS/CDB deposited (LD) surface, and subsequently MB PNIPAM grafts on the d) HD, e) MD, and f) LD surfaces, as well as height images and cross sections of scratches to measure the PNIPAM film thickness grafted from the g) HD, h) MD, and i) LD surfaces.

PNIPAM grafts	Thickness (dry, before) [nm]	Thickness (dry, after) [nm]	PNIPAM grafts	Thickness (dry, before) [nm]	Thickness (dry, after) [nm]
MB-LD	9	4	TB-LD	9	7
MB-MD	96	5	TB-MD	100	90
MB-HD	225	5	TB-HD	220	185

Table 3.1 Thickness (by AFM) of the PNIPAM polymer grafts before and after cell culture MB, monochlorosilane-based, TB, trimethoxysilane-based, HD, high-density, MD, middle density, LD, low-density.

It should be noted that when ATRP is carried out in protic solvents such as water, side reactions affecting the transition metal catalyst may occur. When copper is used, the Cu^{I} complex may undergo disproportionation to Cu^0 and Cu^{II} . In addition, the Cu^{II} halide complex may dissociate, followed by coordination of water to Cu^{II} , which effectively lowers the concentration of deactivator during aqueous ATRP. ATRP is therefore typically faster and less controlled in aqueous media,⁶⁸ i.e. polydispersity may increase. Here, M_n 219 600 g/mol; M_w 519 300 g/mol were obtained for free polymers. Nevertheless, previous studies^{23,24} have shown that PNIPAM grafts can be

synthesized successfully by surface initiated ATRP in aqueous solvents. Here we employed the conditions published in the reference by Zauscher et al.²³ to fabricate our grafts. By varying the surface-immobilized initiator density, grafts with varying height were reliably obtained. AFM analysis showed that the grafts formed possessed smooth surfaces over $10 \times 10 \mu\text{m}^2$ areas. Therefore, even though ATRP in aqueous media may be less controlled than in organic media, we showed that we were able to form PNIPAM grafts with predictable and uniform dimensions.

3.2.2 *In-situ* ellipsometric studies on MB PNIPAM grafts

In reflection ellipsometry, the change in the polarization state of linearly polarized light is measured upon reflection at an interface. The complex reflection coefficient ρ is defined as:

$$\rho = \frac{r_p}{r_s} = \tan \Psi \exp(i\Delta) \quad (3.1)$$

where r_p and r_s are the complex reflection coefficients for the parallel and perpendicular polarizations, respectively, the amplitude ratio is expressed by $\tan \Psi$, while Δ represents the phase difference.⁶⁹ Measurements here were performed as a function of photon energy in the range 1.5-4.5 eV with a step size of 0.1 eV; this corresponds to a wavelength range of 275-827 nm.

Typical ellipsometry spectra at different temperatures are shown in Figure 3.3 for a MB-MD sample. Three spectra are shown corresponding to temperatures (i) well below, (ii) near and (iii) well above the LCST. The variation of the spectra with temperature is obvious from Figure 3.3, showing the optical signature of the temperature-induced transition. For the swollen grafts at relatively low temperatures (squares), features of the silicon substrate can be identified in the spectra, such as for example the peak in Ψ near 3.4 eV and the decreases of Δ near 3.3 eV and 4.3 eV. Owing to the large swelling in water, which is accompanied by a considerably reduced (optical) density of the polymer as compared to that of its collapsed wet or dry conformation, the contribution of the swollen polymer film to the optical spectra becomes hard to distinguish from the solvent. The refractive index of the swollen, diluted polymer is described by an effective medium approximation incorporating the refractive indices of water and the PNIPAM chains. Assuming a low PNIPAM density in the relatively thick diluted layer, its effective refractive index is only slightly larger than that of water, and approximately a linear function of the polymer density. Heating of the system across the LCST gives rise to marked changes in the spectra. A shoulder develops at Ψ values below 3.0 eV, while Δ decreases with temperature below 2.5 eV and

increases markedly at higher photon energies. From these results it is obvious that measurements at a single wavelength, as is often the case with *in-situ* ellipsometry, make it essentially impossible to unambiguously analyse the data. The fact that the temperature response of the system in terms of optical properties depends strongly on photon energy (and thus also wavelength) is clearly shown.

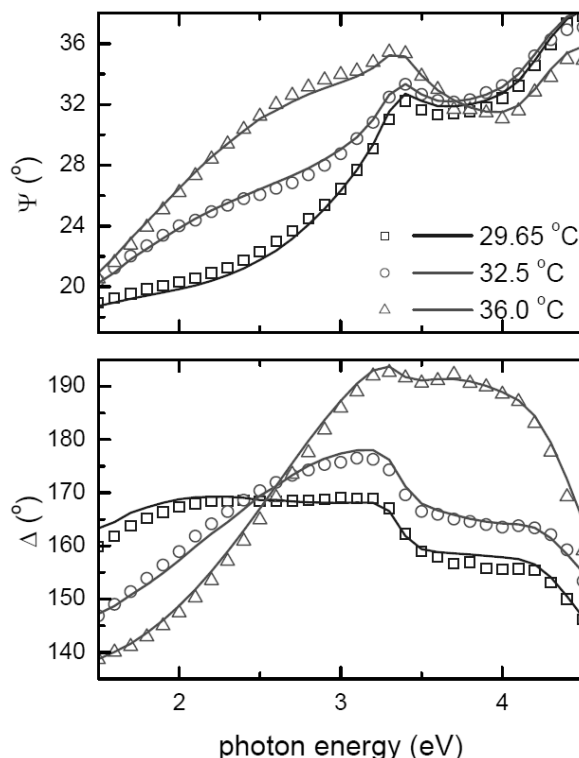


Figure 3.3 Ellipsometry spectra Ψ and Δ measured *in-situ* on a MD PNIPAM grafts at temperatures well below (squares), near (circles) and well above (triangles) the LCST. The data points represent experimental results, while the solid lines are simulated spectra as described in the text.

Typically it takes a few minutes to measure spectra such as shown in Figure 3.3, owing to the relatively slow scan rate of the monochromator and the required integration time at all energy values. To characterize the relatively fast transition of PNIPAM, this may be too slow. As such, we have performed measurements at specific photon energies, keeping the monochromator in a fixed position and continuously monitoring the temperature in our cell. In this way, the time resolution of the experiments is substantially improved.

The experimental results in Figure 3.4 reveal that at temperatures below

approximately 25 °C and above 35 °C, the optical response of the PNIPAM thin films is different, but essentially independent of temperature. The most pronounced changes in the optical response occur near 32-33 °C, in good agreement with many of the reports on PNIPAM available in the literature.^{22,30,31,35-37} However, in the temperature range 25-30 °C already a marked change in the optical properties can be discerned. Also shown in Figure 3.4 are results from the simulated spectra based on the analysis as presented in the next section at fixed temperatures. The pronounced similarity between the measured and simulated data (open and filled symbols, respectively) demonstrates that at all temperatures, the system is in equilibrium.

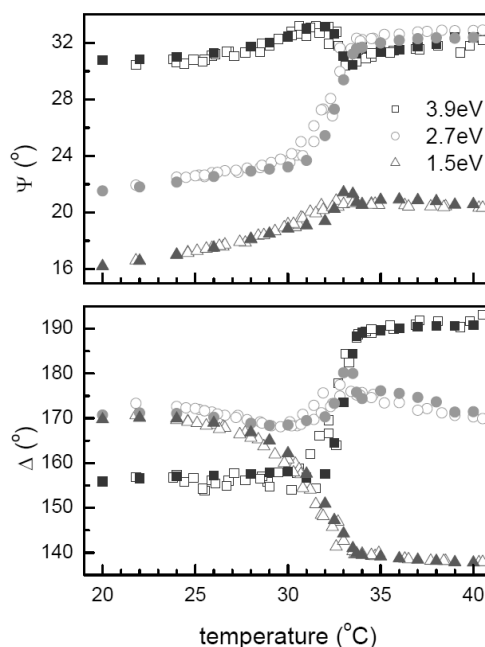


Figure 3.4 Temperature dependence of the ellipsometric quantities Ψ and Δ (top and bottom panels, respectively) at three different photon energies for the MD sample: 3.9 eV (320 nm; squares), 2.7 eV (460 nm; circles) and 1.5 eV (825 nm; triangles). The open and filled symbols represent experimental and simulated data, respectively.

We start the analysis of the ellipsometry spectra by considering the two limiting cases, i.e. at temperatures well below and well above the collapse transition. For the high temperature situation, the optical response of the collapsed films can be modelled using a single layer. The refractive index of this layer is adequately described using a Cauchy model⁶⁹ for the refractive index n :

$$n = A + B/\lambda^2 + C/\lambda^4 \quad (3.2)$$

where we consider the wavelength λ in microns. We neglect absorption, i.e. the

imaginary part of the complex refractive index $k=0$, and consider the films to be transparent. The quantities A, B and C represent fit parameters. In our case we set $C=0$ since it does not yield better fit results.

For the collapsed films, a minor improvement was obtained by included a gradient of A as a function of distance from the substrate. A decrease of A by 2% over the thickness of the film yields a slightly better fit, reflecting a small but discernable segment density gradient within the film. Nevertheless, to simplify the analysis and to keep the number of fit parameters limited, here we neglect this gradient, and consider the Cauchy layer to be homogeneous throughout.

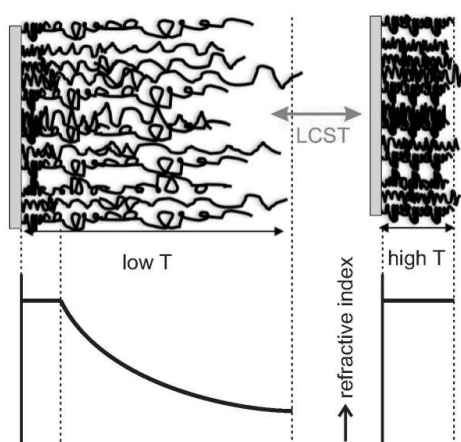


Figure 3.5 Schematic representation of the PNIPAM segment density variation at temperatures below (left) and above (right) the LCST. The corresponding refractive index as a function of distance from the substrate is also schematically shown. At low temperatures, the film is modeled by a double layer, with the outer exhibiting a gradient density profile; at high temperatures, only a single layer with a constant refractive index is considered.

For the swollen grafts at low temperatures, the best fit results are obtained using a two-layer model as schematically outlined in Figure 3.5. At the substrate side of the grafts, i.e. where PNIPAM chains are attached to the substrate, a layer with a constant segment density is considered in the model, with optical properties similar to those of the collapsed film at higher temperatures. On top of this dense layer, a second layer with a marked gradient in the A-parameter (eq. 3.2), representing the decreasing segment density, is included in the model. We assume a large contribution originates from an intrinsic gradient related to a depth distribution of the chain ends, and to the length distribution of the chains. The gradient represents an increasing degree of dilution of the PNIPAM film with larger distance from the substrate. The gradient in the optical density is described by an exponential decrease of the constant A as used in the Cauchy expression (i.e.

$A \sim (d/d_0)^t$, with d the distance within the film, which is normalised to the total thickness d_0 ; the exponent t is also a fit parameter). Using this model, the ellipsometry spectra can be adequately modelled, as shown by the solid lines in Figure 3.5.

An important fit parameter is the thickness of the film, composed of the thicknesses of the dense layer at the substrate side and the graded layer at the solvent side. Note that the effective thickness follows from the fit model used in the analysis of the ellipsometry spectra. In Figure 3.6, the temperature dependence of the thickness for both layers is shown for LD (top panel), MD and HD grafts (bottom panel). The LD film exhibits a relatively smooth transition with temperature, but we note that the accuracy is rather poor due to the inability to unambiguously model both the thickness and the refractive index. The experiment for such low thickness is only sensitive to the product of thickness and refractive index.

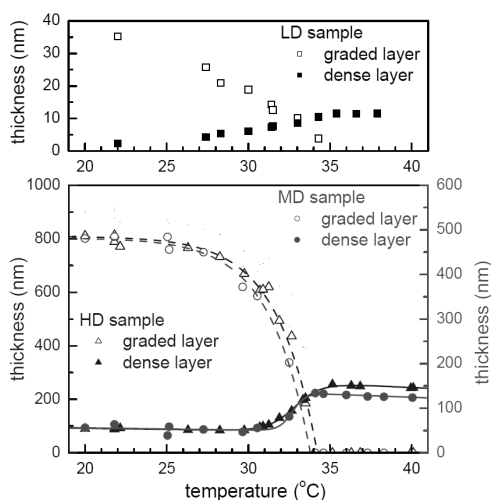


Figure 3.6 Temperature dependence of the PNIPAM thickness as determined from fitting the ellipsometry spectra. In the analysis, the optical response of the PNIPAM films is modeled using a two-layer structure, consisting of a dense, constant segment (optical) density layer (filled symbols) near the substrate, and a more diluted layer on the liquid side (open symbols), exhibiting a decrease of polymer segment density with increasing distance from the substrate. Results are shown for LD (top panel), MD and HD samples (right and left axes of the bottom panel, respectively). Fitted temperature dependencies are represented by solid and dashed lines, corresponding to the dense and diluted layers, respectively.

For the MD and HD samples, the thickness values exhibit very similar behaviour as a function of temperature. Comparing the left and right axes, for the MD and HD samples, the thickness values appear to scale by a factor of

approximately 1.7. At temperatures below 25 °C the thickness for both grafts is constant. With increasing temperature the thickness of the dilute, graded layer decreases until this layer ‘vanishes’ above 33-34 °C. Zooming in on the thickness of the dense layer, a very slight decrease of the thickness is observed for temperatures up to 30 °C. At first this may not seem significant. However, close inspection of the results in Figure 3.4, and more specifically the data for 1.5 eV and 2.7 eV photon energy, reveal a slight variation of the optical response, most likely related to the thickness variation. Upon further heating, an increase of the thickness of the dense layer is observed simultaneously with the collapse of the dilute layer. At temperatures above 35 °C only the dense layer remains, the thickness of which again exhibits a minor decline with temperature.

Using the model described above, we have been able to parameterize all fitting parameters, which in turn can be used to calculate the complete optical response as a function of temperature. This enables us to simulate the temperature response of the Ψ and Δ values. For the MD sample, in Figure 3.4 the simulated values (closed symbols) are compared to the experimental results (open symbols). There is in good agreement between the experimental data and the simulated values, demonstrating the accuracy of our model. At temperatures close to the most pronounced transition, small features in the simulated data can be discerned which are not seen in the experimental data, most likely due to the limited energy-resolution of the monochromator of the ellipsometer.

The parameterization of the optical response of the PNIPAM layer as a function of temperature in terms of graded optical properties enables us to plot the optical density profile throughout the film thickness for different temperatures. Assuming that these correspond in some way (most likely non-linear) to the mass density in the film, a variation of the segment density in the film normal direction across the LCST, and a refined molecular scale picture of the phase transition can be proposed. In Figure 3.7 the density profiles for the HD, MD and LD samples are shown at different temperatures. The profiles demonstrate that upon increasing the temperature across the LCST, the dense layer increases in thickness, while a slight increase of its density is observed. Surprisingly, the refractive index variation for the MD film is markedly larger than that for the HD sample; apparently, collapse of the polymer segments within the constant density layers is more pronounced for HD grafting densities. For the LD sample this increase is absent, since we are not able to fit this parameter for these films; we took a constant value for the refractive index of this layer.

The graded layer exhibits a density gradient, with a decay from the value of the dense layer, to a value almost that of the water. As such, although the optical

modelling yields a well-defined thickness, the exact position of the dividing interface in the actual experiment is difficult to define. From these profiles it directly follows that the collapse occurs by a simultaneous decrease of the thickness of the graded, dilute layer and a growth of the dense layer at the substrate side of the film, in agreement with the thickness variation as shown in Figure 3.6.

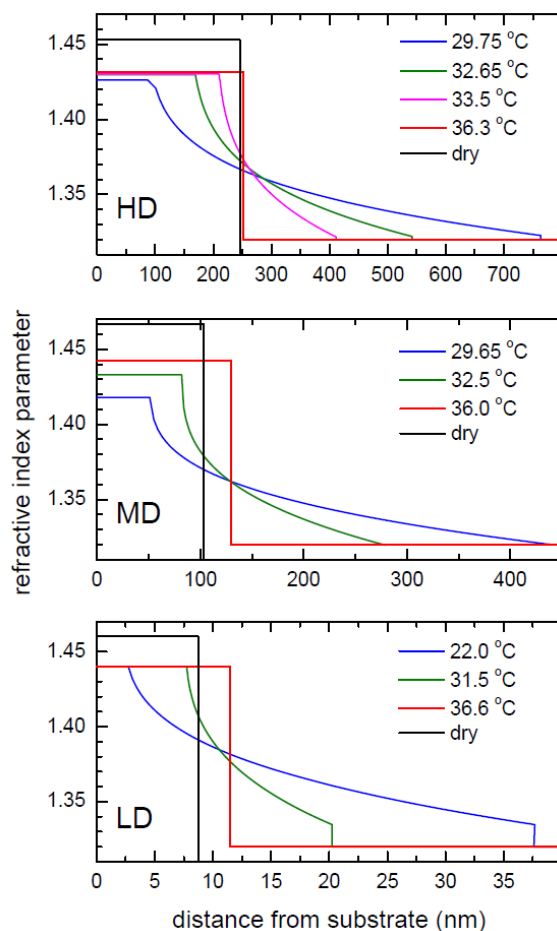


Figure 3.7 Refractive index profiles as a function of distance from the substrate for HD (top), MD (middle) and LD (bottom) PNIPAM samples; note the different distance scales in the panels. The refractive index is represented by the first Cauchy parameter A as described in the text. Results are shown for dry grafts and for samples in contact with water at different temperatures. Specific temperatures for the different samples are indicated in each panel.

Similar behaviour in terms of a dense layer growing at the expense of a more dilute outer layer has been suggested previously both for PNIPAM films^{22,30,37,38,46} as well as thermoresponsive PEG-based brushes.^{47,70} A number of techniques were

employed to assess both the density profiles within the polymer films, as well as the transition. Neutron reflectivity measurements enable a quantitative analysis of density distributions throughout the film, in good agreement with our present ellipsometry experiments. Therewith we have demonstrated the potential of this optical method in probing the polymer films in a truly *in-situ* manner.

The segment density distributions we observe in our experiments are also in line with conclusions based on force-distance curves obtained using an atomic force microscope, while techniques as surface plasmon resonance spectroscopy and quartz crystal microbalance measurements provide additional confirmation of the phase transition. The rapid density variation, and corresponding thickness change as shown in Figure 3.6, are in agreement with contact angle measurements. The latter method is very sensitive primarily to the outer layer of the grafted polymer films, and as such only exhibits a change when the entire film has collapsed (see also Figure 3.7). Finally, the (optical) density of the corresponding dry films are depicted in Figure 3.7 by the solid black line. In all samples with different grafting densities, the refractive index of the dry one is larger than that of the wet one, while the thickness of the dry film is in all cases smaller. This is in agreement with the swelling of the film, even in its collapsed state at elevated temperatures, which leads to a diluted layer with a lower overall density.

The reason for the fact that below the LCST the PNIPAM chains at the substrate side do not swell as much as the outer parts may be a kinetic effect. Alternatively, one can imagine that the driving force for swelling originating from osmotic pressure decays upon moving toward the higher segment density at the substrate film interface, in combination with entropic loss. Over the past decades, different models describing the equilibrium conformation of polymers attached by one end to a substrate and immersed in a solvent have been described. Generally, the grafted polymers are considered to consist of segments, the behaviour of which is determined by the balance of various interactions (segment-segment and segment-solvent) in the solvent. In the pioneering work by Alexander and De Gennes,⁷¹⁻⁷³ the polymer grafts are modelled by a step-like concentration profile, in which the segment density is considered constant throughout the layer. Within the Alexander-De Gennes constant density model, all free ends are estimated to be at the same distance from the surface, therewith imposing severe restrictions on the allowed polymer chain configurations. To circumvent these restrictions, more recently self-consistent field approximations have been used to numerically derive concentration profiles within the polymer thin films.^{74,75} Depending on the specific interactions between the polymer and the solvent, various different gradient profiles have been reported.⁷⁴⁻⁷⁶

3.2.3 AFM force measurements on MB PNIPAM grafts

In the last section, *in-situ* ellipsometry was used to study the temperature induced swelling and collapse of MB grafts in water. Here, to study the impact of co-nonsolvency as well as variation of the grafts height on the mechanical properties of the PNIPAM grafts, force *versus* distance profiles were acquired by AFM to probe the structure and tip-grafts interactions using the colloidal probe approach.⁷⁷ This technique was proved useful for the quantification of surface forces for various soft matter systems.^{55,78,79} The colloidal particle attached to the tip was a silica sphere with a radius of 500 nm. Typical raw data showing the approach section of deflection *vs* piezo-extension curves for the PNIPAM grafts are shown in Figure 3.8. The data were constructed based on 10 individual force curve measurements.

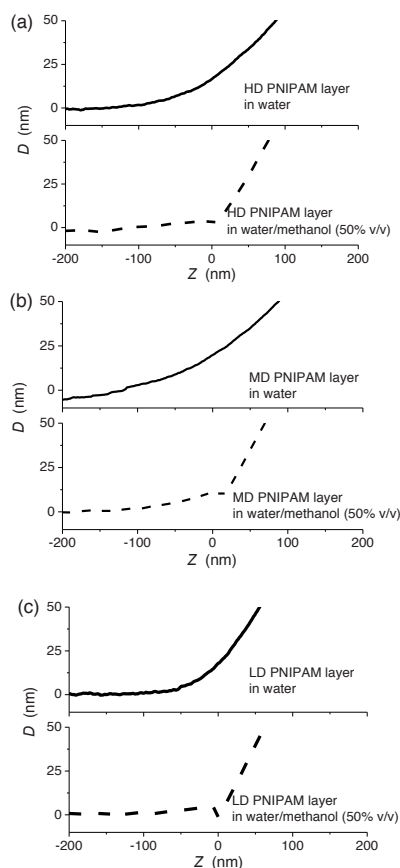


Figure 3.8 AFM cantilever approach deflection *vs* extension curves for PNIPAM grafts with different grafting densities under different solvent conditions as indicated in the legend.

As shown in Figure 3.8, the deflection of the AFM cantilever changed when the PNIPAM grafts were exposed to different solvent conditions. The interaction between the colloidal probe and the surface was repulsive when the polymer was swollen, while it became attractive and jump-to-contact behavior was observed when the solvent environment was changed to a water/methanol (50% v/v) mixture, regardless of differences in height values. Such changes in tip-surface interactions as PNIPAM is brought across the LCST by changing the temperature have been documented in the literature¹⁷ and are also observed here by inducing the transition using a co-nonsolvent. A difference in the slope of the curves after contact is clearly observed when either the grafting density of the PNIPAM layers is changed or when the solvent composition is varied. To elucidate this difference in a quantitative way, the *apparent* Young's modulus of the PNIPAM layer was determined from the recorded curves based on the Hertz model.⁵⁵

From the approach part of the deflection-extension curves the deformation of the PNIPAM grafts can be obtained. Deformation (δ) is calculated from:

$$\delta = |Z - Z_0| - (D - D_0) \quad (3.3)$$

where Z denotes the piezo-extension, Z_0 is the piezo-extension at which tip-surface contact occurs, D and D_0 are the values of deflection of the cantilever and the deflection of cantilever when tip-surface contact occurs, respectively. The load (F) applied onto the polymer grafts is then calculated from:

$$F = k(D - D_0) \quad (3.4)$$

where k represents the spring constant of the AFM cantilever, which is calibrated using the thermal tune function of the instrument software. The Hertz equation (3.5) was used to determine the values of the *apparent* Young's modulus:

$$F = \frac{4\sqrt{r_{tip}}}{3(1-\nu^2)} E \cdot \delta^{3/2} \quad (3.5)$$

where r_{tip} is the radius of the silica colloidal probe, ν is the Poisson ratio and E is the *apparent* Young's modulus of the polymer grafts (assuming an infinitely higher modulus of the probe as compared to the polymer grafts). Typical Hertz plots, in which F was displayed as a function of $\delta^{3/2}$, are shown in Figure 3.9 a-c for PNIPAM grafts with different heights under different solvent conditions. The charts were constructed based on 10 individual measurements.⁸⁰

As can be seen in the figures, PNIPAM grafts are more deformable in water (filled symbols), i.e. deformation is higher at a certain load, than for grafts in a water/methanol (50% v/v) mixture (open symbols), regardless of the film thickness.

This is explained by the fact that under mixed solvent conditions, the polymer chains collapse onto the surface while in water the polymer chains are expanded.

A notable difference in the deformation under the same load was also observed for PNIPAM grafts with different heights under the same solvent conditions. For the LD and MD grafts, the grafts were flattened laterally more than the HD sample. The situation is schematically shown in Figure 3.9d.

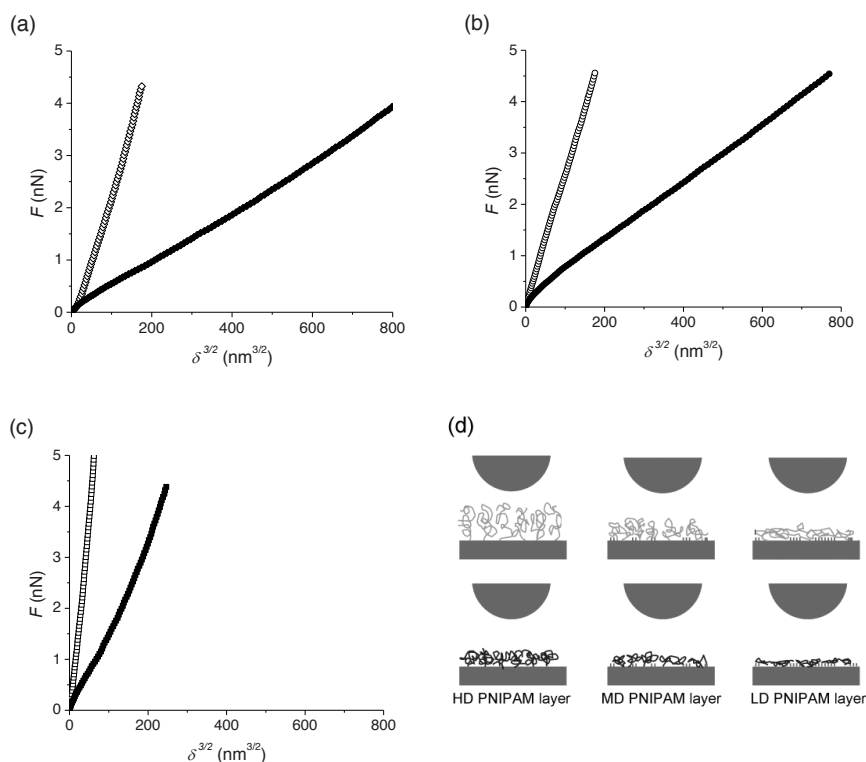


Figure 3.9 Hertz plots of PNIPAM (a) HD, (b) MD and (c) LD grafts under water (filled symbols) and water/methanol (50% v/v) (open symbols). (d) Schematic representation of the contact between the colloidal AFM probe and the PNIPAM layers with different grafting densities under different solvent conditions.

To accurately predict the elastic behavior of the PNIPAM grafts, the initial 20% of the δ value were used to evaluate the *apparent* Young's modulus. We assumed a Poisson ratio of 0.5 and the radius of the colloidal probe (500 nm) was determined by scanning the probe with a tip calibration array. The value of the *apparent* Young's modulus of the PNIPAM grafts^{81,82} was then calculated. Histograms ($N = 50$) of the distributions of the Young's modulus values with different grafting densities under different solvent conditions are shown in Figure 3.10.

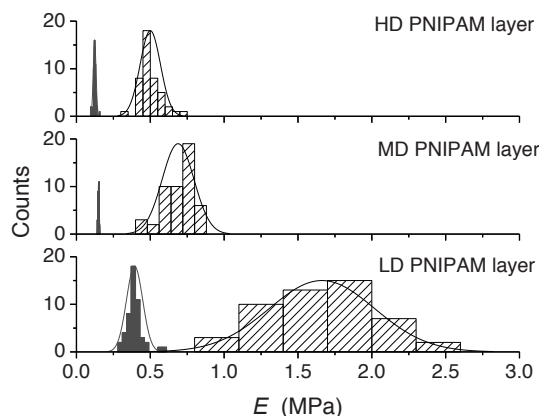


Figure 3.10 Statistical histograms of the Young's modulus of PNIPAM grafts in water (filled) and in water/methanol (50% v/v) (patterned).

The arithmetic mean value of the *apparent* Young's modulus of the HD sample in water is 123 ± 9 kPa, while the values of the *apparent* Young's modulus of the MD and LD samples in water are 150 ± 4 kPa and 394 ± 55 kPa, respectively. In a water/methanol (50% v/v) mixture the modulus value is substantially higher: for the HD sample 500 ± 69 kPa, for the MD sample 688 ± 108 kPa and for the LD sample 1662 ± 358 kPa were found. This fourfold increase of the *apparent* Young's modulus as the PNIPAM grafts is changed from the swollen to the collapsed state corresponds well to literature findings.⁸³⁻⁸⁵ Furthermore a higher value of the *apparent* Young's modulus was observed for the LD PNIPAM grafts as compared to the HD and MD samples. This could be ascribed to the influence of the silicon substrate underneath the polymer grafts,⁸⁶⁻⁸⁸ even though only the top 20% of the deformation was used to evaluate the data.⁸⁹ In addition, as for the LD sample the grafting density was relatively low, structural heterogeneities over the contact area may exist, which could increase the apparent modulus value due to the influence of the stiffer substrate. The presence of contact area heterogeneities could also explain why a broader distribution was obtained for the LD sample.

In order to study the dynamics of the switching of PNIPAM grafts from the swollen to the collapsed state, the adherence (pull-off force)⁹⁰ between the sample surface and the AFM colloidal probe was monitored by recording force curves at constant time intervals. The change in the polymer chain conformation and swelling state causes a change in adherence between the polymer grafts and the AFM probe, as reported earlier.¹⁷ Here the value of the pull-off force was determined from the retract part of the force curve, which is shown in the insets of Figure 3.11a. The obtained

pull-off forces between the HD, MD and LD PNIPAM grafts and the probe were then plotted as a function of time and are displayed in Figure 3.11 a-c.

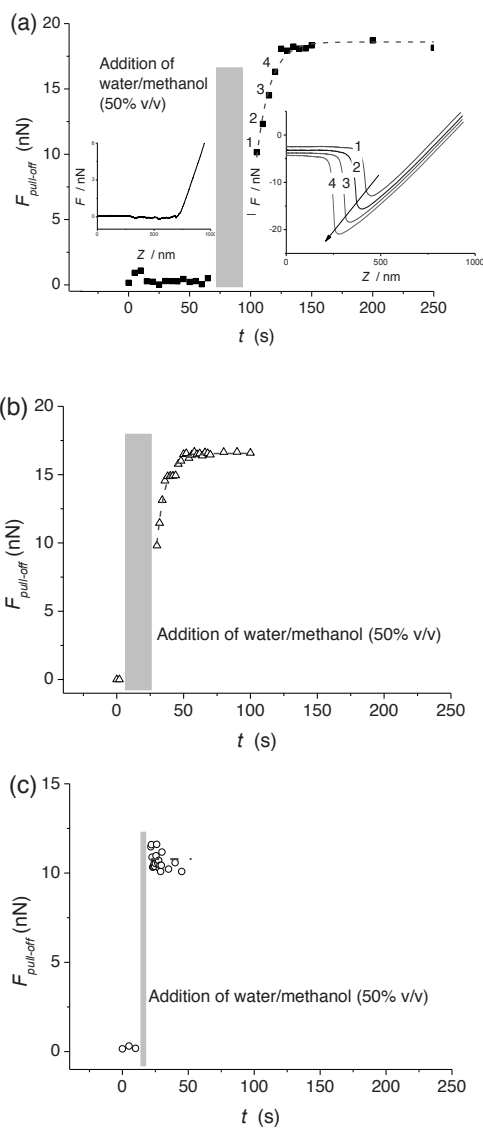


Figure 3.11 The evolution of pull-off forces between the colloidal AFM tip and (a) HD PNIPAM, (b) MD PNIPAM and (c) LD PNIPAM surface. The grey bar indicates the change of solvent environment from pure water to water/methanol (50% v/v) mixture. The retract force-extension curves on HD PNIPAM sample before and after the solvent change are also shown as insets in (a).

Initially the adherence between the grafts and the probe was essentially zero for all grafting densities due to steric interaction between the grafts and the probe.⁹¹ After introducing the co-nonsolvent (i.e. water/methanol, 50% v/v) as indicated by the grey bar in Figure 3.11, the interaction became attractive and pull-off forces on the order of a few tens of nanoNewtons were recorded. The value of the pull-off force generally increased as the thickness of the PNIPAM film increased. This again confirms the transition of PNIPAM chains from swollen to collapsed states due to the co-nonsolvency effect. Changing the solvent environment back to pure water caused the attractive adherence forces to disappear, indicating the reversibility of the process. However, no clear kinetics could be observed in the case of swelling, as equilibration of the system took a very long time and no stable AFM force curves could be recorded. Thus instead of measuring swelling, collapse dynamics of the PNIPAM grafts was monitored. As shown in Figure 3.11a, the pull-off force for the HD sample gradually increased over a period of 25 s from 0 to a plateau value of 19 nN. The collapse dynamics for the LD sample could not be resolved (Figure 3.11c) as after the addition of co-nonsolvent the pull-off force immediately reached the equilibrated value of 11 nN. An intermediate kinetics of the transition was observed for the MD sample, as the adhesion reached the equilibrated 16 nN value in roughly 18s. It should be noted that the precise time of the collapse can be shorter as the transition was already initiated while the co-nonsolvent was introduced (grey bar). A typical equilibration time for the HD and MD samples was 40s while the LD sample equilibrated within 5s. Regardless, a clear and direct correlation could be observed between the collapse dynamics and the film thicknesses of the PNIPAM grafts. We attribute this to the diffusion of solvent molecules into (or out of) the PNIPAM grafts. In the case of a thicker polymer layer, more time is needed for solvent exchange to take place as the collapsed outer layer serves as a diffusion barrier. As well known, in pure water the basis of solubility of PNIPAM is related to the formation of H-bonds between H₂O and the amide groups in the polymer. For the occurrence of LCST, hydrophobic effects are also important.⁴⁸ In a water/methanol (50% v/v) PNIPAM ternary system at room temperature, the solvent-solvent interaction due to the formation of water/methanol complexes is stronger than the solvent-polymer interactions, leading to the desolvation of PNIPAM.⁹²⁻⁹⁴ The timescales of the grafts response to solvent change, as described here, provide important information for the applications of these materials in the fields of e.g. microfluidics and drug release where responsive systems have potential use.

Friction-load plots of the polymer grafts in different liquids were recorded by friction force microscopy (FFM). FFM is a variant of AFM in which lateral deflections of the cantilever are measured as the probe attached to the cantilever

slides across the sample surface.⁹⁵ Here, a microsphere probe (the same as mentioned for adherence measurements) was employed to avoid the extreme contact pressures encountered with typical sharp probes.⁹⁶ The friction images of the MD PNIPAM sample recorded using a SiO₂ microsphere under different solvent environments are shown in Figure 3.12a and b. Cross-section analysis of both images are presented in Figure 3.12c. The friction increases with increasing applied load in both cases, albeit to a different extent. Based on the friction data, friction-load plots were constructed and are shown in Figure 3.12d. The lateral photo-detector signal, which is proportional to the frictional force, was plotted as a function of the applied load. The friction force exhibited a linear relationship with the load, indicative of Amontonian behavior:

$$F_F = \mu F_N + F_F(0) \quad (3.6)$$

where F_F is the friction force, F_N is the load applied perpendicular to the sample surface, $F_F(0)$ is the friction force at zero applied load (related to adhesion) and μ is the coefficient of friction. Here, as we did not determine the lateral spring constant of the cantilever, the obtained friction coefficient was internally normalized to the friction coefficient of a blank silicon substrate under the same solvent environment. It was found that the friction coefficient of the MD PNIPAM in water ($\mu = 0.23 \pm 0.01$) is five times lower than the value of the friction coefficient in the water/methanol (50% v/v) mixture ($\mu = 1.07 \pm 0.06$), indicating a much better lubrication of the PNIPAM grafts in water.

The interaction between the SiO₂ colloidal probe and the PNIPAM surface was repulsive when the polymer was swollen, while it became attractive and jump-to-contact behavior was observed when the solvent environment was changed to a water/methanol (50% v/v) mixture. The effect of solvent on the tribological properties of polymer grafts has been studied by various groups.^{59,96,97} It has been suggested that a high coefficient of friction is associated with the collapsed conformation of polymer grafts, while extended conformations confer a significantly reduced friction force.^{59,96,97} The data shown in Figure 3.12d are in good agreement with these works. For the collapsed grafts, the polymer layer contains disordered, entangled chains in which the molecular conformational changes may readily be induced during “plowing”; in contrast, the swollen grafts retain substantial lubricity because the bound solvent molecules prevent significant deformation of the extended chains and reduce the extent of energy dissipation at a given load.

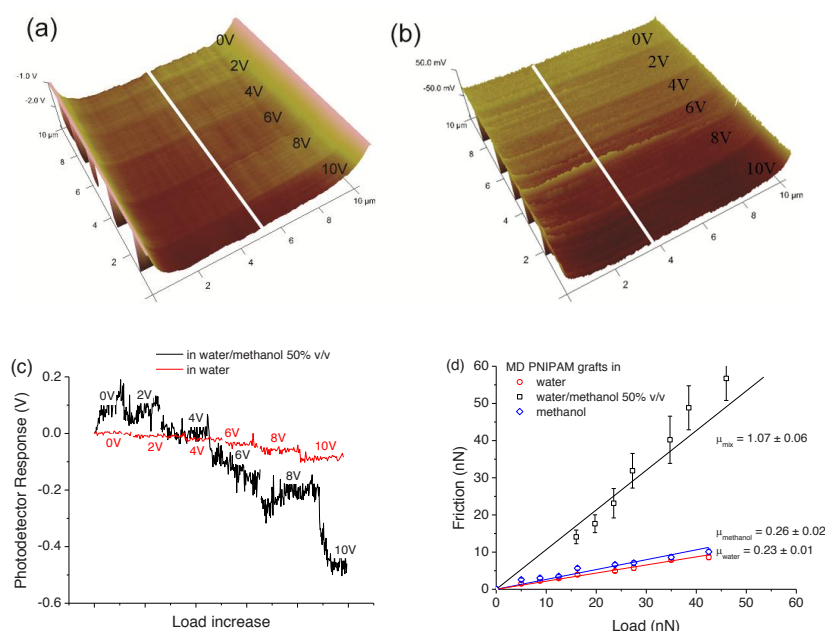


Figure 3.12 Friction images of the MD PNIPAM sample in water/methanol 50% v/v (a) and in pure water (b) while the applied load is increased. Note that the scale of the images is not the same. A cross-section of the indicated white line is shown in (c). (d) Friction of MD PNIPAM sample as a function of load in different solvents as indicated in the legend.

Friction measurements were then carried out on LD, MD and HD PNIPAM grafts. For MD and HD PNIPAM, the coefficient of friction increased by a factor of 4 on switching from water to water/methanol (50% v/v). In contrast, for LD PNIPAM the friction coefficient remained almost the same. As can be seen in Table 3.1, the thickness of the LD sample is substantially lower (one order of magnitude) compared to those of the HD and MD grafts. Although we observed the adherence between the colloidal probe and the LD grafts surface in co-solvent, this seems not to be solely responsible for the friction property of the film as there is no friction contrast of the grafts in different solvents. We believe that the thin PNIPAM layer allowed for exposure of the silicon substrate, resulting in contact area heterogeneity, as observed also previously in determining the mechanical properties of the grafts.

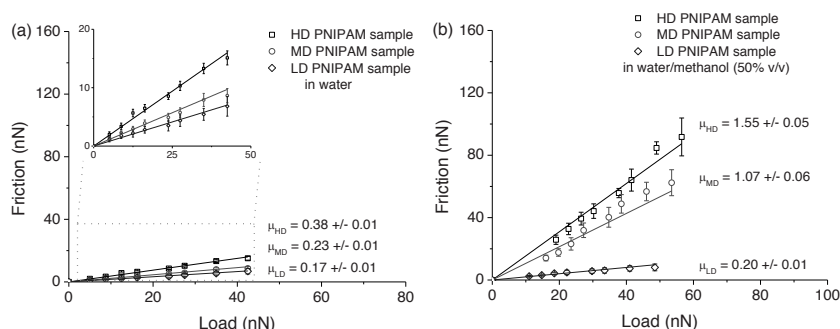


Figure 3.13 Friction of PNIPAM grafts with different grafting densities as a function of load in (a) water and (b) water/methanol (50% v/v). Solid lines are least square fits to the data.

As mentioned earlier, the frictional properties of PNIPAM grafts depend strongly on their “phase state”. To demonstrate the reversibility of the phase change and determine the phase transition kinetics, solvent environment of HD PNIPAM sample was changed *in-situ* while the friction image was recorded in real-time. The obtained friction image and cross-section analysis are shown in Figure 3.14a.

As shown in Figure 3.14a, the friction of the HD PNIPAM shifted between two levels as the solvent environment was cycled between water and water/methanol (50% v/v), indicating the reversibility of the process. The slight offset between the first and the second cycle could be induced by the piezo-movement as resulted from the height difference. From the cross-section analysis (Figure 3.14b) we can see that the photodetector response increased gradually when the co-nonsolvent was introduced (grey bar). The increase was fit to an exponential function and a typical decay time $\tau = 26.7 \pm 2.4$ s was determined. The same experiments were carried out on MD (Figure 3.14c) and LD (Figure 3.14d) samples. The MD sample showed a behavior similar to that of the HD one, the decay time for the MD grafts was determined to be 23.1 ± 2.9 s. No change in friction was found in the case of the LD grafts. These results are consistent with a previous study where the adherence change recorded by AFM force microscopy was monitored. A similar timescale was found for medium and high density polymer grafts while no changes in adherence were found for the low density sample.

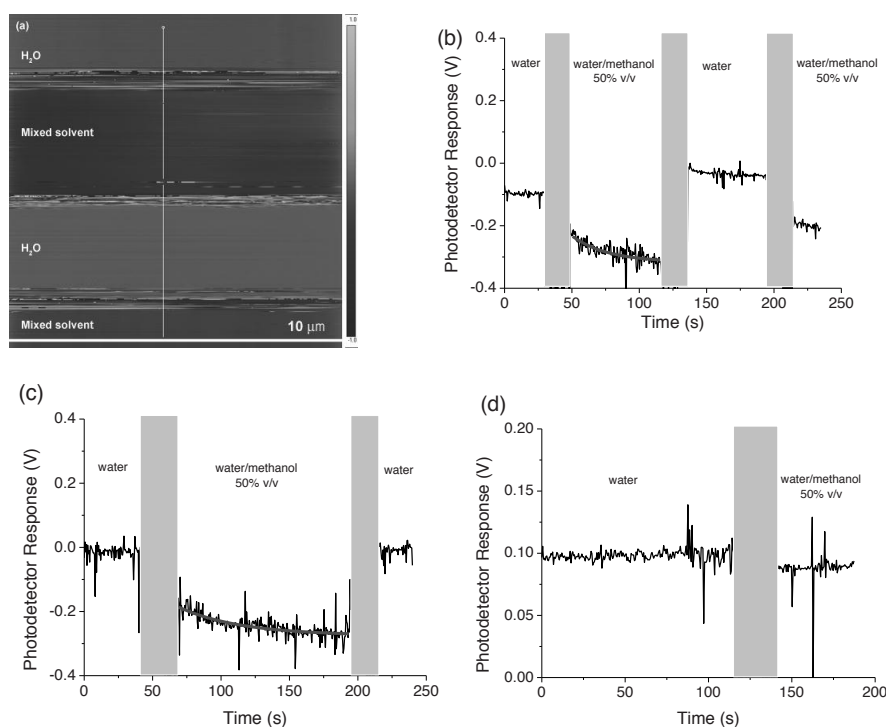


Figure 3.14 (a) AFM friction image of HD PNIPAM sample. The solvent was changed from water to water/methanol 50% v/v as indicated in the image. (b) Cross-section of the white vertical line in (a). Cross-sections of (c) MD and (d) LD PNIPAM sample are also shown. The grey bars indicate the equilibrium time between the solvent exchanges. The solid lines in (b) and (c) are exponential decay fits to the data.

3.2.4 Stability of PNIPAM grafts

To evaluate their stabilities, different PNIPAM grafts were incubated under cell-culture conditions at 37 °C and analysed by AFM following incubation for 24 h. Figure 3.15 shows thickness images and surface morphologies of MB-HD grafts. AFM cross-sectional profiles yielded thickness values decreasing from 210 to 5 nm after incubation. The substrates still showed a relatively smooth surface with a low roughness value for scan sizes of $1 \times 1 \mu\text{m}^2$. These observations indicated an almost complete detachment of the PNIPAM layer. For MB-MD and MB-LD, similar results were observed (Table 3.1). In contrast, a TB-HD grafts did not undergo considerable thickness and morphology changes (Figure 3.16). For all thickness and density values of the studied PNIPAM samples, no considerable thickness change could be observed

on incubation in pure water over 24 h. The difference may be due to two reasons: (i) under cell-culture conditions, the ester bond in the monochlorosilane-based initiator may be somewhat more susceptible to hydrolysis than the amide bond in the trimethoxysilane-based initiator, and (ii) possible siloxane lateral bonds between the trimethoxysilane moieties increase monolayer stability. TB grafts were chosen for further cell-culture studies.

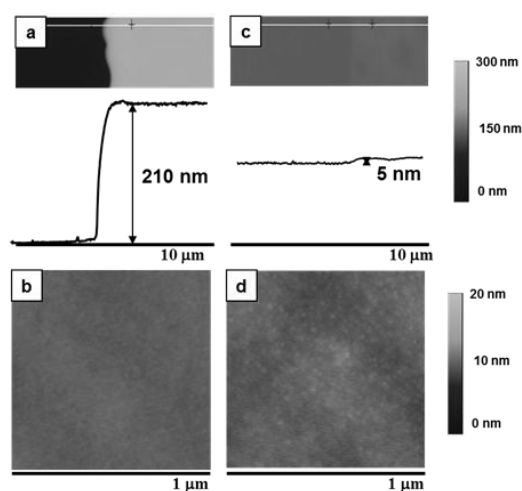


Figure 3.15 Thickness images and surface morphologies of MB PNIPAM grafts by AFM. (a, b) Freshly prepared MB-HD grafts; (c, d) MB-HD grafts after 24 h incubation under cell-culture conditions at 37 °C.

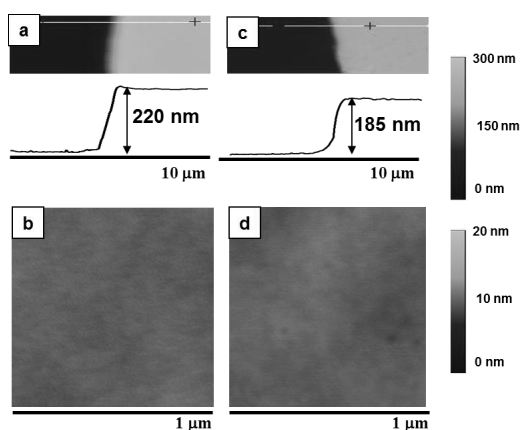


Figure 3.16 Thickness cross-sections and surface morphologies of TB PNIPAM grafts by AFM. (a, b) Freshly prepared TB-HD grafts; (c, d) TB-HD grafts after 24 h incubation under cell-culture conditions at 37 °C.

3.2.5 Cell adhesion and detachment

Cell adhesion and detachment on PNIPAM grafts exhibiting various grafting densities were evaluated by culturing MC-3T3 cells at different incubation temperatures. Control experiments of cell-adhesion behaviour on glass and on initiator-modified glass are shown in Figure 3.17. It can be seen that cells readily attached and proliferated on these surfaces at 37 °C, whereas no cell detachment was observed after 1.5 h at 25 °C.

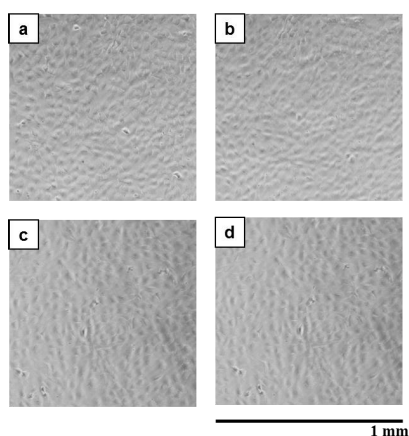


Figure 3.17 Phase-contrast micrographs of MC-3T3 cells cultured on bare glass: (a) at 37 °C for 24 h, (b) at 25 °C for 1.5 h after rinsing; initiator-modified (high-density) substrates: (c) at 37 °C for 24 h, (d) at 25 °C for 1.5 h after rinsing.

Immobilized PNIPAM chain-coated surfaces were applied as cell-culture substrates that enable reversible adhesion and detachment of cells.^{62,83,98-100} Previous studies suggested that thermo-responsive cell adhesion behaviour is dependent on the thickness of the PNIPAM grafts. For PNIPAM grafts beyond a ‘critical thickness range’, cells could not adhere even at 37 °C.^{98,101-103} Here, all grafts showed MC-3T3 adhesion after 24 h of incubation at 37 °C. However, the LD grafts had a much higher cell density with elongated cell morphology, whereas the MD grafts and the HD grafts displayed a progressive decrease of cell density and number of elongated cells, and featured an increase in round, non-elongated cells. These results are in agreement with previous work,^{67,98,101} in which the LD thinner polymer layer was shown to be more dehydrated and restricted. Conversely, in MD and HD thicker layers, the number of chains is larger and inhomogeneously distributed, displaying more freedom and mobility of the outermost layer. After 1.5 h of incubation at 25 °C, almost all cells became detached from the surface as a sheet and could be removed by gentle rinsing (Figure 3.18). This behaviour was reversible and repeatable.

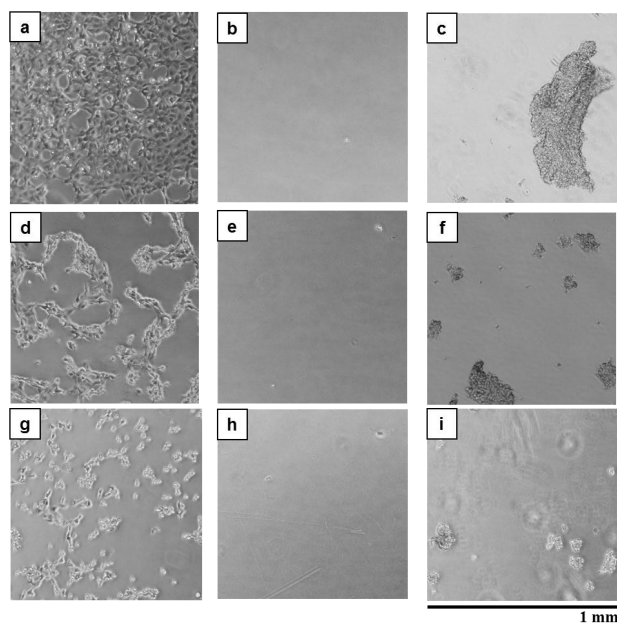


Figure 3.18 (a) Phase-contrast micrographs of MC-3T3 cultured onto TB-LD: (a) at 37 °C for 24 h, (b) at 25 °C for 1.5 h after rinsing, and (c) detached cell sheets; TB-MD: (d) at 37 °C for 24 h, (e) at 25 °C for 1.5 h after rinsing, and (f) detached cell sheets; and TB-HD: (g) at 37 °C for 24 h, (h) at 25 °C for 1.5 h after rinsing, and (i) detached cell sheets.

As is known, the postulated mechanism for cell adhesion and detachment is that as temperature is decreased to below the LCST, PNIPAM chains become hydrated, accompanied by a loss of Young's modulus. This change in hydration and modulus initiates cell detachment.¹⁰⁴ These changes of PNIPAM chains were detected using AFM force measurements, which showed that the interaction between the tip and grafts surface was repulsive when the polymer was swollen, whereas it became attractive and jump-to-contact behaviour was observed when the temperature was above LCST, regardless of differences in thickness values.^{16,17} This indicated that even the outermost layer of the polymer grafts changed from the hydrophilic to the hydrophobic state. This finding was supported by the previous *in-situ* ellipsometry measurements. At 37°C, the collapsed film thickness and optical density values were comparable with those of the dry film. Moreover, transformation of the PNIPAM grafts from the swollen to the collapsed state was also accompanied by a four-fold increase in apparent Young's modulus values, as we discussed in a previous section.

It is worth mentioning that a variation of 'critical thickness' ranges for cell adhesion has been reported.^{67,98,101,105} In addition, grafting densities¹⁰⁶⁻¹⁰⁹ and characteristics of the substrates such as hydrophilicity or hydrophobicity and the

architecture of the PNIPAM layers⁶⁷ all play a role in temperature-controlled cell adhesion and detachment.

3.3 Conclusions

PNIPAM grafts with variable grafting densities were synthesized using substrate-immobilized monochlorosilane- or trimethoxysilane-functional ATRP initiators. *In-situ* spectroscopic ellipsometry was used to study the collapse of PNIPAM grafts as a function of phase state across LCST in real time. A model involving a bi-layer graded density profile was presented, which adequately fits the data therewith enabling a quantitative discussion of the reversible thickness change with varying temperature. The effect of co-nonsolvency, as well as grafting density on the mechanical properties, more specifically the *apparent* Young's moduli of these PNIPAM grafts were studied using an AFM based colloidal probe nano-indentation method. A four-fold increase in *apparent* Young's modulus values was observed when PNIPAM grafts were switched from the swollen to the collapsed state. The collapse dynamics of the PNIPAM grafts was investigated by monitoring the change of adherence between the grafts surface and the colloidal probe. A direct correlation was observed between the time scale of the collapse and the thickness of the PNIPAM layer, indicating that the factor limiting the response time was the diffusion of solvent in and out of the polymer grafts. Lateral force measurements showed low friction forces in water, which greatly increased in water/methanol (50% v/v) for the medium and high density grafts. The observed friction response was fully reversible. We showed that the trimethoxysilane-anchored PNIPAM grafts were much more stable than the monochlorosilane ones under cell-culture medium conditions. Cell-culture studies demonstrated that MC-3T3 cells adhere and proliferate on PNIPAM grafts at 37 °C, whereas they detach from these substrates at 25 °C. Grafting density and film thickness exhibited a clear influence on cell adhesion and detachment. The LD polymer layer with a dry thickness of ~10 nm showed the greatest cell adhesion with elongated morphology, whereas a progressive decrease in cell density and number of elongated cells occurred for the MD layer (dry thickness ~100 nm) and for the HD layer (dry thickness ~220 nm). The latter two grafts did influence cell morphology: an increase in round-shaped cells was observed on these grafts.

3.4 Experimental

Materials:

N-Isopropylacrylamide (NIPAM, Aldrich, 97%) was recrystallized twice from a toluene/hexane solution (50% v/v) and dried under vacuum before use. Copper(I) bromide (CuBr, Aldrich, 98%) was purified by stirring in glacial acetic acid, filtering and washing with ethanol three times, followed by drying under vacuum at room temperature overnight. Methanol (absolute) and toluene (AR) were purchased from Biosolve. Sodium pyruvate (1 mM), copper(II) bromide ($\geq 99\%$), triethylamine (99.5%), *N,N,N',N',N'*-pentamethyldiethylenetriamine (PMDETA) (98%), 2-bromo-2-methylpropionic acid (98%), 2-bromo-2-methylpropionyl bromide (98%), 1-bromocarbonyl-1-methylethyl acetate (96%), (3-aminopropyl)trimethoxysilane (97%) and chlorotrimethylsilane (CTS) ($\geq 97\%$) were used as received. Culture medium α -Minimum Essential Medium and L-glutamine were obtained from Invitrogen. The ATRP initiator 3-(chlorodimethylsilyl)propyl 2-bromo-2-methylpropionate (CDB) was synthesized according to a literature procedure.¹¹⁰ Water used in the experiments was Millipore Milli-Q grade.

Formation of CTS self-assembled monolayers (SAMs):

Silicon substrates were first cleaned with Piranha solution, then rinsed extensively with water, ethanol and dichloromethane. *Caution: Piranha solution reacts violently with many organic materials and should be handled with great care!* Dried substrates were immersed in 25 mL anhydrous toluene solutions containing Et₃N (17.5 μ L, 5 mM) and chlorotrimethylsilane (16 μ L, 5 mM) was added. Reaction was carried out at room temperature for predetermined times. After rinsing with toluene and ethanol, samples were dried in a nitrogen stream and immediately used for the next step.

ATRP initiator vapor phase deposition:

ATRP initiator (30 μ L) was placed in a glass vial at the bottom of a desiccator, the substrates with CTS SAMs and cleaned silicon substrates were placed around the vial. The desiccator was then evacuated by a rotary vane pump for 10 min and subsequently closed. The vapor deposition was allowed to proceed for 10 h. Afterwards the substrates were washed with anhydrous toluene, sonicated in ethanol for 1 min, and dried in a nitrogen stream. The substrates were directly used for SI-ATRP experiments.

Formation of TB ATRP initiator SAMs:

Silicon and glass substrates were first cleaned with Piranha solution, then rinsed extensively with water and ethanol. *Caution: Piranha solution reacts violently with*

many organic materials and should be handled with great care! The dried substrates were placed at the bottom of a desiccator, around a vial containing (3-aminopropyl)-trimethoxysilane (100 μL). The desiccator was then evacuated with a rotary vane pump for 10 min and subsequently closed. Vapour deposition was allowed to proceed overnight. In a beaker, a solution of toluene (40 mL) and triethylamine (5.5 mL) was prepared and subsequently cooled with ice to 0°C. The substrates were immersed into the solution, to which 2-bromo-2-methylpropionyl bromide and 1-bromocarbonyl-1-methylethyl acetate in a predetermined ratio were added dropwise. The reaction was carried out for 20 min, after which the substrates were rinsed with toluene, washed with ethanol and water, and dried under a stream of nitrogen.

ATRP of PNIPAM grafts:

NIPAM (5.73 g, 50 mmol) monomer and PMDETA (314 μL , 1 mmol) were added to a water (18 mL) and methanol (2 mL) mixture. The solution was purged with argon for 30 min. CuBr (71.7 mg, 0.5 mmol) and CuBr₂ (11.2 mg, 0.05 mmol) were added into another reaction flask and also flushed with argon. Monomer, ligand, and catalyst were then combined and stirred for another 30 min to facilitate the formation of the organometallic complex. This solution was then transferred into the flasks containing the substrates covered with SAMs. The flasks were sealed with rubber septa and kept at room temperature under argon. After reaching the desired reaction time, the substrates were removed from the polymerization solution, exhaustively rinsed with water and gently sonicated in EDTA solution (0.1 M, pH 7) for 1 min to remove any unreacted substances not tethered to the surface and subsequently dried in a stream of nitrogen.

Characterization:

The optical experiments were obtained using a Woollam variable angle spectroscopic ellipsometer (VASE) system. All measurements were done *in-situ* using a custom-built, dedicated temperature-controlled cell. Optical access to the sample was achieved through two windows at a fixed angle of incidence $\theta = 63^\circ$. A third window enabled alignment of the sample at normal incidence as well as allowed visual inspection of the sample during *in-situ* experiments. Temperature control was achieved using an externally heated bath from which water was continuously pumped to the cell; the temperature was stabilized using a thermostat with the sensor inside the liquid cell, not more than 1 cm from the sample under investigation. In all cases, the temperature was stable within $\pm 0.5^\circ$ during measurement of the spectra, typically a few minutes. The ellipsometry spectra, i.e. Ψ and Δ as a function of wavelength, were analyzed using the package CompleteEASE (Woollam), employing tabulated dielectric functions for silicon, silicon dioxide and water.¹¹¹ In all cases the

Levenberg-Marquardt multivariate regression algorithm was applied in the fitting procedure.

An atomic force microscope - Dimension D3100 (Digital Instruments, Veeco-Bruker, Santa Barbara, CA, USA) was operated in the tapping mode to measure the thickness and surface morphology of PNIPAM grafts. The PNIPAM grafts were scratched with needles and the thickness differences between the unscratched and the scratched regions were measured to determine the layer thickness.

Force measurements were performed in liquid environment using a NanoScope IIIa multimode atomic force microscope (Digital Instruments/Veeco-Bruker, Santa Barbara, CA, USA) equipped with a standard liquid cell. A silica colloidal probe (Novascan Technologies, Inc. Ames, IA, USA) with a spring constant of 0.050 ± 0.003 N/m (determined using the thermal tune method) and a diameter of 1.00 ± 0.06 μm (determined by scanning a tip array) was used in the experiments. A typical force measurement was carried out in the so-called force volume imaging mode with a z-ramp size of 1 μm , a scan rate of 1 Hz and a deflection trigger of 200 nm and an image area of 10×10 μm . To change the solvent environment, Milli-Q water or a water/methanol mixture (50% v/v) was gently injected into the AFM liquid cell from the outlet within 5s using a syringe.

Quantitative friction measurements were taken from friction loops acquired by obtaining forward–reverse scan cycles along a single line with the microscope employed in scope mode. The friction signal was obtained by subtracting the mean signals in both directions, giving a resultant force that was twice the frictional force. In each measurement, the vertical signal (deflection setpoint) was first minimized to zero and then increased stepwise up to 10 V. Multiple repeat measurements were made at different locations on the samples to verify that the system was stable and provided reproducible data. The lateral spring constant ($k_l = 381.62$ N/m) of the colloidal probe was calculated from the geometry, dimensions and material properties of the V shaped cantilever and the SiO_2 bead according to the analytical approach of Sader et al.¹¹² Dimensions of the cantilever and the SiO_2 bead were determined from SEM measurements. An elastic modulus of 185 GPa and a Poisson ratio of 0.25 for Si_3N_4 was used for the calculation of the lateral spring constant.¹¹³ The lateral photodiode sensitivity (0.34 nm/V) was determined from the measured vertical photodiode sensitivity (73.3 nm/V) in aqueous buffer and the dimensions of the cantilever.¹¹³ Here the assumption was made that under identical small displacements in normal and lateral directions a linear relation between the output voltages can be approximated.

Cell Culture and Cell Image Analysis:

A murine osteoblastic cell line MC-3T3 was cultured at 37 °C in a humidified atmosphere of 5 % carbon dioxide, using as culture medium α -MEM supplemented with 10 % fetal bovine serum, 2 mM L-Glutamine, 1 mM sodium pyruvate, 100 U mL⁻¹ of penicillin, and 100 μ g mL⁻¹ of streptomycin. The cells were seeded at a density of 2×10^4 cells cm⁻² on silica or glass substrates modified with different PNIPAM grafting densities. Metabolic activity was analysed by alamarBlue at 24 and 72 h. Briefly, the samples were immersed in 10 % alamarBlue in cell-culture media; after 4 h of incubation, 200 μ L of supernatant was collected in a white 96-well plate. The fluorescence intensity was measured at an excitation wavelength of 545 nm and an emission wavelength of 590 nm (Victor, Perkin-Elmer). Cell attachment and detachment on the PNIPAM-modified surfaces above or below the LCST was assessed by light microscopy connected with a digital camera (Nikon Eclipse TE 300). Cells were detached by lowering the temperature; after 1.5 h at 25 °C, the surface was gently rinsed with the growth medium and the detached cells collected and reseeded on tissue culture polystyrene for 3 days to confirm their viability. The images of the surfaces taken after the detachment were used to confirm that all the cells were removed from the samples.

3.5 References and notes

- 1 R. Barbey, L. Lavanant, D. Paripovic, N. Schüwer, C. Sugnaux, S. Tugulu and H. A. Klok, *Chem. Rev.*, 2009, **109**, 5437-5527.
- 2 S. Edmondson, V. L. Osborne and W. T. S. Huck, *Chem. Soc. Rev.*, 2004, **33**, 14-22.
- 3 P. M. Mendes, *Chem. Soc. Rev.*, 2008, **37**, 2512-2529.
- 4 S. Minko, *Polym. Rev.*, 2006, **46**, 397-420.
- 5 A. Nelson, *Nat. Mater.*, 2008, **7**, 523-525.
- 6 M. A. C. Stuart, W. T. S. Huck, J. Genzer, M. Müller, C. Ober, M. Stamm, G. B. Sukhorukov, I. Szleifer, V. V. Tsukruk, M. Urban, F. Winnik, S. Zauscher, I. Luzinov and S. Minko, *Nat. Mater.*, 2010, **9**, 101-113.
- 7 I. Luzinov, S. Minko and V. V. Tsukruk, *Soft Matter*, 2008, **4**, 714-725.
- 8 O. Smidsrød and J. E. Guillet, *Macromolecules*, 1969, **2**, 272-277.
- 9 H. G. Schild, *Prog. Polym. Sci.*, 1992, **17**, 163-249.
- 10 E. Kutnyanszky, A. Embrechts, M. A. Hempenius, G. J. Vancso, *Chem. Phys. Lett.*, 2012, **535**, 126-130.
- 11 F. J. Xu, S. P. Zhong, L. Y. L. Yung, E. T. Kang and K. G. Neoh, *Biomacromolecules*, 2004, **5**, 2392-2403.
- 12 M. Mitsuishi, Y. Koishikawa, H. Tanaka, E. Sato, T. Mikayama, J. Matsui and T. Miyashita, *Langmuir*, 2007, **23**, 7472-7474.
- 13 H. Alem, A. S. Duwez, P. Lussis, P. Lipnik, A. M. Jonas and S. Demoustier-Champagne, *J. Membr. Sci.*, 2008, **308**, 75-86.

Chapter 3

- 14 I. Lokuge, X. Wang and P. W. Bohn, *Langmuir*, 2007, **23**, 305-311.
- 15 A. Synytska, E. Svetushkina, N. Pureskiy, G. Stoychev, S. Berger, L. Ionov, C. Bellmann, K. J. Eichhorn and M. Stamm, *Soft Matter*, 2010, **6**, 5907-5914.
- 16 N. Ishida and S. Biggs, *Macromolecules*, 2010, **43**, 7269-7276.
- 17 E. M. Benetti, S. Zapotoczny and J. Vancso, *Adv. Mater.*, 2007, **19**, 268-271.
- 18 M. A. Cole, N. H. Voelcker, H. Thissen, R. G. Horn and H. J. Griesser, *Soft Matter*, 2010, **6**, 2657-2667.
- 19 E. C. Cho, Y. D. Kim and K. Cho, *J. Colloid Interface Sci.*, 2005, **286**, 479-486.
- 20 S. Kidoaki, S. Ohya, Y. Nakayama and T. Matsuda, *Langmuir*, 2001, **17**, 2402-2407.
- 21 S. Mendez, B. P. Andrzejewski, H. E. Canavan, D. J. Keller, J. D. McCoy, G. P. Lopez and J. G. Curro, *Langmuir*, 2009, **25**, 10624-10632.
- 22 K. N. Plunkett, X. Zhu, J. S. Moore and D. E. Leckband, *Langmuir*, 2006, **22**, 4259-4266.
- 23 M. Kaholek, W. K. Lee, S. J. Ahn, H. W. Ma, K. C. Caster, B. LaMattina and S. Zauscher, *Chem. Mat.*, 2004, **16**, 3688-3696.
- 24 I. B. Malham and L. Bureau, *Langmuir*, 2010, **26**, 4762-4768.
- 25 X. Zhu, C. Yan, F. M. Winnik and D. Leckband, *Langmuir*, 2007, **23**, 162-169.
- 26 H. Yim, M. S. Kent, S. Mendez, G. P. Lopez, S. Satija and Y. Seo, *Macromolecules*, 2006, **39**, 3420-3426.
- 27 W. Wang, G. Kaune, J. Perlich, C. M. Paradakis, A. M. B. Koumba, A. Laschewsky, K. Schlage, R. Rohlsberger, S. V. Roth, R. Cubitt and P. Muller-Buschbaum, *Macromolecules*, 2010, **43**, 2444-2452.
- 28 N. Ishida and S. Biggs, *Langmuir*, 2007, **23**, 11083-11088.
- 29 G. M. Liu and G. Z. Zhang, *J. Phys. Chem. B*, 2005, **109**, 743-747.
- 30 H. W. Ma, L. Fu, W. Li, Y. Z. Zhang and M. W. Li, *Chem. Commun.*, 2009, 3428-3430.
- 31 C. A. Naini, S. Franzka, S. Frost, M. Ulbricht and N. Hartmann, *Angew. Chem. -Int. Edit.*, 2011, **50**, 4513-4516.
- 32 E. Bittrich, S. Burkert, M. Muller, K. J. Eichhorn, M. Stamm and P. Uhlmann, *Langmuir*, 2012, **28**, 3439-3448.
- 33 C. Y. Xue, N. Yonet-Tanyeri, N. Brouette, M. Sferrazza, P. V. Braun and D. E. Leckband, *Langmuir*, 2011, **27**, 8810-8818.
- 34 L. Patra, A. Vidyasagar and R. Toomey, *Soft Matter*, 2011, **7**, 6061-6067.
- 35 S. B. Rahane, J. A. Floyd, A. T. Metters and S. M. Kilbey, *Adv. Funct. Mater.*, 2008, **18**, 1232-1240.
- 36 D. Schmaljohann, M. Nitschke, R. Schulze, A. Eing, C. Werner and Y. J. Eichhorn, *Langmuir*, 2005, **21**, 2317-2322.
- 37 S. Balamurugan, S. Mendez, S. S. Balamurugan, M. J. O'Brien and G. P. Lopez, *Langmuir*, 2003, **19**, 2545-2549.
- 38 M. E. Harmon, T. A. M. Jakob, W. Knoll and C. W. Frank, *Macromolecules*, 2002, **35**, 5999-6004.
- 39 E. B. Zhulina, O. V. Borisov, V. A. Pryamitsyn and T. M. Birshtein, *Macromolecules*, 1991, **24**, 140-149.
- 40 X. Laloyaux, B. Mathy, B. Nysten and A. M. Jonas, *Langmuir*, 2010, **26**, 838-847.
- 41 Spectroscopic ellipsometry involves the measurement of the optical response in terms of ellipsometric parameters over a wide spectral range.
- 42 S. Edmondson, N. T. Nguyen, A. L. Lewis and S. P. Armes, *Langmuir*, 2010, **26**, 7216-7226.
- 43 H. Tu, C. E. Heitzman and P. V. Braun, *Langmuir*, 2004, **20**, 8313-8320.
- 44 S. Q. Wang and Y. X. Zhu, *Langmuir*, 2009, **25**, 13448-13455.

- 45 H. Yim, M. S. Kent, S. Mendez, S. S. Balamurugan, S. Balamurugan, G. P. Lopez and S. Satija, *Macromolecules*, 2004, **37**, 1994-1997.
- 46 H. Yim, M. S. Kent, S. Satija, S. Mendez, S. S. Balamurugan, S. Balamurugan and G. P. Lopez, *Phys. Rev. E*, 2005, **72**.
- 47 X. Gao, N. Kucerka, M. P. Nieh, J. Katsaras, S. P. Zhu, J. L. Brash and H. Sheardown, *Langmuir*, 2009, **25**, 10271-10278.
- 48 F. M. Winnik, H. Ringsdorf and J. Venzmer, *Macromolecules*, 1990, **23**, 2415-2416.
- 49 H. G. Schild, M. Muthukumar and D. A. Tirrell, *Macromolecules*, 1991, **24**, 948-952.
- 50 E. Meyer, *Prog. Surf. Sci.*, 1992, **41**, 3-49.
- 51 X. F. Sui, S. Zapotoczny, E. M. Benetti, P. Schön and G. J. Vancso, *J. Mater. Chem.*, 2010, **20**, 4981-4993.
- 52 Y. H. Lin, J. Teng, E. R. Zubarev, H. Shulha and V. V. Tsukruk, *Nano Lett.*, 2005, **5**, 491-495.
- 53 M. C. LeMieux, Y. H. Lin, P. D. Cuong, H. S. Ahn, E. R. Zubarev and V. V. Tsukruk, *Adv. Funct. Mater.*, 2005, **15**, 1529-1540.
- 54 A. J. Parnell, S. J. Martin, R. A. L. Jones, C. Vasilev, C. J. Crook and A. J. Ryan, *Soft Matter*, 2009, **5**, 296-299.
- 55 H. J. Butt, B. Cappella and M. Kappl, *Surf. Sci. Rep.*, 2005, **59**, 1-152.
- 56 M. Kobayashi, Y. Terayama, N. Hosaka, M. Kaido, A. Suzuki, N. Yamada, N. Torikai, K. Ishihara and A. Takahara, *Soft Matter*, 2007, **3**, 740-746.
- 57 M. K. Vyas, K. Schneider, B. Nandan and M. Stamm, *Soft Matter*, 2008, **4**, 1024-1032.
- 58 A. J. Morse, S. Edmondson, D. Dupin, S. P. Armes, Z. Zhang, G. J. Leggett, R. L. Thompson and A. L. Lewis, *Soft Matter*, 2010, **6**, 1571-1579.
- 59 N. Nordgren and M. W. Rutland, *Nano Lett.*, 2009, **9**, 2984-2990.
- 60 Z. Y. Zhang, A. J. Morse, S. P. Armes, A. L. Lewis, M. Geoghegan and G. J. Leggett, *Langmuir*, 2011, **27**, 2514-2521.
- 61 A. Kumar, A. Srivastava, I. Y. Galaev and B. Mattiasson, *Prog. Polym. Sci.*, 2007, **32**, 1205-1237.
- 62 M. Yamato, Y. Akiyama, J. Kobayashi, J. Yang, A. Kikuchi and T. Okano, *Prog. Polym. Sci.*, 2007, **32**, 1123-1133.
- 63 M. A. Cooperstein and H. E. Canavan, *Langmuir*, 2010, **26**, 7695-7707.
- 64 J. E. Gautrot, B. Trappmann, F. Ocegüera-Yanez, J. Connelly, X. M. He, F. M. Watt and W. T. S. Huck, *Biomaterials*, 2010, **31**, 5030-5041.
- 65 Y. X. Zhang, J. A. He, Y. Zhu, H. Chen and H. W. Ma, *Chem. Commun.*, 2011, **47**, 1190-1192.
- 66 S. Tugulu and H. A. Klok, *Biomacromolecules*, 2008, **9**, 906-912.
- 67 L. H. Li, Y. Zhu, B. Li and C. Y. Gao, *Langmuir*, 2008, **24**, 13632-13639.
- 68 N. V. Tsarevsky and K. Matyjaszewski, *Chem. Rev.*, 2007, **107**, 2270-2299.
- 69 R. M. A. Azzam, N. M. Bashara, *Ellipsometry and polarized light*, North-Holland Pub. Co. 1977.
- 70 X. Laloyaux, B. Mathy, B. Nysten and A. M. Jonas, *Langmuir*, 2010, **26**, 838-847.
- 71 S. Alexander, *Journal De Physique*, 1977, **38**, 983-987.
- 72 P. G. Degennes, *Macromolecules*, 1980, **13**, 1069-1075.
- 73 P. G. Degennes, *Adv. Colloid Interface Sci.*, 1987, **27**, 189-209.
- 74 I. Bahar and B. Erman, *Macromolecules*, 1987, **20**, 1696-1701.
- 75 S. T. Milner, T. A. Witten and M. E. Cates, *Macromolecules*, 1988, **21**, 2610-2619.
- 76 O. Guiselin, *Europhys. Lett.*, 1992, **17**, 225-230.
- 77 A. Halperin, *Langmuir*, 2010, **26**, 8933-8940.
- 78 S. Kessel, S. Schmidt, R. Muller, E. Wischerhoff, A. Laschewsky, J. F. Lutz, K. Uhlig, A. Lankenau, C. Duschl and A. Fery, *Langmuir*, 2010, **26**, 3462-3467.

Chapter 3

- 79 E. C. Cho, Y. D. Kim and K. Cho, *Polymer*, 2004, **45**, 3195-3204.
- 80 We note that for deformable materials the “zero distance” becomes a matter of definition. There is an error of a few nanometers due to the determination of the point of contact, which is shown in Figure 3.8a-c.
- 81 It should be noted that the obtained Young’s modulus value here is the apparent Young’s modulus, as the effect of the solid support cannot be neglected, even though only a small amount of deformation was probed.
- 82 M. E. McConney, S. Singamaneni and V. V. Tsukruk, *Polym. Rev.*, 2010, **50**, 235-286.
- 83 S. Schmidt, M. Zeiser, T. Hellweg, C. Duschl, A. Fery and H. Möhwald, *Adv. Funct. Mater.*, 2010, **20**, 3235-3243.
- 84 M. E. Harmon, D. Kucking and C. W. Frank, *Langmuir*, 2003, **19**, 10660-10665.
- 85 O. Tagit, N. Tomczak and G. J. Vancso, *Small*, 2008, **4**, 119-126.
- 86 E. K. Dimitriadis, F. Horkay, J. Maresca, B. Kachar and R. S. Chadwick, *Biophys. J.*, 2002, **82**, 2798-2810.
- 87 H. Shulha, A. Kovalev, N. Myshkin and V. V. Tsukruk, *Eur. Polym. J.*, 2004, **40**, 949-956.
- 88 D. Filip, V. I. Uricanu, M. H. G. Duits, W. G. M. Agterof and J. Mellema, *Langmuir*, 2005, **21**, 115-126.
- 89 For this film, the stress field does not decay within the brush, thus there is a finite force acting on the substrate which will influence the modulus measured.
- 90 We use here “adherence” to describe the practical work of adhesion to emphasize differences between its value and the magnitude of thermodynamic adhesion. The latter, if expressed in work of adhesion, corresponds to the reversible free energy change per unit surface area when two contacting surfaces are moved apart from contact to infinite distance of separation. Thus, adherence also includes the energy dissipated during separation of the contacting surfaces from each other.
- 91 S. Yamamoto, M. Ejaz, Y. Tsujii and T. Fukuda, *Macromolecules*, 2000, **33**, 5608-5612.
- 92 G. M. Liu and G. Z. Zhang, *Langmuir*, 2005, **21**, 2086-2090.
- 93 G. Z. Zhang and C. Wu, *J. Am. Chem. Soc.*, 2001, **123**, 1376-1380.
- 94 J. K. Hao, H. Cheng, P. Butler, L. Zhang and C. C. Han, *J. Chem. Phys.*, 2010, **132**, 154902.
- 95 R. W. Carpick and M. Salmeron, *Chem. Rev.*, 1997, **97**, 1163-1194.
- 96 M. A. Brady, F. T. Limpoco and S. S. Perry, *Langmuir*, 2009, **25**, 7443-7449.
- 97 F. T. Limpoco, R. C. Advincula and S. S. Perry, *Langmuir*, 2007, **23**, 12196-12201.
- 98 A. Mizutani, A. Kikuchi, M. Yamato, H. Kanazawa and T. Okano, *Biomaterials*, 2008, **29**, 2073-2081.
- 99 Q. Yu, Y. X. Zhang, H. Chen, F. Zhou, Z. Q. Wu, H. Huang and J. L. Brash, *Langmuir*, 2010, **26**, 8582-8588.
- 100 N. Matsuda, T. Shimizu, M. Yamato and T. Okano, *Adv. Mater.*, 2007, **19**, 3089-3099.
- 101 K. Fukumori, Y. Akiyama, Y. Kumashiro, J. Kobayashi, M. Yamato, K. Sakai and T. Okano, *Macromol. Biosci.*, 2010, **10**, 1117-1129.
- 102 Y. Akiyama, A. Kikuchi, M. Yamato and T. Okano, *Langmuir*, 2004, **20**, 5506-5511.
- 103 K. Fukumori, Y. Akiyama, M. Yamato, J. Kobayashi, K. Sakai and T. Okano, *Acta Biomater.*, 2009, **5**, 470-476.
- 104 T. Okano, N. Yamada, M. Okuhara, H. Sakai and Y. Sakurai, *Biomaterials*, 1995, **16**, 297-303.
- 105 A. Kikuchi and T. Okano, *J. Control. Release*, 2005, **101**, 69-84.
- 106 N. Singh, X. F. Cui, T. Boland and S. M. Husson, *Biomaterials*, 2007, **28**, 763-771.

Engineering of Surface Grafted PNIPAM Layers Across the Length Scales

- 107 Y. Mei, T. Wu, C. Xu, K. J. Langenbach, J. T. Elliott, B. D. Vogt, K. L. Beers, E. J. Amis and N. R. Washburn, *Langmuir*, 2005, **21**, 12309-12314.
- 108 R. R. Bhat, B. N. Chaney, J. Rowley, A. Liebmann-Vinson and J. Genzer, *Adv. Mater.*, 2005, **17**, 2802-2807.
- 109 M. Zelzer, R. Majani, J. W. Bradley, F. R. A. J. Rose, M. C. Davies and M. R. Alexander, *Biomaterials*, 2008, **29**, 172-184.
- 110 B. Lego, W. G. Skene and S. Giasson, *Langmuir*, 2008, **24**, 379-382.
- 111 E. D. Palik. *Handbook of optical constants of solids II*, Academic Press, Boston, 1991.
- 112 J. E. Sader, *Rev. Sci. Instrum.*, 2003, **74**, 2438-2443.
- 113 E. Tocha, H. Schönherr and G. J. Vancso, *Langmuir*, 2006, **22**, 2340-2350.

Chapter 4

Grafting Mixed Responsive Layers of Poly(*N*-isopropylacrylamide) and Poly(methacrylic acid) from Gold by Selective Initiation

In this chapter, mixed polymer grafts consisting of poly(*N*-isopropylacrylamide) (PNIPAM) and poly(methacrylic acid) (PMAA) were prepared at room temperature by a sequential combination of surface-initiated atom transfer radical polymerization (SI-ATRP) and iniferter-mediated photopolymerization (SI-IMP). Mixed monolayers of disulfides of ATRP initiator and IMP iniferter on gold substrates were employed for independent initiation of the two polymer components. As the polymerization of PNIPAM and PMAA was performed in successive steps, the chain length and corresponding grafts height of the constituents could be individually controlled. Grazing angle Fourier transform infrared spectroscopy (FTIR) and ellipsometry were performed to monitor the component-specific formation of the grafts. The responsive behavior of the mixed polymer grafts under different pH was investigated by contact angle measurements (CA), atomic force microscopy (AFM) and *in-situ* ellipsometry. Reversible structural reorganization, variation of grafts thickness and of wetting characteristics were monitored.

* Parts of this chapter have been published in: Sui, X.; Zapotoczny, S.; Benetti, E. M.; Memesa, M.; Hempenius M. A. and Vancso. G. J. *Polym. Chem.*, **2011**, 2, 879-884.

4.1 Introduction

Responsive films made of surface-tethered macromolecules have been widely applied to a variety of substrates and used to control surface wetting and friction, in fabrication of micro- and nanostructures, for preparing actuators, for regulation of cell and protein attachment and for many other purposes.¹⁻¹¹ These responsive films with well-defined structural properties are usually obtained by controlled surface-initiated radical polymerization methods.¹² The surface properties of stimuli responsive homopolymer grafts usually exhibit sharp transitions between e.g. two different physical states in response to a small change of an external “environmental” trigger (e.g. temperature, pH or light). In mixed grafts, it is possible to switch the surface performance between the properties of the two different polymer components, which allows for control of the targeted property in a broader range compared to the single constituents.¹³⁻¹⁹

Two different strategies are generally used to synthesize mixed polymer grafts: the so-called “grafting to” and “grafting from” techniques.⁸ In the first approach, binary grafts platforms can be obtained by sequential attachment of two different polymers onto reactive substrates.^{20,21} As an example, this specific strategy allowed the surface grafting of polybases and polyacids within the same grafts film. The obtained mixed polyelectrolyte grafts were characterized by surface charge polarity and density which could be precisely tuned by immersion in media presenting different pH values.²² Despite its broad applications, “grafting to” approaches present several limitations, i.e. relatively low grafting densities and film thicknesses are usually achieved by this preparation method. Hence, *in-situ* growth of polymer grafts from pre-functionalized surfaces by a “grafting from” approach is usually preferred. Surface-initiated polymerization from immobilized initiator adsorbates was used in several instances to obtain mixed grafts with adjustable thicknesses and high grafting densities. The mixed monolayer approach is attractive since it is possible to immobilize two or more initiators that may be activated independently. After the first polymer is grafted, the film may be cleaned and reactivated under different conditions in order to synthesize the second grafted polymer. The net result is a mixed graft structure where two kinds of polymer chains are intercalated between each other.²³⁻²⁶

The preparation and the stimuli-responsive behavior of PNIPAM and PMAA homopolymer, random copolymer and block copolymer grafts were described in some reports.^{27,28} However, to our knowledge, the preparation and the responsive behavior of PNIPAM-PMAA mixed grafts by selective initiation have not been investigated. PNIPAM and PMAA are often employed in responsive systems, hence we chose these two constituents for this study.

Grafting Mixed Grafts of PNIPAM and PMAA from Gold by Selective Initiation

In this work, we combined two surface-initiated controlled radical polymerization techniques, i.e. surface-initiated atom transfer radical polymerization (SI-ATRP) and iniferter-mediated photopolymerization (SI-IMP), to create mixed homopolymer grafts of PNIPAM and PMAA on gold substrates at room temperature. We chose SI-ATRP to synthesize the first graft component (PNIPAM) and subsequently SI-IMP for the second grafts (PMAA). The particular step-wise fabrication, using ATRP and IMP, was selected as they allowed us to sequentially control grafts synthesis by the two different mechanisms of polymerization. This is ensured as activation of an ATRP initiator with a metal complex is a bimolecular process, while the free radicals in IMP are formed by photo decomposition, which is a unimolecular process. A unimolecular activation mechanism was preferred for the grafting of the *second grafts component* due to the steric hindrance induced by the existing polymer chains. We also mention that SI-IMP was well suited for the direct synthesis of PMAA grafts since it alleviated the problems of catalyst complexation, dissociation, or disproportionation which could occur when ATRP of electrolytic monomers in protic media is performed.^{15,29}

The choice of gold as a substrate presented several advantages over the use of frequently reported silicon surfaces. Self-assembled monolayers (SAMs) of disulfides/thiols on Au surfaces are well ordered, they can be easily formed under environmental conditions and their compositions may be easily varied by tuning the relative concentration of the different adsorbates in the feeding solutions.^{3,30-32}

The grafts synthesis used here is outlined in Figure 4.1. The behavior of the mixed grafts was characterized and investigated in different media. In particular, the pH responsive behavior was monitored by contact angle measurements, AFM and *in-situ* ellipsometry.

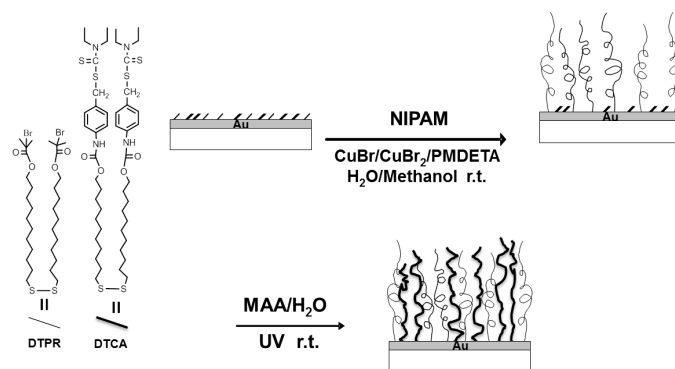


Figure 4.1 Synthetic strategy for mixed polymer grafts from immobilized precursors on gold by combining SI-ATRP and SI-IMP.

4.2 Results and discussion

4.2.1 Preparation of mixed PNIPAM-PMAA grafts

The preparation of mixed PNIPAM-PMAA grafts was carried out as summarized in Figure 4.1. During the first step, mixed SAMs were deposited on Au from chloroform solutions of mixtures of DTPR and DTCA. The formation of the SAMs was confirmed by FTIR and by XPS measurements. Quantitative determination of the surface composition was performed on the mixed SAMs as the feed composition and the surface composition can differ due to differences in the absorption kinetics of the individual components onto Au. The surface concentration of DTPR molecules as obtained by XPS was 37.5 mol %, which was lower than the value for the corresponding feed solution (70 mol %). This difference was attributed to the higher polarity of DTCA functionalities with respect to the DTPR, which makes the chemisorption of DTCA on the Au surface energetically favored.³³⁻³⁶

Following deposition of the mixed initiating SAMs, PNIPAM was grafted from the functionalized Au surfaces by SI-ATRP. The formation of PNIPAM grafted layers was confirmed by ellipsometry and contact angle measurements. Ellipsometry demonstrated the formation of a PNIPAM graft layer with a dry film thickness value of 64 ± 2 nm following 30 min polymerization time. The contact angle value of this graft layer was $56 \pm 2^\circ$, which is typical for PNIPAM films.³⁷ We note that recent studies showed that alkyl dithiocarbamate iniferters for IMP can also initiate ATRP in the presence of copper catalysts with nitrogen-based ligands. These studies showed that the initiation efficiency was strongly dependent on the molecular structure of the iniferter and on the reaction conditions. Also there was essentially no “halogen exchange” between the iniferter reagent and Br in the catalyst solution.³⁸⁻⁴³ In order to confirm the activity of only DTPR molecules as initiators for SI-ATRP from the mixed SAMs and the consequent inertness of DTCA adsorbates during ATRP, control experiments under the same polymerization conditions were performed using pure DTCA monolayers. We observed no formation of any grafted polymer. Pure DTPR SAMs stimulated the growth of graft layers with an average ellipsometric thickness of 155 ± 3 nm over a 30 min polymerization time.

To synthesize binary mixed PNIPAM/PMAA grafts with various PMAA chain lengths, samples from the same PNIPAM graft batch featuring a 64 ± 2 nm dry height were exposed to photopolymerization conditions at room temperature for various polymerization times. The resulting thickness values were determined by

Grafting Mixed Grafts of PNIPAM and PMAA from Gold by Selective Initiation

ellipsometry and AFM (Figure 4.2). As shown in Figure 4.2, the dry graft thickness increased monotonically with the irradiation time. The thickness results obtained by ellipsometry were in good agreement with the height increments recorded by AFM in air. To confirm that PMAA chains were indeed initiated from the adsorbed photoinitiators, we exposed a pure ATRP initiator monolayer to the typical IMP conditions. After cleaning, no considerable changes were observed in the graft layer thickness, confirming the high specificity of the DTCA molecules.

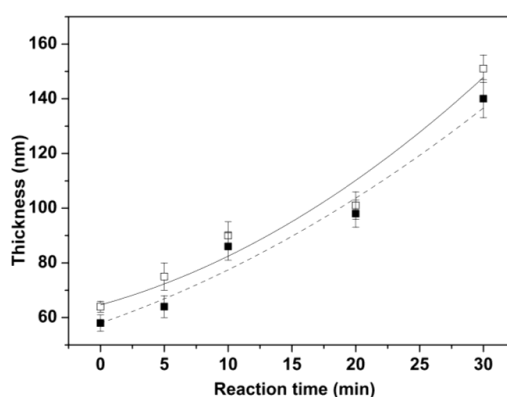


Figure 4.2 Film thickness vs. IMP polymerization time for the mixed grafts, starting with PNIPAM grafts, measured by ellipsometry (open squares, solid line) and AFM (filled squares, dashed line). The fitted lines are meant to guide the eye.

It should be noted that the thickness of PNIPAM layers synthesized from mixed monolayers is significantly smaller than the thickness of a PNIPAM layer synthesized from a pure DTPR SAM under the same time interval. This difference is most likely due to the lower initiator concentration.^{33,44} The thickness of PMAA initiated from a PNIPAM layer is also smaller than the one obtained from a full DTCA monolayer. In this case the lower growth rate is most likely caused by the limited diffusion of the monomer to the surface already partially covered by PNIPAM grafts.

FTIR analysis confirmed the presence of PMAA and PNIPAM immobilized on the surface of the substrates. In representative spectra shown in Figure 4.3a, C=O stretching yields a strong band at 1650 cm^{-1} , while the two bands at 1370 and 1390 cm^{-1} are assigned to the two methyl groups in the isopropyl functionality of PNIPAM. In Figure 4.3e (one component PMAA grafts), the intense peak around 1730 cm^{-1} is assigned to the C=O stretching vibration in the carboxylic acid groups of PMAA. In addition, C-O stretching bands, characteristic to PMAA, can be observed at 1203 and 1269 cm^{-1} . The FTIR spectra of the mixed grafts captured in Figure 4.3b, c and d have characteristic peaks for both PMAA and PNIPAM. The

increasing content of PMAA in the mixed grafts with the polymerization time was also verified. The ratio of the heights of the peak at 1730 cm^{-1} (PMAA) and the peak at 1650 cm^{-1} (PNIPAM) increased with the irradiation time.

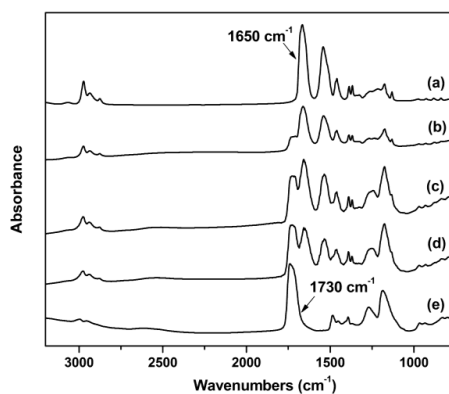


Figure 4.3 FTIR spectra of (a) PNIPAM homopolymer grafts; (b-d) mixed polymer grafts: starting from the same height of PNIPAM, after various photopolymerization times for PMAA: (b) 5 min, (c) 10 min, (d) 20 min; and (e) PMAA homopolymer grafts.

4.2.2 pH responsive behavior of mixed PNIPAM-PMAA grafts

The sample following 20 min of IMP of MAA (53 mol % of PMAA) was chosen to investigate the responsive behavior of binary PNIPAM/PMAA films (sample named as PNIPAM/PMAA-20min).

PMAA undergoes a marked pH-induced conformational transition in aqueous solutions. At low pH values, PMAA chains are weakly charged and adopt a collapsed conformation to prevent exposure of the hydrophobic methyl groups to the polymer-water interface. At high pH values the charge density along the PMAA chains markedly increases causing intramolecular repulsion and a subsequent stretching of the polymer chains.⁴⁵

In-situ ellipsometry at room temperature ($22\text{ }^{\circ}\text{C}$) shows that exposure of a dry PNIPAM/PMAA-20min sample to a pH= 3 buffer solution swells the layer 1.5 times to its dry-layer thickness, while immersion in pH= 8 buffer solution results in a 4.0 times change as compared to the dry-layer thickness. For subsequent measurements, the PNIPAM/PMAA-20 min samples were immersed in a buffer solution with pH= 3 or 8 for 10 min. After each treatment, the samples were quickly rinsed with anhydrous ethanol, dried in a stream of nitrogen and immediately used for AFM and contact angle analyses.

The surface morphology of the different polymer graft films following

treatment at acidic and basic pH values was subsequently studied by tapping mode AFM (TM-AFM).⁴⁶ One-component graft samples of PNIPAM and PMAA revealed fairly smooth surfaces following treatment with buffer at different pH (Figure 4.4a-f, Table 4.1). For mixed grafts a sharp morphological transition was observed by immersing the films alternatively in pH= 3 and pH= 8 (Figure 4.4g and 4h). Following immersion in pH= 3 buffer, both polymer components were uncharged. The root mean square (RMS) roughness value derived from the corresponding micrograph (Figure 4.4g) resulted in a value of 1.80 nm (scan area = $1 \times 1 \mu\text{m}^2$; see Table 4.1). Charging of the PMAA chains at high pH values and their consequent extension leads to confinement of PNIPAM aggregates close to the substrate surface while PMAA extends out at the interface. As a result, the RMS roughness values of the mixed graft surface markedly increased to 4.65 nm over a scan area of $1 \times 1 \mu\text{m}^2$ (Figure 4.4h). The difference in the roughness values was very significant, thus it can be expected that surface roughness plays a significant role in the contact angle results.

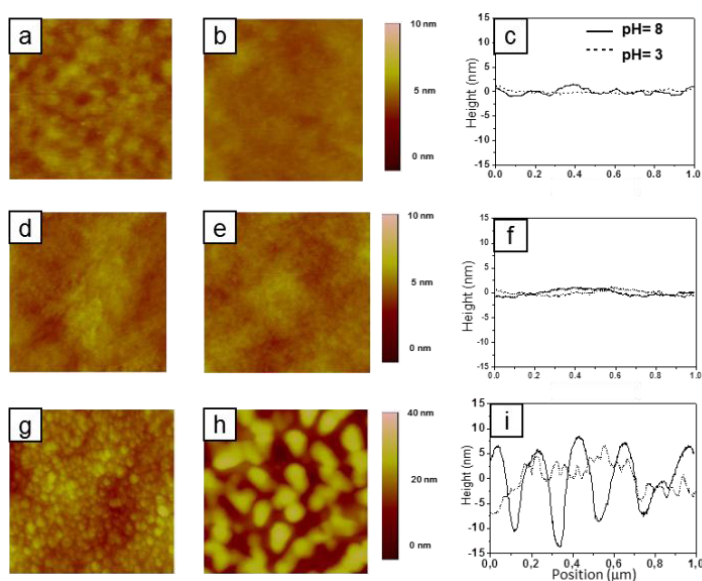


Figure 4.4 AFM surface height images in air and the representative cross-section of various polymer grafts systems following treatments with buffer of different pH (scan area = $1 \times 1 \mu\text{m}^2$). (a) PNIPAM homopolymer grafts after immersion in pH 3 buffer, (b) PNIPAM homopolymer grafts after immersion in pH 8 buffer, and (c) the corresponding cross-sections; (d) PMAA homopolymer grafts after immersion in pH 3 buffer, (e) PMAA homopolymer grafts after immersion in pH 8 buffer, and (f) the corresponding cross-sections; (g) PNIPAM/PMAA-20 min mixed grafts after immersion in pH 3 buffer, (h) PNIPAM/PMAA-20 min mixed grafts after immersion in pH 8 buffer, and (i) the corresponding cross sections.

Static water contact angle analysis (θ) on the different polymer graft films was subsequently performed and the corresponding results are reported in Table 4.1. PNIPAM graft surfaces treated with different buffer solutions display similar wettability (contact angle 56°) suggesting no response to pH changes. For PMAA surfaces, a pH change from pH= 3 to pH= 8 induced a shift in contact angle values from 52° for the collapsed state to 10° for the highly hydrophilic swollen state. Similar behavior has already been reported.⁴⁷ For the mixed grafts sample PNIPAM/PMAA-20min, the contact angle value was quite different compared to single component PMAA and PNIPAM grafts at the corresponding pH values. It is known that the surface roughness can influence the apparent contact angles through many different and subtle ways and contact angles are only affected by the first few nanometers of contacted solids at the air/liquid interface.^{15,48} At pH= 3, the RMS roughness is 1.80 nm and the contact angle is similar for both PNIPAM and PMAA grafts. However at pH 8, the RMS roughness increased to 4.65 nm in the mixed grafts (see Figure 4.4). This behavior was paralleled by a contact angle increase to $80 \pm 5^\circ$ (see Table 4.1) in line with earlier reports. High contact angles were observed even on hydrophilic surfaces due to high surface roughness.⁴⁹ Since both grafts at pH 8 are hydrophilic, the high starting contact angle at pH= 8 decreases gradually to 20° in one minute due to the reorganization of grafts upon water drop deposition.

	Contact angle ($^\circ$) at pH= 3	RMS roughness (nm)	Contact angle ($^\circ$) at pH= 8	RMS roughness (nm)
PNIPAM	56 ± 2	0.37	56 ± 2	0.33
PMAA	52 ± 2	0.13	<10	0.17
PNIPAM/PMAA -20 min mixed grafts	60 ± 5	1.80	80 ± 5 (gradually decreasing to 20)	4.65

Table 4.1 Static water contact angle and root mean square roughness as determined by AFM in air (scan area = $1 \times 1 \mu\text{m}^2$) on different samples treated previously with buffer solution of different pH.

4.3 Conclusions

The successful synthesis of binary, mixed PNIPAM/PMAA grafts on gold surfaces at room temperature was described. A simple approach from binary mixed monolayers of initiators by combining two surface-initiated controlled radical polymerization methods, i.e. SI-ATRP and SI-IMP, was employed. The method enabled one to achieve height control for both components of the grafts

independently in contrast to the previously reported mixed grafts on silicon and the other “grafting to” methods. We found that the mixed grafts undergo reorganization in response to changes in pH, exhibiting reversible changes in swollen/collapsed thicknesses, water contact angles and surface morphology. The stimulus responsive behavior unveiled in this study could find applications in creating functional thin films with reversibly switchable surfaces or adaptive chemical properties.

4.4 Experimental

Materials:

N-isopropylacrylamide (NIPAM, Aldrich, 97%) was recrystallized twice from a toluene/hexane solution (50% v/v) and dried under vacuum prior to use. Methacrylic acid (MAA, Aldrich, 99%) was purified by vacuum distillation. Copper(I) bromide (CuBr, Aldrich, 98%) was purified by stirring in glacial acetic acid, filtering, and washing with ethanol three times, followed by drying in vacuum at room temperature overnight. Copper(II) bromide (Aldrich, $\geq 99\%$), methanol (Biosolve, absolute) and *N,N,N',N'',N''*-pentamethyldiethylenetriamine (PMDETA) (98%, Acros Organics) were used as received. The ATRP initiator, dithiodiundecane-11,1-diylbis[2-bromo-2-methylpropanoate] (DTPR, depicted in Scheme 1), was synthesized according to literature procedures.⁵⁰ The photoiniferter, dithiodiundecane-11,1-diylbis[4-((diethylamino)carbonothioyl)thioethyl] phenyl)carbamate] (DTCA, depicted in Figure 4.1) was synthesized following the procedure reported previously.³ Gold substrates (200 nm thick Au layer) were obtained from Ssens BV, Hengelo, The Netherlands. Buffer solutions, pH 4.0, and pH 8.0, were obtained from Merck. Water was purified with a Millipore desktop system. All other chemicals were received from Aldrich and were used without further purification.

Formation of mixed SAMs on gold substrates:

Mixed SAMs were prepared by immersing gold substrates in chloroform solutions containing predetermined amounts of the ATRP initiator (DTPR) and of the photoiniferter (DTCA). The substrates were previously cleaned with “piranha” solution, and rinsed with water, ethanol and dichloromethane extensively. *Caution: ‘Piranha’ solutions react violently with many organic materials and should be handled with great care.* The total concentration of the adsorbates was 1 mM. Substrates covered with only one monolayer (DTPR or DTCA) were also prepared for reference experiments. The typical deposition time was 16 h. The substrates were rinsed sequentially with dichloromethane and ethanol, dried in a stream of N₂ and

immediately used for grafts growth. For most of the reported polymerizations the mixed SAMs were prepared from a solution containing DTPR and DTCA with a molar ratio of 70:30 in the feed.

Synthesis of PNIPAM grafts by SI-ATRP:

Figure 4.1 displays the synthetic pathway for the preparation of PNIPAM grafts on Au. NIPAM (5.73 g, 50 mmol) monomer and PMDETA (314 μ L, 1 mmol) were added to a water (18 mL) and methanol (2 mL) mixture. The solution was purged with argon for 30 min. CuBr (71.7 mg, 0.5 mmol) and CuBr₂ (11.2 mg, 0.05 mmol) were added into another reaction flask and also flushed with argon. Monomer, ligand and catalyst were then combined and stirred for another 0.5 h to facilitate the formation of the organometallic complex. This solution was then transferred into the flasks containing the substrates covered with SAMs. The flasks were sealed with rubber septa and kept at room temperature under argon. After reaching the desired reaction time (30 min), the substrates were removed from the polymerization solution, exhaustively rinsed with water to remove any unreacted and not surface tethered substances and subsequently dried in a stream of nitrogen.

Synthesis of PMAA polymer grafts by SI-IMP:

The substrates were placed in flasks containing 1.0 M aqueous solution of MAA, they were extensively purged with argon and finally irradiated for the pre-determined polymerization time by an array of six UV-B lamps (15 W, G15T8E, Ushio, Japan; sample-to-lamp distance, 20 cm). Following completion of photopolymerization, the samples were extensively rinsed with water to remove all traces of the polymerization solution, and subsequently dried in a stream of nitrogen.

Characterization:

Static contact angle measurements with water were performed by the sessile drop technique using an optical contact angle device equipped with an electronic syringe unit (OCA15, Dataphysics, Germany). At least three different measurements of each sample were performed.

X-ray photoelectron spectroscopy (XPS) was used to evaluate the actual surface concentration in SAMs. XPS spectra were obtained by a Quantera XPS instrument (Physical Electronics) using monochromatized Al K α radiation (1486.6 eV) with an X-ray beam diameter of 100 μ m and a take-off angle of 30°, relative to the substrate's surface. Each sample was measured over a set of eight different locations. To evaluate the relative concentration of DTCA and DTPR on the surface, high-resolution XPS elemental scans for the O1s, N1s and Br3p signals were recorded. By combining the

values obtained for each sample, the relative composition of the SAMs was determined.

Grazing angle FTIR spectroscopy was employed to determine the actual surface composition of the polymer grafts. FTIR spectra were obtained using a BIO-RAD FTS575C spectrometer equipped with a nitrogen-cooled cryogenic mercury telluride detector. A background spectrum was obtained by scanning a clean gold substrate. For reference purposes, a set of nine thin polymer films with known, different compositions of PNIPAM and PMAA homopolymer mixtures was prepared by drop casting from methanol solutions onto silicon substrates. FTIR spectra of these mixed homopolymer samples were used for calibration. The relative intensities of the deconvoluted peaks at 1730 cm^{-1} (characteristic for PMAA) and at 1650 cm^{-1} (characteristic for PNIPAM) were plotted against the known compositions of the films and a calibration curve was constructed. The composition of the mixed grafts was derived from their FTIR spectra using the so-obtained calibration.

The thickness of dry layers was measured using a rotating analyzer ellipsometer (J. A. Woollam VASE) at 10 nm intervals at wavelengths from 380 to 800 nm at an angle of incidence of 70° . The measurements were performed at $22\text{ }^\circ\text{C}$ at 30% relative humidity. The thickness and refractive index determination were performed on at least 5 spots for each sample. *In-situ* ellipsometric measurements were conducted at $22\text{ }^\circ\text{C}$ with the same instrument using a quartz flow cell with thin walls fixed at an angle of 70° with respect to the sample plane. The angle of incidence of the light was set such that its path was normal to the window. The samples were immersed in different buffer solution for at least 15 min to ensure full swelling. The measured values of amplitude ratio upon reflection and phase shift were used to obtain the optical constants of the samples by the standard WVASE 32 software package (J. A. Woollam Co.).

AFM in the tapping mode (TM-AFM) was employed to study the morphology of the grafts surfaces. A Dimension D3100 (AFM, Digital Instruments, Veeco-Bruker, Santa Barbara, CA) was used.

4.5 References

- 1 M. A. C. Stuart, W. T. S. Huck, J. Genzer, M. Müller, C. Ober, M. Stamm, G. B. Sukhorukov, I. Szleifer, V. V. Tsukruk, M. Urban, F. Winnik, S. Zauscher, I. Luzinov and S. Minko, *Nat.Mater.*, 2010, **9**, 101-114.
- 2 S. T. Milner, *Science*, 1991, **251**, 905-914.
- 3 E. M. Benetti, S. Zapotoczny and G. J. Vancso, *Adv. Mater.*, 2007, **19**, 268-271.
- 4 S. Zapotoczny, E. M. Benetti and G. J. Vancso, *J. Mater. Chem.*, 2007, **17**, 3293-3296.

Chapter 4

- 5 M. Navarro, E. M. Benetti, S. Zapotoczny, J. A. Planell and G. J. Vancso, *Langmuir*, 2008, **24**, 10996-11002.
- 6 X. F. Sui, J. Y. Yuan, W. Z. Yuan and M. Zhou, *Prog. Chem.*, 2008, **20**, 1122-1127.
- 7 P. M. Mendes, *Chem. Soc. Rev.*, 2008, **37**, 2512-2529.
- 8 Y. Tsujii, K. Ohno, S. Yamamoto, A. Goto and T. Fukuda, *Adv. Polym. Sci.*, 2006, **197**, 1-45.
- 9 S. Edmondson, V. L. Osborne and W. T. S. Huck, *Chem. Soc. Rev.*, 2004, **33**, 14-22.
- 10 S. G. Boyes, A. M. Granville, M. Baum, B. Akgun, B. K. Mirous and W. J. Brittain, *Surf. Sci.*, 2004, **570**, 1-12.
- 11 S. Minko, *Polym. Rev.*, 2006, **46**, 397-420.
- 12 R. Barbey, L. Lavanant, D. Paripovic, N. Schüwer, C. Sugnaux, S. Tugulu and H. A. Klok, *Chem. Rev.*, 2009, **109**, 5437-5527.
- 13 M. C. LeMieux, S. Peleshanko, K. D. Anderson and V. V. Tsukruk, *Langmuir*, 2007, **23**, 265-274.
- 14 B. Zhao, *Langmuir*, 2004, **20**, 11748-11755.
- 15 B. Zhao, R. T. Haasch and S. MacLaren, *J. Am. Chem. Soc.*, 2004, **126**, 6124-6134.
- 16 S. Minko, M. Müller, M. Motornov, M. Nitschke, K. Grundke and M. Stamm, *J. Am. Chem. Soc.*, 2003, **125**, 3896-3900.
- 17 P. Uhlmann, L. Ionov, N. Houbenov, M. Nitschke, K. Grundke, M. Motornov, S. Minko and M. Stamm, *Prog. Org. Coat.*, 2006, **55**, 168-174.
- 18 T. P. Russell, *Science*, 2002, **297**, 964-967.
- 19 D. Julthongpiput, Y. H. Lin, J. Teng, E. R. Zubarev and V. V. Tsukruk, *J. Am. Chem. Soc.*, 2003, **125**, 15912-15921.
- 20 L. Ionov, A. Sidorenko, M. Stamm, S. Minko, B. Zdyrko, V. Klep and I. Luzinov, *Macromolecules*, 2004, **37**, 7421-7424.
- 21 S. Minko, I. Luzinov, V. Luchnikov, M. Müller, S. Patil and M. Stamm, *Macromolecules*, 2003, **36**, 7268-7279.
- 22 N. Houbenov, S. Minko and M. Stamm, *Macromolecules*, 2003, **36**, 5897-5901.
- 23 B. Zhao, *Polymer*, 2003, **44**, 4079-4084.
- 24 S. Santer, A. Kopyshchev, H. K. Yang and J. Rühe, *Macromolecules*, 2006, **39**, 3056-3064.
- 25 J. X. Feng, R. T. Haasch and D. J. Dyer, *Macromolecules*, 2004, **37**, 9525-9537.
- 26 E. Bittrich, M. Kuntzsch, K. J. Eichhorn and P. Uhlmann, *J. Polym. Sci. Pol. Phys.*, 2010, **48**, 1606-1615.
- 27 M. Kaholek, W. K. Lee, J. X. Feng, B. LaMattina, D. J. Dyer and S. Zauscher, *Chem. Mat.*, 2006, **18**, 3660-3664.
- 28 S. B. Rahane, J. A. Floyd, A. T. Metters and S. M. Kilbey, *Adv. Funct. Mater.*, 2008, **18**, 1232-1240.
- 29 A. J. Parnell, S. J. Martin, C. C. Dang, M. Geoghegan, R. A. L. Jones, C. J. Crook, J. R. Howse and A. J. Ryan, *Polymer*, 2009, **50**, 1005-1014.
- 30 J. C. Love, L. A. Estroff, J. K. Kriebel, R. G. Nuzzo and G. M. Whitesides, *Chem. Rev.*, 2005, **105**, 1103-1169.
- 31 M. Niwa, M. Date and N. Higashi, *Macromolecules*, 1996, **29**, 3681-3685.
- 32 R. Heeb, R. M. Bielecki, S. Lee and N. D. Spencer, *Macromolecules*, 2009, **42**, 9124-9132.
- 33 D. M. Jones, A. A. Brown and W. T. S. Huck, *Langmuir*, 2002, **18**, 1265-1269.
- 34 H. Schönherr and H. Ringsdorf, *Langmuir*, 1996, **12**, 3891-3897.
- 35 H. Schönherr, H. Ringsdorf, M. Jaschke, H. J. Butt, E. Bamberg, H. Allinson and S. D. Evans, *Langmuir*, 1996, **12**, 3898-3904.

Grafting Mixed Grafts of PNIPAM and PMAA from Gold by Selective Initiation

- 36 E. M. Benetti, E. Reimhult, J. de Bruin, S. Zapotoczny, M. Textor and G. J. Vancso, *Macromolecules*, 2009, **42**, 1640-1647.
- 37 L. H. Li, Y. Zhu, B. Li and C. Y. Gao, *Langmuir*, 2008, **24**, 13632-13639.
- 38 W. Zhang, X. L. Zhu, Z. P. Cheng and J. Zhu, *J. Appl. Polym. Sci.*, 2007, **106**, 230-237.
- 39 W. Zhang, X. L. Zhu, J. Zhu and J. Y. Chen, *J. Polym. Sci. Pol. Chem.*, 2006, **44**, 32-41.
- 40 R. Nicolay, Y. Kwak and K. Matyjaszewski, *Macromolecules*, 2008, **41**, 4585-4596.
- 41 Y. Kwak, R. Nicolay and K. Matyjaszewski, *Macromolecules*, 2008, **41**, 6602-6604.
- 42 Y. Kwak and K. Matyjaszewski, *Macromolecules*, 2008, **41**, 6627-6635.
- 43 W. Tang, Y. Kwak, W. Braunecker, N. V. Tsarevsky, M. L. Coote and K. Matyjaszewski, *J. Am. Chem. Soc.*, 2008, **130**, 10702-10714.
- 44 Z. Y. Bao, M. L. Bruening and G. L. Baker, *Macromolecules*, 2006, **39**, 5251-5258.
- 45 A. J. Parnell, S. J. Martin, R. A. L. Jones, C. Vasilev, C. J. Crook and A. J. Ryan, *Soft Matter*, 2009, **5**, 296-299.
- 46 R. Dong, M. Lindau and C. K. Ober, *Langmuir*, 2009, **25**, 4774-4779.
- 47 X. F. Sui, S. Zapotoczny, E. M. Benetti, P. Schön and G. J. Vancso, *J. Mater. Chem.*, 2010, **20**, 4981-4994.
- 48 C. Dorrer and J. Rühle, *Langmuir*, 2008, **24**, 1959-1964.
- 49 M. Lemieux, D. Usov, S. Minko, M. Stamm, H. Shulha and V. V. Tsukruk, *Macromolecules*, 2003, **36**, 7244-7255.
- 50 R. R. Shah, D. Merreceyes, M. Husemann, I. Rees, N. L. Abbott, C. J. Hawker and J. L. Hedrick, *Macromolecules*, 2000, **33**, 597-605.

Chapter 5

Electrochemical Sensing by Surface-immobilized

Poly(ferrocenylsilane) Grafts

This chapter describes the fabrication of chemically modified electrodes, which were decorated with covalently tethered poly(ferrocenylsilane) (PFS) chains. Robust, relatively dense redox-active films with a height of around 10 nm were successfully formed by reaction of poly(ferrocenyl(3-iodopropyl)methylsilane) (PFS-I) with amine-terminated monolayers on silicon or gold surfaces. The electrochemical properties of the surface-immobilized PFS chains were studied using cyclic voltammetry (CV) and differential pulse voltammetry (DPV), both in aqueous and organic media. Information on the properties of these films as a function of redox state was gained using quantitative adherence measurements between the films and AFM tips. An ascorbic acid electrochemical sensor based on these surface-anchored PFS chains, exhibiting a high sensitivity and stability, was fabricated. The PFS layers described are easily derivatized, thus forming a platform for creating highly tailorable redox-active interfaces.

* Parts of this chapter have been published in: Sui, X.; Feng, X. (co-first author); Song, J.; Hempenius, M. A. and Vancso, G. J. *J. Mater. Chem.*, **2012**, 22, 11261-11267.

5.1 Introduction

This chapter reports on the formation and redox characteristics of electrodes modified by substrate-tethered redox responsive organometallic poly(ferrocenylsilane) (PFS)¹⁻⁴ chains and their use in the electrochemical detection of ascorbic acid.

Ascorbic acid, a water-soluble vitamin, is present naturally in fruits and vegetables. It is an important preservative and antioxidant agent used in food industry, pharmaceutical formulations and cosmetic applications. Thus the development of a simple and rapid method for its detection has attracted great attention.⁵⁻⁸

Electrodes chemically modified by conducting polymers, carbon nanotubes or graphene, ferrocene derivatives and other transition metal complexes play a central role in the detection of many biologically important species.⁹⁻¹³ Such chemical modifications are aimed at tailoring electrochemical responses to analytes to improve detection sensitivity, selectivity and device stability.¹⁴⁻¹⁸ In addition, chemically modified electrodes may be combined with biospecific recognition entities such as redox enzymes for the detection of e.g. glucose.¹⁹ In this case, redox-active components are often employed to serve as redox mediators, facilitating charge transfer between enzyme and electrode.

PFS, composed of alternating ferrocene and silane units in the main chain, are a fascinating class of processable materials with redox characteristics suitable for the electrochemical detection of biological analytes.^{20,21} Several reports have appeared on the formation of thin PFS films on electrode surfaces using layer-by-layer (LbL) deposition²²⁻²⁴ of PFS polyions or by solution-casting of PFS homo- or block copolymers.^{25,26} However, only a few accounts of covalently surface-tethered PFS films, including thiol end-functionalized PFS chains attached to gold by chemisorption, have been reported in the literature.^{21,27-29}

Here we describe a "grafting to" approach^{19,30} for the covalent attachment of PFS chains to an electrode surface, employing amine alkylation reactions. The fabrication of such chemically modified electrodes, decorated with stable, ultrathin redox-active films is of interest for electrochemical sensing applications. In addition to cyclic voltammetry measurements, quantitative adherence measurements between the immobilized PFS films and Atomic Force Microscopy (AFM) tips were conducted to gain further information on the behavior of the thin films in the oxidized and reduced states, respectively. An ascorbic acid electrochemical sensor based on these PFS films exhibited a high sensitivity, stable responses, and a lower detection limit below 5 μM which is comparable to other reported ascorbic acid sensors.³¹ The grafted-to layers described here are readily derivatized further and can therefore be regarded as a versatile platform for creating tailor-made redox-active interfaces.

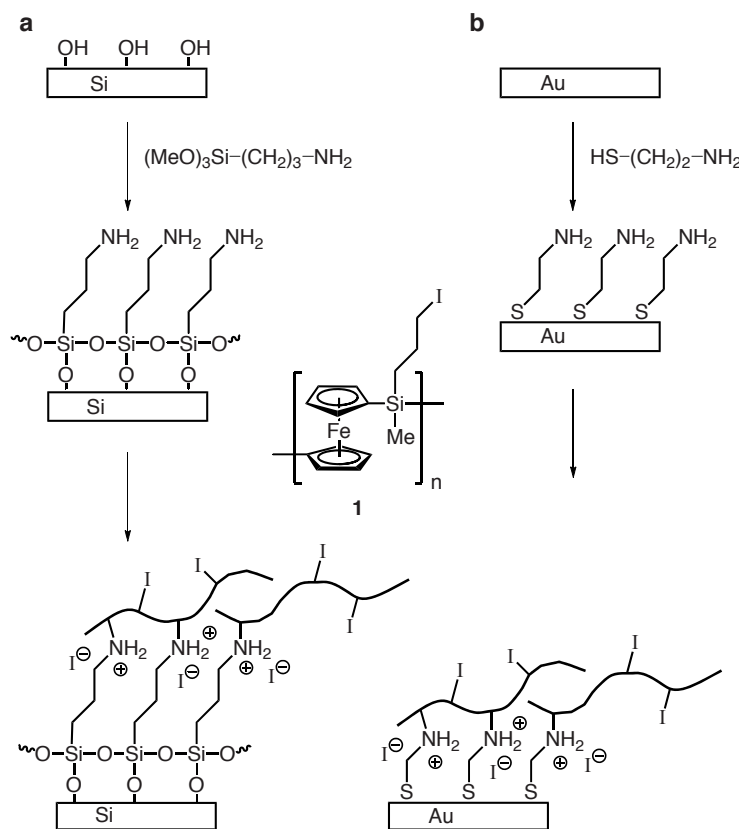


Figure 5.1 Schematic representation of the covalent surface-attachment of PFS chains, (a) on a silicon substrate and (b) on a gold substrate.

5.2 Results and discussion

5.2.1 Preparation of PFS grafts

Surface grafted PFS layers were obtained in two steps: firstly, an amine-terminated monolayer was formed, then poly(ferrocenyl(3-iodopropyl)methylsilane) (PFS-I) was covalently bound onto the surface by amination of the PFS side groups at 50 °C (Figure 5.1). Control experiments were carried out to study the stability of PFS-I. A TGA study (Figure 5.2) showed that PFS-I remained thermally stable up to 250 °C.

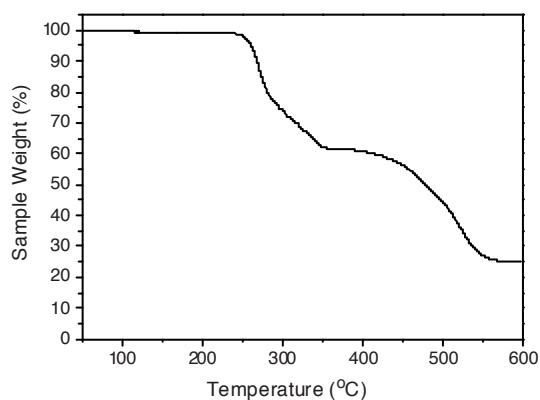


Figure 5.2 Thermogravimetric analysis of PFS-I.

The integrity of the surface-bound PFS layer was investigated electrochemically as the desorption of physisorbed, non-covalently bound PFS chains is easily monitored in this way. Cyclic voltammograms were recorded before and after soaking a covalently bound PFS film and an inert poly(ferrocenyldimethylsilane) (PFDMs) film in THF (Figure 5.3). The voltammogram observed for PFS-I grafts showed no change prior to, and following soaking in THF, providing evidence that PFS-I forms a stable layer²¹ on amine functionalized gold surfaces. For the physisorbed, non-reactive PFDMs, no appreciable current signal was found.

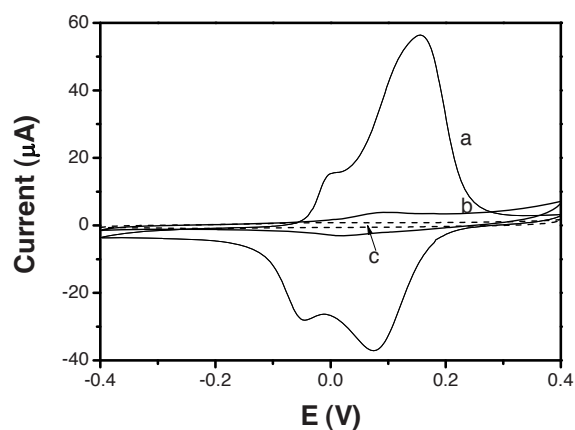


Figure 5.3 Cyclic voltammogram of a) PFS-I covalently bound to an amine-terminated (cysteamine) SAM on gold; b) PFDMs on the gold substrate with the cysteamine SAM; c) bare gold in 0.1 M NaClO₄ with Pt wires as the reference and counter electrode. All the substrates were soaked in THF overnight before measurements.

Since substrate anchoring occurs through the PFS side groups, the layer is envisaged to be composed of tethered polymer strands of varying length with some

fraction of polymer loops. The surface morphology and film height were imaged by tapping mode AFM (Figure 5.4). In the dry state, the PFS films showed a uniform thickness of 9 nm on silicon substrates.³² SEM images also confirmed this film thickness and the uniformity of the PFS layer over larger areas (Figure 5.5).

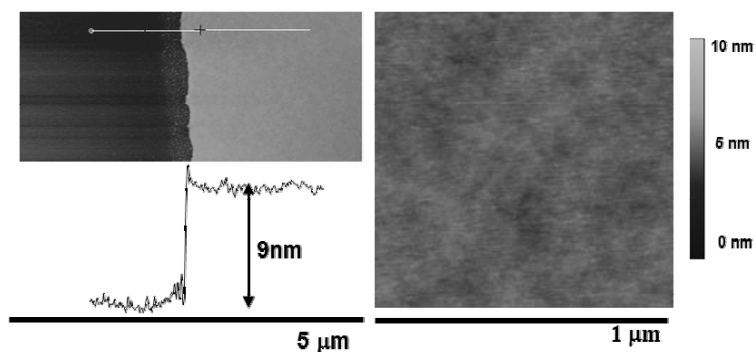


Figure 5.4 Height image and surface morphology of the PFS film immobilized on silicon.

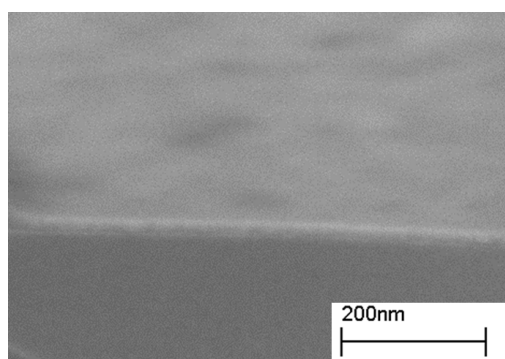


Figure 5.5 SEM image of the covalently anchored PFS film on silicon.

FTIR was used to verify the presence of PFS chains on the gold surface (Figure 5.6). The spectra for the surface-bound PFS and PFS-I in bulk showed similar absorptions in both the high energy (C-H stretch peaks belonging to the ferrocene rings, 3087 cm^{-1}) and the low energy regions (asymmetric ring in-plane vibration for ferrocene, 1165 cm^{-1} and the out-of-plane C-H vibration for ferrocene, 1037 cm^{-1}).²⁸

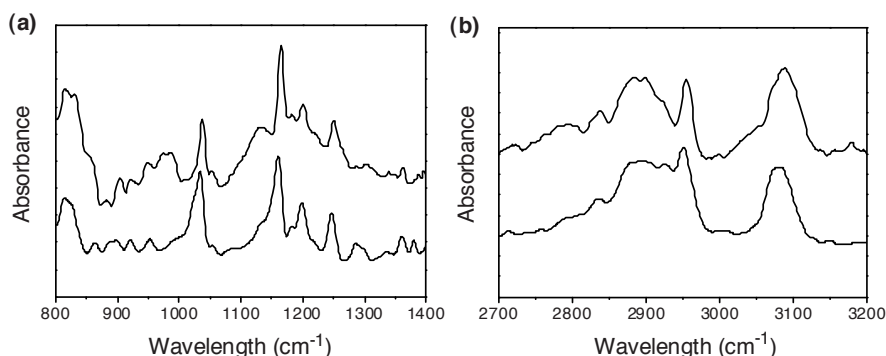


Figure 5.6 FTIR spectra of PFS-I in bulk (bottom) and PFS grafts (top) on gold; (a) low energy region; (b) high energy region.

Static contact angles for water were measured to gauge the efficiency of the PFS anchoring step. On gold substrates, the contact angle changed from 60° for the amine-terminated monolayer to 90° after attachment of the PFS chains, confirming the formation of a hydrophobic layer. The surface coverage of ferrocene units was calculated to be 3.8×10^{-9} mol cm^{-2} from electrochemical measurements, which is a factor of 1.5 to 1.8 higher than previously found for "grafting to" layers formed from thiol end-functionalized PFDMS chains of varying molar mass.^{28,29} These results indicate that thin, uniform, relatively dense PFS films were introduced by covalent attachment to gold and silicon substrates.

5.2.2 Electrochemical properties of PFS grafts

The electrochemical properties of the PFS films were investigated by cyclic voltammetry (CV) and differential pulse voltammetry (DPV) in water and organic solvent. Figure 5.7 shows the results in 0.1 M aqueous NaClO_4 with a potential range between -0.4 and 0.4 V *versus* the reference electrode. The double-wave voltammogram (Figure 5.7a) indicates that repulsive interactions exist between the neighboring ferrocene units along the PFS chain.³³ A DPV curve, recorded after performing the CV measurements, is shown in Figure 5.7b. The best fit of the area under the DPV curve was obtained by considering multiple oxidation events where oxidation potentials are influenced by intra- and interchain interactions and also by the distance of the redox centers to the electrode surface. In this case, an accurate fit was obtained by using a peak area ratio of 1:1.2:2.

When immersed in aqueous NaClO_4 , the hydrophobic PFS chains will be in a collapsed state. Our experimental results show that in the first oxidation step a quarter of the ferrocene units are oxidized, probably predominantly those that are in close

proximity to the gold surface. Another quarter of the remaining Fe atoms are oxidized if a higher potential is applied. The electrochemical oxidation is completed if the potential is increased further. This behaviour is in accordance with that of end-grafted PFDMS chains on gold.²⁸

In order to probe the reversibility of the redox process, the separation between the anodic peak potential (E_{pox}) and cathodic peak potential (E_{pred}), ΔE ($\Delta E(1) = E_{\text{pox1}} - E_{\text{pred1}}$, $\Delta E(2) = E_{\text{pox2}} - E_{\text{pred2}}$) was plotted with the scan rate (Figure 5.7c). A reversible one electron transfer should exhibit a ΔE of 59 mV.³⁴ In aqueous NaClO_4 , the surface-bound PFS layers display electrochemical reversibility up to a scan rate of 30 mV s^{-1} for $\Delta E(2)$, and 100 mV s^{-1} or higher for $\Delta E(1)$. This is consistent with previous findings.²⁸ Peak currents plotted against scan rate are shown in Figure 5.7d. Linear dependencies were found for all oxidation and reduction peaks which is characteristic for surface-confined electroactive layers.³⁴

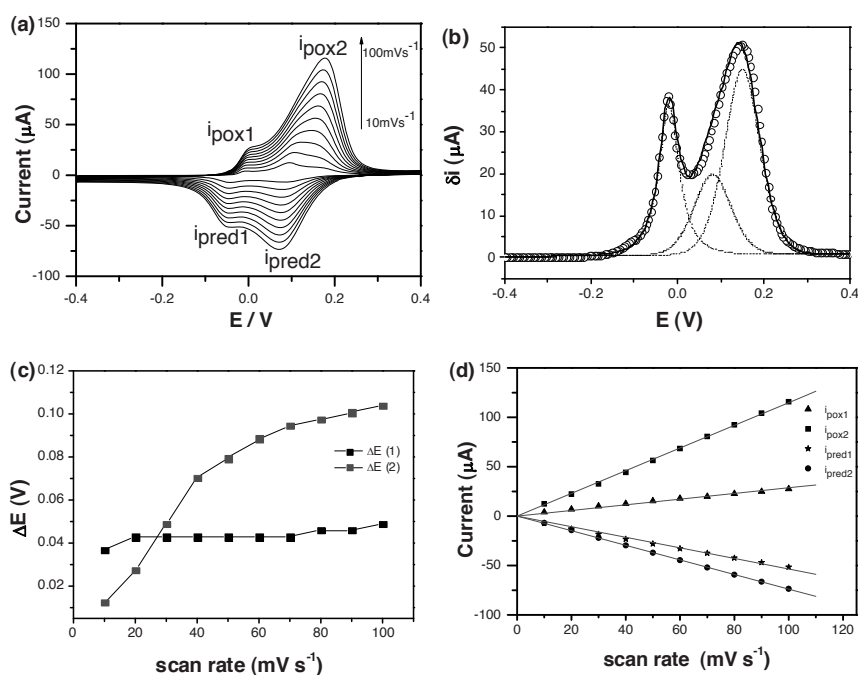


Figure 5.7 (a) CVs of PFS films immobilized on gold at different scan rates (in 0.1 M aqueous NaClO_4 , Pt reference and counter electrode); (b) DPV recorded for these PFS films (scan rate 5 mV/s), the line with open circles represents the measured data; the dashed lines are fitted curves; (c) ΔE versus scan rate; (d) plots of peak current i_p versus scan rate.

As is well-known, swellability of surface-confined redox-active polymer films in the medium used for cyclic voltammetry greatly facilitates the diffusion of solvated electrolyte ions into the film, which strongly influences electrode processes in the

film.³⁵ Electrochemical studies on the immobilized PFS films were also performed in CH_2Cl_2 , a good solvent for PFS, using 0.1 M NBu_4PF_6 as supporting electrolyte. The shape of the cyclic voltammograms obtained (Figure 5.8a) is clearly different from those recorded in aqueous electrolyte. The area under the DPV curve (Figure 5.8b) was again fitted using multiple oxidation waves, in this case a peak area ratio of 1:1:1 gave the best fit result.

The swollen grafts in CH_2Cl_2 provide a higher electrolyte permeability and lower diffusion resistivity, leading to readily accessible electroactive centers on the PFS chains and an increased homogeneity within the redox-active film. Compared to Figure 5.7, we can conclude that the oxidation reaction of PFS appears to be particularly sensitive to its solvation in the electrolyte medium. In Figure 5.8c, both $\Delta E(1)$ and $\Delta E(2)$ showed electrochemical reversibility with scan rates of up to 100 mV s^{-1} or higher. Peak currents plotted against scan rate showed a linear dependence and the $i_{\text{pox}}/i_{\text{pred}}$ ratio was close to unity. These characteristics indicated that the redox process on these electrodes was controlled by charge-transfer kinetics¹¹ and confirmed that PFS grafts were immobilized on the gold surface.

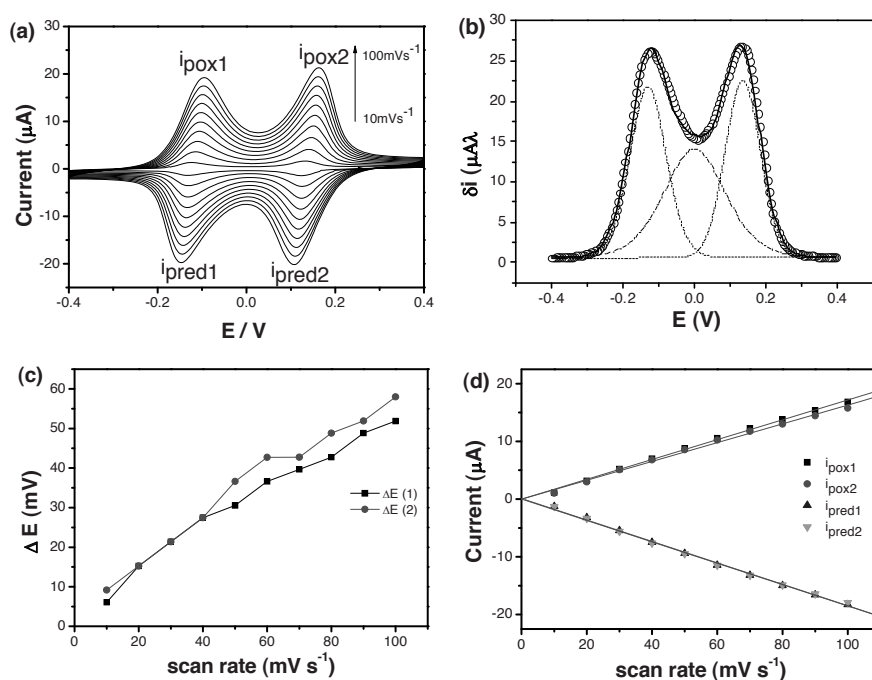


Figure 5.8 (a) CVs for PFS grafts on gold at different scan rates (in 0.1 M NBu_4PF_6 in CH_2Cl_2 , Pt reference and counter electrode); (b) DPV recorded for the tethered PFS chains (scan rate 5 mV/s), the line with open circles represents the measured data; the dashed lines are fitted curves. (c) ΔE versus scan rate; (d) plots of peak current i_p versus scan rate.

The electrochemical stability of PFS films was examined by successive potential cycling in both aqueous and CH_2Cl_2 media from -0.4 to $+0.4$ V *versus* Pt with a potential sweep rate of 50 mV s^{-1} . The peaks in the CVs were unchanged and reproducible after 20 potential cycles (Figure 5.9). Clearly, no PFS chains desorbed from the substrate surface.

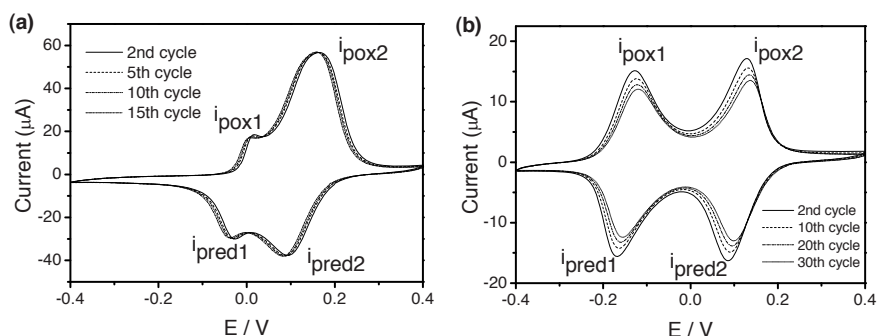


Figure 5.9 Cyclic voltammograms of PFS grafts on gold at different scan rates, Pt reference and counter electrode. (a) In aqueous NaClO_4 (0.1 M); (b) in CH_2Cl_2 containing NBu_4PF_6 (0.1 M).

To gain further information on the influence of the oxidation state on the properties of the surface-anchored films, the adherence between the PFS grafts and an AFM tip was assessed by electrochemical Atomic Force Microscopy (ECAFM).³⁶⁻³⁹ Force measurements were performed in 0.1 M NaClO_4 aqueous solution at room temperature, using a standard Si_3N_4 tip.

A representative set of pull-off force distributions in form of force histograms obtained at different applied potentials is presented in Figure 5.10. With the PFS film in the neutral state, the average of the distribution of the observed pull-off forces is clearly higher than for films in the oxidized state. As untreated silicon nitride tips have a hydrophobic surface,^{36,40,41} they will interact more strongly with PFS films in the unoxidized state. The lower adhesion force measured between the AFM tip and the oxidized PFS film provides evidence of the increased hydrophilicity of the film upon oxidation.

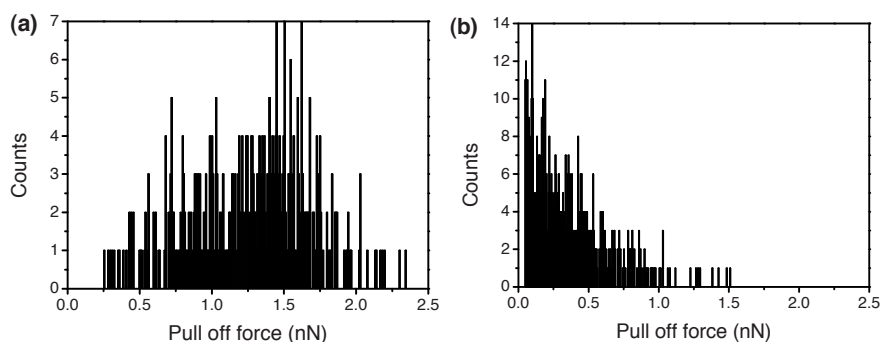


Figure 5.10 Histogram of pull-off force recorded for a reduced (a) and oxidized (b) PFS-layer in 0.1 M aqueous NaClO_4 . The applied electrochemical potential was -0.05 V(a) and $+0.65$ V(b) vs Ag electrode.

5.2.3 Electrochemical sensing of ascorbic acid

The PFS-decorated gold substrates are of interest as the active component in electrochemical sensors. Figure 5.11 shows the electrocatalytic responses of bare gold (Figure 5.11a) and of a PFS layer on gold (Figure 5.11b) in 0.1 M aqueous NaClO_4 , in the presence and absence of 0.6 mM ascorbic acid. The PFS-modified electrode showed a quasi-reversible redox response in the absence of ascorbic acid.

The bare gold electrode showed only a redox wave corresponding to ascorbic acid oxidation.⁴² For the gold electrode modified with PFS grafts, however, upon ascorbic acid oxidation, the CV displayed a well-defined peak around $+0.34$ V (vs Pt) and greatly enhanced peak currents. This behavior shows that the immobilized PFS films on gold can effectively catalyze the oxidation of ascorbic acid. The defined amperometric response forms the basis for the use of these PFS films in electrochemical sensor applications.

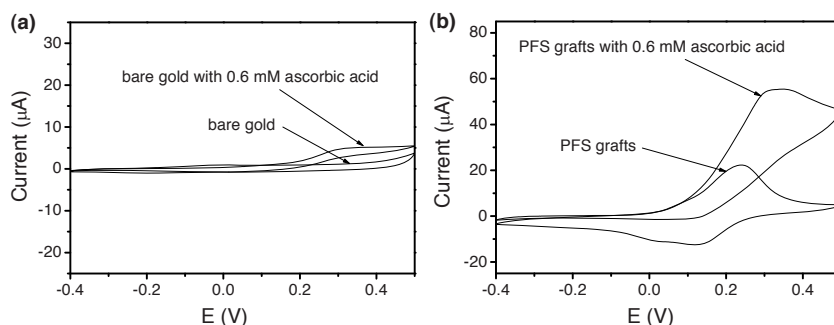


Figure 5.11 Cyclic voltammogram of bare gold (a) and modified electrode (b) in the absence and presence of 0.6 mM ascorbic acid in 0.1 M NaClO_4 aqueous solution. Scan rate is 50 mV/s, Pt wires were used as the reference and counter electrode.

The amperometric response of the modified electrode to successive additions of ascorbic acid was evaluated by applying a fixed potential of +0.3 V. The current-time curve shown in Figure 5.12 indicates that the PFS films show a rapid response and high sensitivity. The nearly equal current steps observed for each addition reflect a stable and predictable catalytic activity. A linear relationship between oxidation current and ascorbic acid concentration was obtained up to 40 μM . At high ascorbic acid concentrations a deviation from the straight line was observed. This deviation is likely attributed to the rate of ascorbic acid delivery to the electroactive sites.⁴³ Similar deviations from linearity have been observed in the literature for other amperometric biosensors.^{44,45} Overall, the ascorbic acid electrochemical sensor based on these PFS films exhibits a high sensitivity, stable responses, and a low detection limit which compares favorably to other reported ascorbic acid sensors based on ferrocene derivatives.⁴⁶⁻⁴⁹

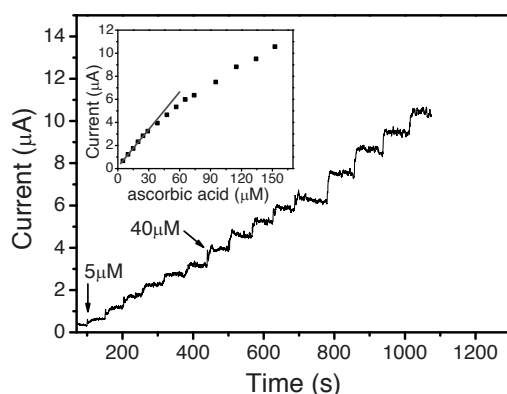


Figure 5.12 Amperometric response of the sensor to successive additions of ascorbic acid into stirred aqueous 0.1 M NaClO_4 at room temperature, Pt wires were used as reference and counter electrode. The first six additions increased the concentration of ascorbic acid by 5 μM each, later each injection increased the concentration by 10 μM . The inset was the calibration curve. Applied potential = 0.3 V ($R=0.99908$).

5.3 Conclusions

The present study demonstrates a novel approach to the development of electrochemical sensors based on surface-immobilized PFS chains. Surface-anchored PFS films were formed by an alkylation reaction of an amine monolayer on silicon or gold surfaces with PFS chains featuring iodopropyl side groups. AFM and SEM measurements showed the formation of thin, relatively dense PFS films. The electrochemical properties of these films were studied both in water and in methylene chloride. In a good solvent which could swell the films, such as CH_2Cl_2 , a more

reversible redox behaviour was observed than in water. Due to the covalent anchoring, PFS chains remained on the substrate during repeated redox cycling. Furthermore, adherence between Si_3N_4 tips and the immobilized PFS films was assessed by ECAFM to gain information on the hydrophobicity / hydrophilicity of the films as a function of redox state. A higher adhesion was found when the PFS film was in the reduced state, which can be attributed to a stronger interaction with the hydrophobic untreated Si_3N_4 tip. The PFS films exhibited a high sensitivity and stable responses to ascorbic acid, which renders these films of interest in electrochemical sensing. The anchored PFS chains possess unreacted iodopropyl side groups which are readily derivatized into a range of functionalities including cationic, anionic, hydrophilic, hydrophobic etc. moieties. These robust redox-active films, possessing tunable characteristics, therefore constitute a highly versatile platform for the chemical modification of electrodes.

5.4 Experimental

Materials:

Poly(ferrocenyl(3-iodopropyl)methylsilane) (PFS-I) (1) (M_w : 3.7×10^5 g/mol, M_n : 1.7×10^5 g/mol, M_w/M_n : 2.1)⁵⁰ and poly(ferrocenyldimethylsilane) (PFDMS)⁵¹ were prepared according to established procedures. (3-Aminopropyl)trimethoxysilane, cysteamine, polyethyleneimine, sodium perchlorate (NaClO_4), tetrabutylammonium hexafluorophosphate (NBu_4PF_6), dichloromethane (CH_2Cl_2) and ascorbic acid were used as received. Tetrahydrofuran (THF) was purified by distillation from sodium-benzophenone under argon. All water used in the experiments was Milli-Q grade.

Formation of (3-aminopropyl)trimethoxysilane SAMs:

Silicon substrates were first cleaned with Piranha solution, then rinsed extensively with water and ethanol. *Caution: Piranha solution reacts violently with many organic materials and should be handled with great care!* The dried substrates were placed at the bottom of a desiccator, around a vial containing 100 μL of (3-aminopropyl)trimethoxysilane. The desiccator was then evacuated by a rotary vane pump for 10 min and subsequently closed. Vapor phase silanization was allowed to proceed overnight. The substrates were then rinsed with ethanol, dried in a stream of N_2 and immediately used for PFS attachment.

Formation of cysteamine SAMs:

Gold substrates were cleaned with Piranha solution, and extensively rinsed with water, ethanol and dichloromethane. Cysteamine SAMs were prepared by immersing gold substrates in ethanol solutions, containing 1% cysteamine, for 16 h. The

substrates were then rinsed with ethanol, dried in a stream of N₂ and immediately used for PFS anchoring.

Attachment of PFS chains to amine-terminated SAMs:

A solution of PFS-I (1) in THF (10 mg/mL, 50 μL) was deposited on the functionalized silicon or gold substrate surfaces. Another 50 μL of PFS-I solution was added onto the surface after 30 min. Then the substrates were left to react overnight at 50 °C in a vacuum oven. The PFS-I modified substrates were soaked three times in THF for 30 min to remove physisorbed polymer chains.

Characterization:

Static contact angle measurements were performed by the sessile drop technique using an optical contact angle device equipped with an electronic syringe unit (OCA15, Dataphysics, Germany). The sessile drop was deposited onto the surface of the materials with the syringe, and the drop contour was fitted by the Young-Laplace method. At least three different measurements of each sample were performed.

The thermal stability of samples was examined on a Perkin Elmer Thermo Gravimetric Analyzer (TGA 7, Waltham, MA, U.S.A.) with a heating rate of 20 °C/min from 50 to 600 °C under a nitrogen atmosphere. All samples were dried under vacuum for 24 h prior to TGA measurements.

Grazing angle Fourier transform infrared spectroscopy was employed to establish which groups are present in the tethered films after substrate anchoring. FTIR spectra were obtained using a Bruker Vertex 70v spectrometer. A background spectrum was obtained by scanning a clean gold substrate.

A Dimension D3100 (Digital Instruments, Veeco-Bruker, Santa Barbara, CA) was operated in tapping mode to obtain the thickness and surface morphology of the PFS graft layers.

SEM images of PFS films were captured with a HR-LEO 1550 FEF SEM instrument.

Cyclic voltammetry (CV) and differential pulse voltammetry (DPV) were carried out with PFS films on gold substrates in aqueous NaClO₄ (0.1 M) or NBu₄PF₆ in CH₂Cl₂ (0.1 M) using an Autolab PGSTAT 10 electrochemical workstation (Ecochemie, Utrecht, The Netherlands). Cyclic voltammograms were recorded between -0.4 V and +0.4 V at different scan rates, using a Pt reference electrode and a Pt counter electrode. The amperometric sensing of ascorbic acid was performed by using the immobilized PFS films as the working electrode and aqueous NaClO₄ (0.1 M) as the electrolyte, the potential was set at 0.3 V for a certain time to stabilize the current. Successively, ascorbic acid-water solution was added to the sensing system and mixed

under magnetic stirring to form a homogenous solution with a controlled concentration. Simultaneously, the current response was recorded.

A NanoScope IVa scanning probe microscope (Veeco-Digital Instruments (DI), Santa Barbara, CA) with standard Si₃N₄ tips was used in combination with an Autolab PGSTAT10 potentiostat. The AFM was connected to an external potentiostat. The electrochemical measurements were carried out using a three-electrode arrangement. The gold substrate with immobilized PFS chains was used as the working electrode. The reference (Ag wire) and counter (Pt wire) electrodes were mounted through the holes of the AFM electrochemical liquid cell. An electrolyte was injected or drained through the inlet or the outlet of the liquid cell. Cyclic voltammograms were recorded between (-0.05 V vs Ag) and (0.65 V vs Ag) with a scan rate of 50 mV/s. Prior to the experiments, the electrolyte was degassed by purging the solution with nitrogen gas for 5 min. The cantilever was calibrated after a given experiment by measuring the thermal excitation of the tip to compute its spring constant. Adhesion force curves were collected at a ramp size of 500 nm and scan rate of 1 Hz.

5.5 References and notes

- 1 I. Manners and A. S. Abd-El-Aziz, *Frontiers in transition metal-containing polymers*, John Wiley and Sons, Hoboken, New Jersey, 2007.
- 2 G. R. Whittell and I. Manners, *Adv. Mater.*, 2007, **19**, 3439-3468.
- 3 V. Bellas and M. Rehahn, *Angew Chem. Int. Edit*, 2007, **46**, 5082-5104.
- 4 X. F. Sui, L. van Ingen, M. A. Hempenius and G. J. Vancso, *Macromol. Rapid Commun.*, 2010, **31**, 2059-2063.
- 5 C. J. Weng, Y. S. Jhuo, Y. L. Chen, C. F. Feng, C. H. Chang, S. W. Chen, J. M. Yeh and Y. Wei, *J. Mater. Chem.*, 2011, **21**, 15666-15672.
- 6 A. Bossi, S. A. Piletsky, E. V. Piletska, P. G. Righetti and A. P. F. Turner, *Anal. Chem.*, 2000, **72**, 4296-4300.
- 7 N. Malashikhina and V. Pavlov, *Biosens. Bioelectron.*, 2012, **33**, 241-246.
- 8 D. W. Kimmel, G. LeBlanc, M. E. Meschievitz and D. E. Cliffel, *Anal. Chem.*, 2012, **84**, 685-707.
- 9 E. Lorenzo, F. Pariente, L. Hernandez, F. Tobalina, M. Darder, Q. Wu, M. Maskus and H. D. Abruna, *Biosens. Bioelectron.*, 1998, **13**, 319-332.
- 10 N. G. Shang, P. Papakonstantinou, M. McMullan, M. Chu, A. Stamboulis, A. Potenza, S. S. Dhessi and H. Marchetto, *Adv. Funct. Mater.*, 2008, **18**, 3506-3514.
- 11 T. Kondo, H. Hoshi, K. Honda, Y. Einaga, A. Fujishima and T. Kawai, *J. Phys. Chem. C*, 2008, **112**, 11887-11892.
- 12 B. Fabre, S. Ababou-Girard, P. Singh, J. Kumar, S. Verma and A. Bianco, *Electrochem. Commun.*, 2010, **12**, 831-834.
- 13 W. J. Hong, H. Bai, Y. X. Xu, Z. Y. Yao, Z. Z. Gu and G. Q. Shi, *J. Phys. Chem. C*, 2010, **114**, 1822-1826.
- 14 S. Liu, J. Q. Tian, L. Wang, Y. L. Luo and X. P. Sun, *Analyst*, 2011, **136**, 4898-4902.
- 15 G. Krishnamoorthy, E. T. Carlen, H. L. deBoer, A. van den Berg and R. B. M. Schasfoort, *Anal. Chem.*, 2010, **82**, 4145-4150.

- 16 O. Azzaroni, M. Mir, M. Alvarez, L. Tiefenauer and W. Knoll, *Langmuir*, 2008, **24**, 2878-2883.
- 17 N. Carolan, R. J. Forster and C. O'Fagain, *Bioconjugate Chem.*, 2007, **18**, 524-529.
- 18 A. M. Yu, Z. J. Liang, J. H. Cho and F. Caruso, *Nano Lett.*, 2003, **3**, 1203-1207.
- 19 T. K. Tam, J. Zhou, M. Pita, M. Ornatska, S. Minko and E. Katz, *J. Am. Chem. Soc.*, 2008, **130**, 10888-10889.
- 20 J. Song and G. J. Vancso, *Langmuir*, 2011, **27**, 6822-6829.
- 21 M. Péter, R. G. H. Lammertink, M. A. Hempenius, M. van Os, M. W. J. Beulen, D. N. Reinhoudt, W. Knoll and G. J. Vancso, *Chem. Commun.*, 1999, 359-360.
- 22 M. A. Hempenius, M. Péter, N. S. Robins, E. S. Kooij and G. J. Vancso, *Langmuir*, 2002, **18**, 7629-7634.
- 23 Y. J. Ma, W. F. Dong, E. S. Kooij, M. A. Hempenius, H. Möhwald and G. J. Vancso, *Soft Matter*, 2007, **3**, 889-895.
- 24 M. A. Hempenius, N. S. Robins, R. G. H. Lammertink and G. J. Vancso, *Macromol. Rapid Comm.*, 2001, **22**, 30-33.
- 25 X. J. Wang, L. Wang, J. J. Wang and T. Chen, *Electrochimica Acta*, 2007, **52**, 3941-3949.
- 26 T. Chen, L. Wang, G. H. Jiang, J. J. Wang, X. C. Dong, X. J. Wang, J. F. Zhou, C. L. Wang and W. Wang, *J. Phys. Chem. B*, 2005, **109**, 4624-4630.
- 27 M. Péter, M. A. Hempenius, E. S. Kooij, T. A. Jenkins, S. J. Roser, W. Knoll and G. J. Vancso, *Langmuir*, 2004, **20**, 891-897.
- 28 M. Péter, R. G. H. Lammertink, M. A. Hempenius and G. J. Vancso, *Langmuir*, 2005, **21**, 5115-5123.
- 29 S. Zou, Y. J. Ma, M. A. Hempenius, H. Schönherr and G. J. Vancso, *Langmuir*, 2004, **20**, 6278-6287.
- 30 T. K. Tam, G. Strack, M. Pita and E. Katz, *J. Am. Chem. Soc.*, 2009, **131**, 11670-11671.
- 31 A. Malinauskas, R. Garjonyte, R. Mazeikiene and I. Jureviciute, *Talanta*, 2004, **64**, 121-129.
- 32 T. K. Tam, M. Pita, O. Trotsenko, M. Motornov, I. Tokarev, J. Halamek, S. Minko and E. Katz, *Langmuir*, 2010, **26**, 4506-4513.
- 33 R. Rulkens, A. J. Lough, I. Manners, S. R. Lovelace, C. Grant and W. E. Geiger, *J. Am. Chem. Soc.*, 1996, **118**, 12683-12695.
- 34 A. J. Bard and L. R. Faulkner, *Electrochemical Methods: Fundamentals and Applications*, Wiley, 2001.
- 35 X. J. Wang, L. Wang, J. J. Wang and T. Chen, *J. Phys. Chem. B*, 2004, **108**, 5627-5633.
- 36 H. J. Chung, J. Song and G. J. Vancso, *Appl. Surf. Sci.*, 2009, **255**, 6995-6998.
- 37 G. K. Rowe and S. E. Creager, *Langmuir*, 1991, **7**, 2307-2312.
- 38 J. E. Hudson and H. D. Abruna, *J. Am. Chem. Soc.*, 1996, **118**, 6303-6304.
- 39 L. L. Norman and A. Badia, *J. Am. Chem. Soc.*, 2009, **131**, 2328-2337.
- 40 S. H. Xu and M. F. Arnsdorf, *P. Natl. Acad. Sci. USA*, 1995, **92**, 10384-10388.
- 41 Cleaning procedures may influence the surface hydrophobicity/ hydrophilicity of Si₃N₄ tips. By cleaning with piranha, negative charges may be introduced at the tip surface.
- 42 G. P. Keeley, A. O'Neill, N. McEvoy, N. Peltekis, J. N. Coleman and G. S. Duesberg, *J. Mater. Chem.*, 2010, **20**, 7864-7869.
- 43 H. Razmi and M. Harasi, *Int. J. Electrochem. Sc.*, 2008, **3**, 82-95.
- 44 V. S. Tripathi, V. B. Kandimalla and H. X. Ju, *Biosens. Bioelectron.*, 2006, **21**, 1529-1535.
- 45 Z. B. Zhang, S. J. Yuan, X. L. Zhu, K. G. Neoh and E. T. Kang, *Biosens. Bioelectron.*, 2010, **25**, 1102-1108.
- 46 J. B. Raoof, R. Ojani and A. Kiani, *J. Electroanal. Chem.*, 2001, **515**, 45-51.

Chapter 5

- 47 M. H. Pournaghi-Azar and R. Ojani, *Talanta*, 1995, **42**, 1839-1848.
- 48 B. Kazakevičienė, G. Valincius, G. Niaura, Z. Talaikytė, M. Kažemėkaitė, V. Razumas, D. Plaušinitis, A. Teišerskienė and V. Lisauskas, *Langmuir*, 2007, **23**, 4965-4971.
- 49 S. F. Wang and D. Du, *Sens. Actuator B-Chem.*, 2004, **97**, 373-378.
- 50 M. A. Hempenius, F. F. Brito and G. J. Vancso, *Macromolecules*, 2003, **36**, 6683-6688.
- 51 P. Gomez-Elipe, R. Resendes, P. M. Macdonald and I. Manners, *J. Am. Chem. Soc.*, 1998, **120**, 8348-8356.

Chapter 6

Preparation of a Rapidly Forming Poly(ferrocenylsilane)-

Poly(ethylene glycol)-based Hydrogel *via* Thiol-Michael

Addition Click Reaction

In this chapter, a rapidly forming redox responsive poly(ferrocenylsilane)-poly(ethylene glycol) (PFS-PEG)-based hydrogel was synthesized *via* thiol-Michael addition click reaction. PFS bearing acrylate side groups (PFS-acryl) was synthesized by side group modification of poly(ferrocenyl(3-iodopropyl)methylsilane) (PFS-I) (previously described in Chapter 5) and characterized with ^1H NMR, ^{13}C NMR and FTIR spectroscopies. Poly(ethylene glycol)dithiol (PEG-dithiol) was selected as the thiol cross-linker. The equilibrium swelling ratio, morphology, rheology and redox responsive properties of the PFS-PEG-based hydrogel were reported.

* Parts of this chapter have been published in: Sui, X.; van Ingen, L.; Hempenius, M. A. and Vancso, G. J. *Macromol. Rapid Comm.*, **2010**, 31, 2059-2063.

6.1 Introduction

Poly(ferrocenylsilane) (PFS) chains are composed of alternating ferrocene and silane units and can be reversibly oxidized and reduced by chemical and electrochemical means.¹⁻⁵ This organometallic polymer has received considerable attention due to its interesting optical, electronic and magnetic properties.¹ Although most of these studies involve linear, uncross-linked chains, it has been shown that cross-linking imparts further novel and useful characteristics to these organometallic polymers.⁴ For example, by introducing cross-linking chains, the ceramic yield of PFS can be increased dramatically, which leads to shaped ceramics with tunable magnetic properties.⁶ In the presence of solvents, these organometallic networks swell to form gels which show stimulus-responsive properties. PFS networks that swell in organic solvents have been prepared by various methods: thermal cross-linking,^{7,8} photopolymerization,⁹ thiol-ene addition¹⁰ or hydrolysis of PFS ethoxysilane derivatives.¹¹ These gels have been used to fabricate polychromic metallopolymer gel photonic crystals and displays.¹²⁻¹⁴

Hydrogels are crosslinked polymeric networks which absorb and retain large amounts of water. Stimulus-responsive hydrogels are highly attractive materials for use in specific areas ranging from biomedical to actuator applications.¹⁵⁻²² Although the preparation of PFS-based gels has been widely investigated, the hydrogels and their responsive behavior have received little attention. Recently our group reported on the synthesis and characterization of the first PFS-based hydrogel. Two distinct types of PFS polyion network, featuring permanent positively or negatively charged side groups, were successfully prepared using covalent cross-linking approaches.^{4,15} These PFS polyelectrolyte hydrogels have a high water swelling ratio and show reversible redox responsive behavior.

Here, we report the rapid formation of a PFS-based hydrogel by the thiol-Michael addition click reaction. Thiol-Michael polymer networks have significant advantages over traditional polymer networks as they form rapidly and quantitatively under ambient conditions and are insensitive to the presence of water and oxygen, resulting in uniform polymer networks.¹⁶⁻¹⁸ PFS featuring acrylic side groups⁹ was chosen as the redox-responsive component and poly(ethylene glycol)dithiol (PEG-dithiol) was selected as the thiol cross-linker due to its excellent water solubility and proven biocompatibility.^{19,20} The equilibrium swelling ratio, morphology, rheology and redox responsive properties of the PFS-PEG-based hydrogel were investigated.

PFS-PEG-based Hydrogel *via* Thiol–Michael Addition Click Reaction

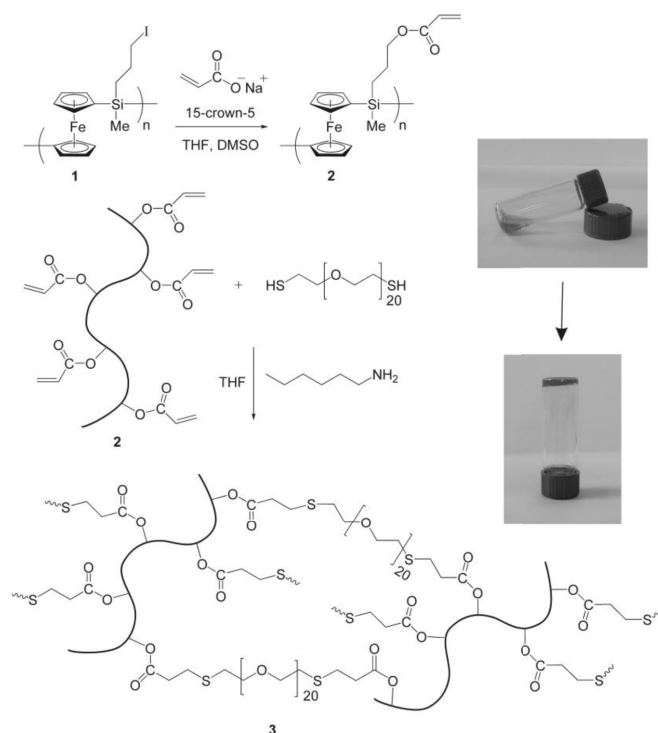


Figure 6.1 Schematic representation of the synthesis of PFS-PEG-based hydrogel and photographs of the gel formation.

6.2 Results and discussion

6.2.1 Synthesis and characterization of PFS-acryl

The synthesis of PFS bearing acrylate side groups is outlined in Figure 6.1. The iodo groups of PFS-I are easily replaced by a variety of nucleophiles under mild conditions.^{21,22} A weak nucleophile, sodium acrylate, could be attached in the presence of the crown ether 15-crown-5 with quantitative conversion. The formation of PFS with acrylate side groups (PFS-acryl) was confirmed by ¹H NMR, ¹³C NMR and FTIR spectroscopies. Figure 6.2 shows the ¹H NMR spectra of polymers PFS-I and PFS-acryl in CDCl₃. The peak at 3.2 ppm (-CH₂I) in the NMR spectrum of PFS-I disappeared in the NMR spectrum of PFS-acryl, and a new signal appeared at 4.15 ppm (-CH₂O(C=O)-C=C) in the spectra of PFS-acryl, indicating complete conversion. Integration values of the double bond peaks (5.81-6.43 ppm, 3H) matched with those of the methyl group at silicon (0.41 ppm) in the PFS main chain, confirming the full conversion of PFS-I into PFS-acryl. Figure 6.3 displays the FTIR spectra for PFS-I (a)

and PFS-acryl (b). The stretching vibration of the carbonyl group in the acrylate moiety appeared at 1718 cm^{-1} and the C-C double bond appeared at 1638 cm^{-1} for PFS-acryl. However, these peaks were absent in the IR spectrum of its precursor, which indicates that the acrylate group was successfully introduced.

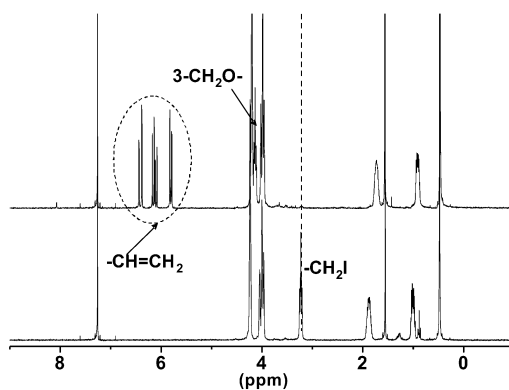


Figure 6.2 ^1H NMR spectra and the assignments of PFS-I (bottom) and PFS-acryl (top).

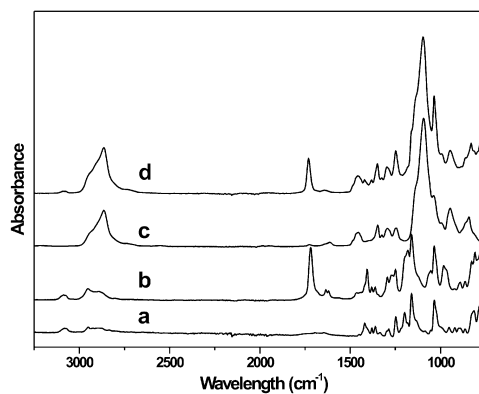


Figure 6.3 FTIR spectra of (a) PFS-I, (b) PFS-acryl, (c) PEG-dithiol and (d) PFS-PEG-based hydrogel.

6.2.2 Formation of PFS-PEG hydrogel

Acrylate moieties are known to react rapidly with thiols by the thiol-Michael addition click reaction.¹⁶ A mixture of acrylate bearing PFS and PEG-dithiol formed a gel within 30 s upon addition of 1-hexylamine (Figure 6.1). FTIR spectra of the PFS-PEG-based hydrogel (Figure 6.3d) display characteristic peaks for both PFS (774 , 1035 cm^{-1}) and PEG (1098 cm^{-1}). The spectra also show the disappearance of the C-

C double bond signal at 1638 cm^{-1} and a characteristic shift in the carbonyl stretch from 1718 to 1731 cm^{-1} as the C-C double bond was converted into a single bond.

The time to form a gel, denoted as gelation time, was determined using the vial tilting method.²³ Absence of flow within 1 min after inverting the vial indicated the formation of the gel state. Two hours after this point, THF was added to the gel, and then replaced by immersing the gel several times in Milli-Q water to remove any unreacted polymer and residual catalyst. To prove that hydrogels were formed, water-uptake measurements were performed. Upon swelling in deionized water, the PFS-based hydrogel became transparent and turned an amber color. The swelling ratio (by weight)²⁴ $SW = (W_h - W_d)/W_d$, where W_h and W_d are the hydrated and dry sample weights, respectively, was calculated to be ~ 3.6 . The swelling ratio strongly depends on the effective crosslink density, the affinity of the network for the solvent, and external conditions such as ionic strength, pH and temperature.²⁵ The relatively low value of $SW = 3.6$ indicates that a rather densely crosslinked network was formed.

The mechanical performance of the hydrogels was characterized by dynamic mechanical measurements. Dependencies of storage moduli (G') and loss moduli (G'') on angular frequency were used to characterize the viscoelastic behavior. From the frequency sweep experiments (Figure 6.4a), it was found that the hydrogels were elastic and that the storage modulus did not depend on the frequency in the employed frequency range. G' showed a constant value of $\sim 6.5\text{ kPa}$. The magnitude of G'' was substantially lower, indicating successful network formation. The complex viscosity (η^*) was also obtained in these dynamic mechanical measurements as a function of frequency (Figure 6.4b). It decreases with frequency due to the dynamics of the mechanical energy dissipation in entangled networks.²⁶

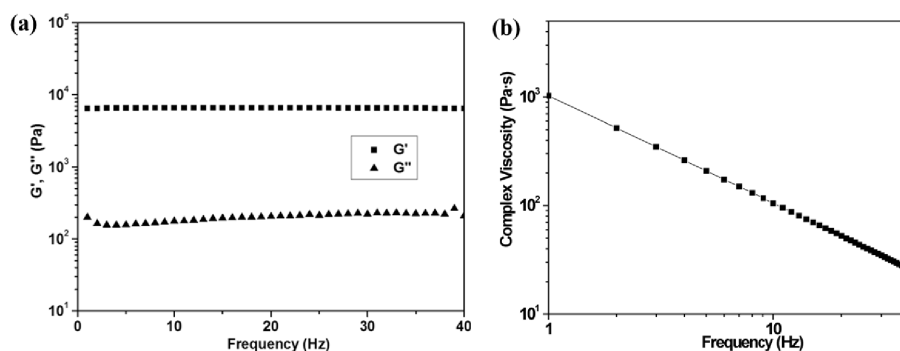


Figure 6.4 (a) Frequency dependence of storage moduli (G') and loss moduli (G'') for the obtained hydrogel and (b) Frequency dependence of the complex viscosity for the PFS-PEG-based hydrogel.

6.2.3 Redox responsive properties of PFS-PEG hydrogel

Redox stimuli can be used to trigger the release of molecular payloads embedded in the gel, making use of hydrophobic-hydrophilic switching. Upon oxidation, positive charges are generated in the PFS main chain, accompanied by a migration of counterions to the ferrocenium sites to compensate for the positive charge buildup. The PFS-PEG gels described here contain hydrophilic PEG chains and hydrophobic PFS chains. PFS-PEG gels can be loaded with drugs, making use of hydrophobic interactions between PFS chains and the drug. Under the influence of redox stimuli, these hydrophobic interactions might be disrupted when the PFS chains become oxidized, thus triggering drug release. The potential of using hydrophobic interactions for drug loading and release was recently described.²⁷

The PFS-PEG hydrogels could be reversibly oxidized and reduced both chemically and electrochemically. Chemical oxidation of PFS chains can readily be achieved by using FeCl_3 .²⁸ Figure 6.5 displays the hydrogel in its neutral and oxidized state. A rapid color change from orange to dark blue occurred when the hydrogel was immersed in 1.0 mol/L aqueous FeCl_3 solution. The oxidized hydrogel could be reduced back to the neutral state by immersion into 1.0 mol/L aqueous ascorbic acid solution. After swelling in deionized water, the swelling ratio of oxidized PFS-PEG-based hydrogel was calculated to be ~ 4.5 , which is slightly higher than that of the neutral state and indicates that the overall polarity of the gel can be influenced by redox chemistry. Chemical oxidation-reduction may lead to chain scission due to side reactions, e.g., nucleophilic attack at the ferrocenium sites.²⁹ It can be seen (Figure 6.6) that the storage moduli (G') and loss moduli (G'') of the obtained hydrogel decreased slightly after chemical oxidation and reduction. This may be caused by some minor chain scission occurring during chemical oxidation and reduction.

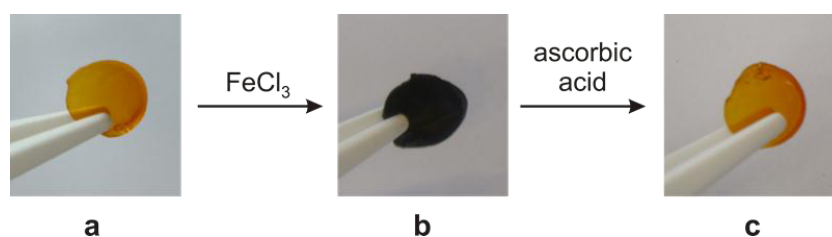


Figure 6.5 Reversible chemical oxidation and reduction of the PFS-PEG-based hydrogel. Oxidation is accompanied by a color change from amber to dark blue.

PFS-PEG-based Hydrogel via Thiol–Michael Addition Click Reaction

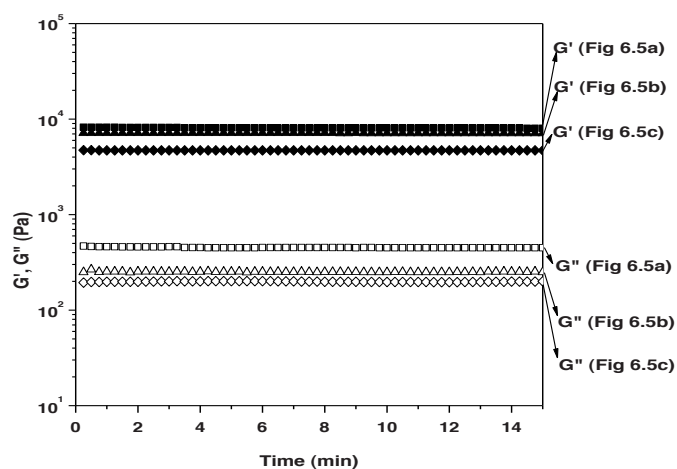


Figure 6.6 Storage moduli (G') and loss moduli (G'') of the PFS-PEG-based hydrogel before and after chemical oxidation and reduction.

Electrochemical oxidation of PFS allows for mild and improved control over the degree of oxidation, which fully depends on the potential applied.^{30,31} We noticed that in aqueous NaClO_4 , cyclic voltammetry (CV) peak currents of the hydrogel increased gradually with each successive sweep and then reached a steady state at which stable and reproducible current-potential curves were obtained (Figure 6.7). This "break-in" behavior³² is typical for a range of neutral electroactive polymer films and for neutral PFS chains in aqueous electrolyte solutions.³⁰ By holding the potential at 0.8 V, a gradual color change from orange to dark-blue was observed due to the oxidation of PFS.

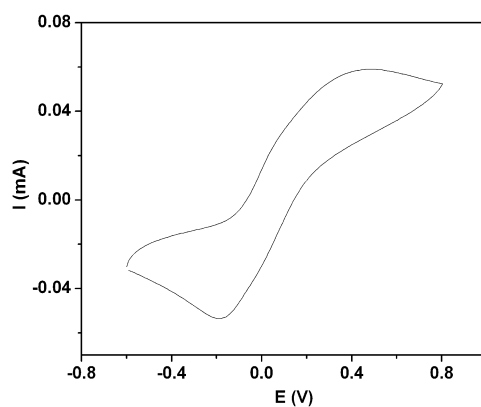


Figure 6.7 Cyclic voltammogram of the PFS-PEG-based hydrogel, swollen in 0.1 M NaClO_4 . Scan rate 50 mV/s.

6.3 Conclusions

A redox responsive PFS-PEG-based hydrogel was synthesized by thiol-Michael addition click reaction with PEG-dithiol under mild conditions. PFS bearing acrylate side groups was obtained by side-group modification of poly(ferrocenyl(3-iodopropyl)methylsilane) and characterized with ^1H NMR, ^{13}C NMR and FTIR spectroscopies. The equilibrium swelling ratio, morphology, dynamic mechanical properties and redox responsive properties of the hydrogel were studied. The redox state of the PFS chains in the gel could be tuned reversibly, allowing one to control their polarity, as became apparent from differences in the degree of swelling of the hydrogel between oxidation states. The reported method allows one to easily tune the degree of cross-linking and thereby the swelling and mechanical properties by performing the thiol-Michael addition reaction with PEG-dithiol in the presence of monothiols. This PFS-PEG-based hydrogel may have potential use as a redox controlled drug release carrier where release is based on hydrophobic-hydrophilic switching.

6.4 Experimental

Materials:

Poly(ferrocenyl(3-iodopropyl)methylsilane) (PFS-I) (**1**) (M_w : 3.7×10^5 g/mol, M_n : 1.7×10^5 g/mol, M_w/M_n : 2.1) was prepared according to established procedures.^{21,22} Dimethylsulfoxide (DMSO) and tetrahydrofuran (THF) were obtained from Biosolve and used without further purification. Sodium acrylate (97%), 1-hexylamine (99%), PEG-dithiol 1000 (average mol wt 1019 g/mol), 15-Crown-5 (98%) were obtained from Aldrich and used without further purification.

Synthesis of PFS-acryl:

To a solution of PFS-I (0.20 g, 0.5 mmol repeat units) in THF (6 mL), DMSO (3 mL), sodium acrylate (0.24 g, 2.5 mmol) and 15-crown-5 (0.55 g, 2.5 mmol) were added and the reaction mixture was stirred at room temperature for 7 days under a nitrogen atmosphere. The resulting mixture was precipitated into cold methanol and the resulting solid was collected and washed thoroughly with water and methanol. PFS-acryl was dried under vacuum, affording a yellow solid. Yield: 0.15 g. ^1H NMR (CDCl_3 , ppm): δ 0.41 (s, Si- CH_3), 0.98 (m, Si- CH_2), 1.87 (m, CH_2), 4.15 (t, $-\text{CH}_2\text{-O}-$), 3.94-4.21 (m, Cp rings), 5.81 (m, $=\text{CH}$), 6.18 (m, $-\text{CH}=\text{}$) and 6.43 (m, $=\text{CH}$). ^{13}C NMR (CDCl_3 , ppm): δ -3.6 (Si- CH_3), 12.4 (Si- CH_2), 23.3 (CH_2), 67.3 ($-\text{CH}_2\text{-O}-$), 69.7-73.2 (Cp rings), 128.1 ($-\text{CH}=\text{}$), 130.6 ($=\text{CH}_2$) and 166.2 (C=O).

PFS-based hydrogel formation and gelation time:

PFS-acryl (**2**) (20 mg) and PEG-dithiol (36 mg) (1:1.1 molar ratio) were mixed in THF (200 μ L) in vials. 1-Hexylamine (2 μ L) was added as a catalyst. The time to form a gel (denoted as gelation time) was determined using the vial tilting method.²³ In order to completely remove THF, the Milli-Q water was replaced several times.

Characterization:

¹H and ¹³C NMR spectra were recorded using a Varian Unity Inova (300 MHz) instrument at 299.89 MHz and 75.52 MHz, respectively. The chemical shift of the CDCl₃ solvent peak at $\delta = 7.26$ and 77.0 ppm, respectively, was used as a reference. Fourier transform infrared (FTIR) spectra were measured with a Bruker ALPHA.

Gel permeation chromatography (GPC) measurements were carried out in THF (flow rate 2.0 mL/min) at 25 °C, using microstyrigel columns (bead size 10 μ m) with pore sizes of 10⁵, 10⁴, 10³ and 10⁶ Å (Waters) and a dual detection system consisting of a differential refractometer (Waters model 410) and a differential viscometer (Viscotek model H502).

Swelling measurements were carried out by immersing dry gel samples in water. The hydrogels were allowed to equilibrate for 24 h until a constant weight was reached. The surface water was carefully wiped off before weighing. The swelling ratio (by weight), SW, was calculated as follows: $SW = (W_h - W_d)/W_d$, where W_h and W_d are the hydrated and dry sample weights, respectively.

Rheological experiments were carried out with a MCR 301 rheometer (Anton Paar) using parallel plates (25 mm diameter, gap 0.8 mm) configuration at 25 °C in the oscillatory mode.

Electrochemical measurements were carried out on hydrogels swollen in 0.1 M aqueous NaClO₄ using an Autolab, PGSTAT 10 electrochemical workstation. Cyclic voltammograms were recorded between -0.6 and +0.8 V at a scan rate of 50 mV/s, using a Hg/Hg₂SO₄ reference electrode, a Pt counter electrode, and an indium-tin oxide (ITO) surface, supporting the hydrogel, as a working electrode.

6.5 References

- 1 G. R. Whittell, M. D. Hager, U. S. Schubert and I. Manners, *Nat. Mater.*, 2011, **10**, 176-188.
- 2 V. Bellas and M. Rehahn, *Angew. Chem. -Int. Edit.*, 2007, **46**, 5082-5104.
- 3 Y. J. Ma, W. F. Dong, M. A. Hempenius, H. Möhwald and G. J. Vancso, *Nat. Mater.*, 2006, **5**, 724-729.
- 4 M. A. Hempenius, C. Cirimi, F. Lo Savio, J. Song and G. J. Vancso, *Macromol. Rapid Commun.*, 2010, **31**, 772-783.

Chapter 6

- 5 D. A. Foucher, B. Z. Tang and I. Manners, *J. Am. Chem. Soc.*, 1992, **114**, 6246-6248.
- 6 M. J. MacLachlan, M. Ginzburg, N. Coombs, T. W. Coyle, N. P. Raju, J. E. Greedan, G. A. Ozin and I. Manners, *Science*, 2000, **287**, 1460-1463.
- 7 K. Kulbaba, M. J. MacLachlan, C. E. B. Evans and I. Manners, *Macromol. Chem. Phys.*, 2001, **202**, 1768-1775.
- 8 M. J. MacLachlan, A. J. Lough and I. Manners, *Macromolecules*, 1996, **29**, 8562-8564.
- 9 P. W. Cyr, D. A. Rider, K. Kulbaba and I. Manners, *Macromolecules*, 2004, **37**, 3959-3961.
- 10 D. P. Puzzo, A. C. Arsenault, I. Manners and G. A. Ozin, *Angew. Chem. -Int. Edit.*, 2009, **48**, 943-947.
- 11 J. J. McDowell, N. S. Zacharia, D. Puzzo, I. Manners and G. A. Ozin, *J. Am. Chem. Soc.*, 2010, **132**, 3236-3237.
- 12 A. C. Arsenault, H. Miguez, V. Kitaev, G. A. Ozin and I. Manners, *Adv. Mater.*, 2003, **15**, 503-507.
- 13 A. C. Arsenault, V. Kitaev, I. Manners, G. A. Ozin, A. Mihi and H. Miguez, *J. Mater. Chem.*, 2005, **15**, 133-138.
- 14 A. C. Arsenault, D. P. Puzzo, I. Manners and G. A. Ozin, *Nat. Photonics*, 2007, **1**, 468-472.
- 15 M. A. Hempenius, C. Cirmi, J. Song and G. J. Vancso, *Macromolecules*, 2009, **42**, 2324-2326.
- 16 C. E. Hoyle and C. N. Bowman, *Angew. Chem. -Int. Edit.*, 2010, **49**, 1540-1573.
- 17 C. Hiemstra, L. J. van der Aa, Z. Y. Zhong, P. J. Dijkstra and J. Feijen, *Macromolecules*, 2007, **40**, 1165-1173.
- 18 A. Metters and J. Hubbell, *Biomacromolecules*, 2005, **6**, 290-301.
- 19 B. V. Slaughter, S. S. Khurshid, O. Z. Fisher, A. Khademhosseini and N. A. Peppas, *Adv. Mater.*, 2009, **21**, 3307-3329.
- 20 C. C. Lin and K. S. Anseth, *Pharm. Res.*, 2009, **26**, 631-643.
- 21 M. A. Hempenius and G. J. Vancso, *Macromolecules*, 2002, **35**, 2445-2447.
- 22 M. A. Hempenius, F. F. Brito and G. J. Vancso, *Macromolecules*, 2003, **36**, 6683-6688.
- 23 B. Jeong, S. W. Kim and Y. H. Bae, *Adv. Drug Deliv. Rev.*, 2002, **54**, 37-51.
- 24 G. R. Deen and L. H. Gan, *Polymer*, 2006, **47**, 5025-5034.
- 25 J. M. G. Swann and A. J. Ryan, *Polym. Int.*, 2009, **58**, 285-289.
- 26 K. D. Anderson, D. Lu, M. E. McConney, T. Han, D. H. Reneker and V. V. Tsukruk, *Polymer*, 2008, **49**, 5284-5293.
- 27 K. Peng, I. Tomatsu, A. V. Korobko and A. Kros, *Soft Matter*, 2010, **6**, 85-87.
- 28 Y. J. Ma, M. A. Hempenius and G. J. Vancso, *J. Inorg. Organomet. Polym. Mater.*, 2007, **17**, 3-18.
- 29 N. G. Connelly and W. E. Geiger, *Chem. Rev.*, 1996, **96**, 877-910.
- 30 X. J. Wang, L. Wang, J. J. Wang and T. Chen, *J. Phys. Chem. B*, 2004, **108**, 5627-5633.
- 31 M. Péter, R. G. Lammertink, M. A. Hempenius and G. J. Vancso, *Langmuir*, 2005, **21**, 5115-5123.
- 32 G. Inzelt, "Mechanism of Charge Transport in Polymer-Modified Electrodes", in: *Electroanalytical Chemistry*, A. J. Bard., Ed., Marcel Dekker, Inc., New York 1994, p. 89-241.

Chapter 7

Poly(*N*-isopropylacrylamide)-Poly(ferrocenylsilane) Dual-responsive Hydrogels: Synthesis, Characterization and Antimicrobial Applications

This chapter describes the formation of novel hydrogels composed of thermo-responsive poly(*N*-isopropylacrylamide) (PNIPAM) and redox-responsive poly(ferrocenylsilane) (PFS) macromolecules by photopolymerization. PFS chains bearing acrylate side groups (PFS-acryl, Chapter 6) were copolymerized with NIPAM and *N,N'*-methylenebisacrylamide in tetrahydrofuran in a predetermined ratio under ultraviolet light-emitting diode (UV-LED) irradiation at a wavelength of 365 nm, in the presence of a photoinitiator. Crosslinking occurred under mild conditions, providing homogeneous hydrogels. The equilibrium swelling ratio, rheology and morphology of these hybrid PNIPAM-PFS-based hydrogels were investigated. The thermo-responsive properties of the hydrogels were studied as a function of the PFS oxidation state. *In-situ* fabrication of silver nanoparticles inside the hydrogel network *via* reduction of silver nitrate by the PFS chains led to hydrogel composites. These composites showed strong antimicrobial activity while maintaining a high biocompatibility with cells.

* Parts of this chapter have been submitted for publication: Sui, X.; Feng, X.; Di Luca, A.; van Blitterswijk, C. A.; Moroni, L.; Hempenius, M. A. and Vancso, G. J. "Poly(*N*-isopropylacrylamide)-poly(ferrocenylsilane) dual-responsive hydrogels: synthesis, characterization and antimicrobial applications."

7.1 Introduction

Stimuli responsive hydrogels are water-swollen, chemically or physically crosslinked three-dimensional polymeric structures that may undergo relatively large variations in volume or shape due to specific changes in their environment.¹⁻¹⁰ These materials have found widespread use in the field of biotechnology, such as in tissue engineering applications,¹¹ as scaffolds for cell culture,¹² for the controlled release of drugs,¹³ as sensors¹⁴ and actuators.¹⁵⁻¹⁷ One of the most commonly studied classes of hydrogels is made from poly(*N*-isopropylacrylamide) (PNIPAM) networks, as PNIPAM possesses a lower critical solution temperature (LCST) in water around physiological temperature (~ 32 °C) and has excellent biocompatible properties. PNIPAM chains are hydrated below the LCST, while above LCST, they adopt a dehydrated and compact form.¹⁸⁻²⁰ A volume phase transition accompanies the reversible hydration and dehydration of the chains. The thermally induced volume phase transition allows PNIPAM hydrogels to be used in *e.g.* controlled drug delivery and tissue engineering, in permeation-controlled filters and as actuators.^{17,21-23}

Incorporation of other functional co-monomers with PNIPAM can provide a wide variety of stimuli responsivities.^{24,25} As a complementary functional component, we chose to introduce poly(ferrocenylsilane) (PFS),^{5,26-28} which is composed of alternating ferrocene and silane units in the main chain and can be reversibly oxidized and reduced by chemical and electrochemical means.²⁹ This organometallic polymer has received considerable attention due to its interesting optical, electronic and magnetic properties.^{27,28} In previous studies, our group has reported on the synthesis and characterization of various kinds of PFS-based hydrogels.^{5,26,30} Two distinct types of PFS polyion networks, featuring permanent positively or negatively charged side groups, were prepared using covalent crosslinking approaches.³⁰ A rapidly forming PFS-poly(ethylene glycol) (PFS-PEG) hydrogel (Chapter 6) was obtained *via* a thiol-Michael addition click reaction.²⁶

The development and applications of functional nanoparticle-polymer hydrogel composites have attracted a growing interest in the past decade.³¹⁻³³ For instance, silver nanoparticle-polymer hydrogel composites have been identified as promising materials for use in biological and medical applications.³⁴⁻³⁷ Typically, nanoparticle synthesis involves external reducing agents and toxic organic solvents, which pose potential environmental and biological risks.^{38,39} The Fe-(II) inside the PFS chains was reported to be able to reduce silver ions to the corresponding metal.⁴⁰⁻⁴²

Here, we reported the formation of a PNIPAM-PFS-based hydrogel by photopolymerization. The resulting hybrid networks were swellable in water due to the presence of PNIPAM chains. The equilibrium swelling ratio, rheology and morphology of the PNIPAM-PFS hydrogels were investigated. The thermo-

responsive properties were studied as a function of the oxidation state of the PFS chains. Uniformly distributed silver nanoparticles were prepared in the hydrogel networks *via in-situ* reduction of silver nitrate with PFS. These composites showed strong antimicrobial activity while maintaining a high biocompatibility with cells.

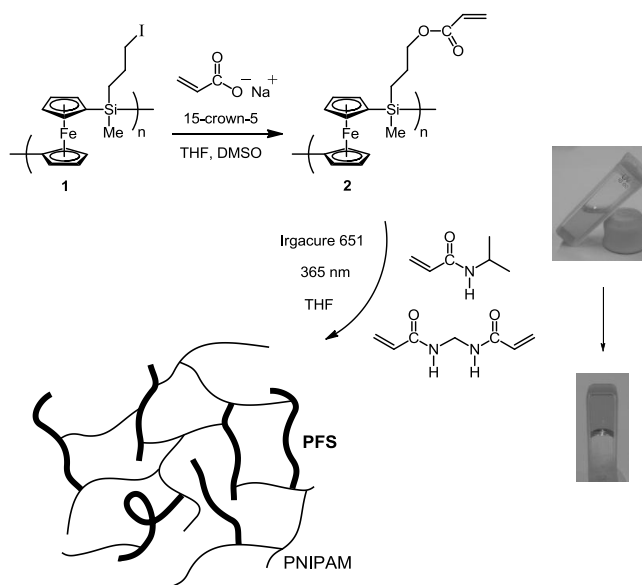


Figure 7.1 Schematic representation of the synthesis of PNIPAM-PFS hydrogel and photographs of the gel formation.

7.2 Results and discussion

7.2.1 Synthesis and characterization of PNIPAM-PFS hydrogel

The synthesis of the hybrid PNIPAM-PFS hydrogel is presented in Figure 7.1. First, PFS main chains bearing polymerizable acrylate side groups (PFS-acryl), were obtained with quantitative conversion by treating poly(ferrocenyl(3-iodopropyl)methylsilane) with the weak nucleophile sodium acrylate.²⁶ The resulting PFS-acryl underwent photopolymerization⁴³ with NIPAM and *N,N'*-methylenebisacrylamide at room temperature in THF. The UV source employed in this work consisted of a commercial high-power ultraviolet light-emitting diode (UV-LED) which emitted in a narrow wavelength region (365 ± 5 nm) where the PFS chains and the acrylamide monomers show little absorption.⁴⁴ The narrow emission spectrum of UV-LEDs is known to be highly beneficial for controlled polymerization reactions.⁴⁴ A gel state was reached within 5 min of irradiation. To achieve a high

conversion of monomers, a further 30 min irradiation was applied for all the samples. The gels acquired a darker amber colour as the PFS content increased (Figure 7.2). Figure 7.3 displays the FTIR spectra of PNIPAM-PFS hydrogels possessing various concentrations of PFS. The typical stretching vibration of the carbonyl group in the acrylate moiety of PFS-acryl appeared at 1718 cm^{-1} . Another typical peak for PFS-acryl was found at 1037 cm^{-1} (out-of-plane C-H vibration for ferrocene), while the carbonyl stretching vibration of the PNIPAM amide groups occurred at 1650 cm^{-1} . Both absorptions were present in the spectra of the PNIPAM-PFS hybrid hydrogels. With the increasing amount of PFS, the intensity of the peak 1037 cm^{-1} and 1718 cm^{-1} also increased.

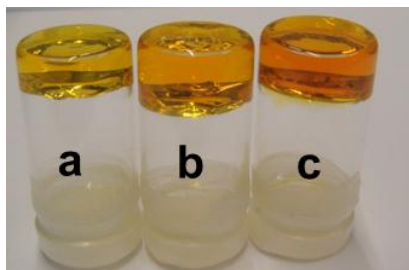


Figure 7.2 Photographs of the formed gels: (a) PNIPAM-1% PFS, (b) PNIPAM-2% PFS and (c) PNIPAM-5% PFS.

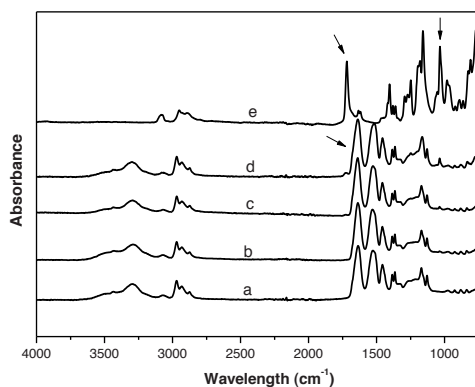


Figure 7.3 FTIR spectra of (a) PNIPAM hydrogel, (b) PNIPAM-1% PFS hydrogel, (c) PNIPAM-2% PFS hydrogel, (d) PNIPAM-5% PFS hydrogel and (e) PFS-acryl.

Thermogravimetric analysis was used to study the decomposition pattern and the thermal stability of the hybrid network. As seen in Figure 7.4a, the thermal decomposition of PNIPAM occurred by a one-step mechanism, displaying a maximum degradation at 475 °C with a significant mass loss (97%). For PFS-acryl

(Figure 7.4e), a relatively poor thermal stability was found which can be ascribed to the presence of ester bonds (320 °C). Its residual mass (60%), however, was quite high due to the presence of the non-volatile elements iron and silicon in the PFS main chain. The PNIPAM-PFS hybrid hydrogel samples (Figure 7.4b-d) display a decomposition temperature and residual mass between PNIPAM and PFS-acryl. This shows that the higher the PFS ratio in the hydrogel, the lower is the decomposition temperature and the higher is the residual mass.

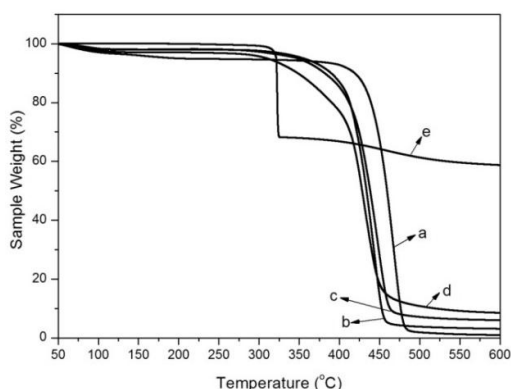


Figure 7.4 TGA traces of (a) PNIPAM hydrogel, (b) PNIPAM-1% PFS hydrogel, (c) PNIPAM-2% PFS hydrogel, (d) PNIPAM-5% PFS hydrogel and (e) PFS-acryl.

Water-uptake measurements, dynamic mechanical measurements and a study of the inner network morphology of PNIPAM-PFS hydrogels were performed. The swelling ratio strongly depended on the effective crosslink density. In these hydrogels, the effective crosslink density not only depends on the employed amount of *N,N'*-methylenebisacrylamide, but also on PFS-acryl which itself acts as a macro-crosslinker. For PNIPAM-1% PFS hydrogel, the SW can go to 20, while for PNIPAM-5% PFS hydrogel sample, a relatively low value of SW = 6 indicates that a rather densely crosslinked network was formed (Table 7.1).

Hydrogel	PNIPAM-1% PFS	PNIPAM-2% PFS	PNIPAM-5% PFS
Storage modulus (G' , Pa)	500 ± 30	$2,200 \pm 200$	$1000,000 \pm 1,000$
Loss modulus (G'' , Pa)	25 ± 10	120 ± 30	$19,000 \pm 1,000$
Swelling ratio (by weight), SW	20	10	6

Table 7.1 Storage modulus (G'), loss modulus (G'') and swelling ratios for the obtained hydrogels.

The mechanical properties of the hydrogels were characterized by means of dynamic mechanical measurements. From frequency sweep experiments, it was found that the hydrogels displayed the typical behaviour of an elastic solid. The magnitude of the loss modulus G'' was substantially lower than that of the storage modulus G' ,

and the value of the storage modulus was independent of frequency in the employed frequency range (Figure 7.5). These characteristics indicate successful network formation. The values of G' and G'' also depended on the PFS content, where more PFS resulted in dramatically higher values.

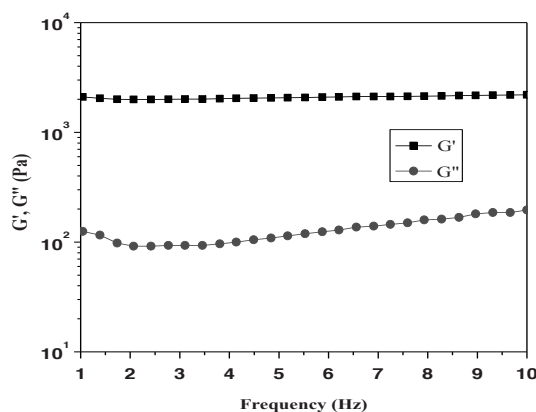


Figure 7.5 Frequency dependence of storage moduli (G') and loss moduli (G'') for the obtained PNIPAM-2% PFS hydrogel.

SEM images were obtained from freeze dried PNIPAM-PFS hydrogel samples to characterize their interior structures in the swollen state. Clearly, the hydrogels possess a homogeneous, porous structure. As shown in Figure 7.6, all the hydrogels exhibit porous structures, with the pore size decreasing as the PFS content increases. This result is consistent with water-uptake and mechanical measurements. Thus, more PFS in the hydrogels results in a higher crosslink density.

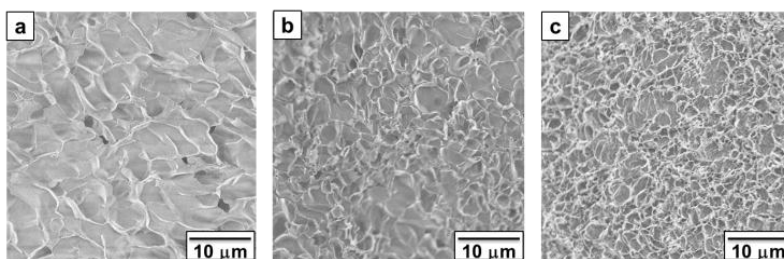


Figure 7.6 SEM images of hydrogels (a) PNIPAM-1% PFS, (b) PNIPAM-2% PFS and (c) PNIPAM-5% PFS (freeze dried).

It has been reported that the value of the LCST of PNIPAM is influenced by the oxidation state of redox-responsive monomers, incorporated in the PNIPAM chain by copolymerization with NIPAM.⁴⁵⁻⁴⁸ For example, by incorporation of 3 mol% vinylferrocene in PNIPAM, the LCST of the aqueous copolymer increased

significantly (8 °C) upon oxidation of the ferrocene moiety.⁴⁹ Here, the thermosensitive character of the as prepared PNIPAM-PFS hydrogels was studied by means of DSC.⁵⁰⁻⁵³ Chemical oxidation of the PFS chains inside the hydrogels was achieved by using FeCl₃. A colour change from yellow to dark blue occurred when the hydrogel was immersed in 1.0 mmol/L aqueous FeCl₃. DSC showed that the introduction of PFS (up to 5 mol%) into the PNIPAM hydrogel only led to a slight upward shift of the transition temperature (up to 2 °C) upon oxidation (Figure 7.7). A possible explanation for the limited influence of the PFS chains on the PNIPAM transition temperature is that the ferrocene groups are confined in the PFS main chains, instead of being incorporated as comonomers in the PNIPAM chains. Figure 7.8 shows the typical DSC curves and images of PNIPAM-2% PFS hydrogel at different oxidation states.

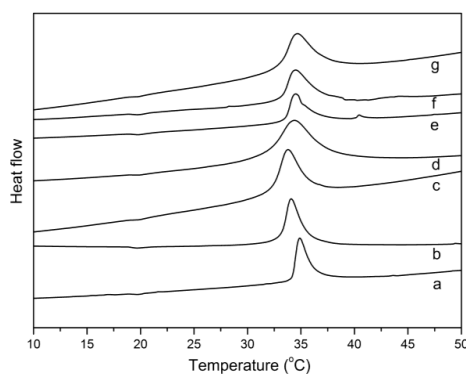


Figure 7.7 DSC measurements of the various hydrogels: (a) PNIPAM, (b) PNIPAM-1% PFS, (c) PNIPAM-2% PFS, (d) PNIPAM-5% PFS, (e) PNIPAM-1% PFS after oxidation, (f) PNIPAM-2% PFS after oxidation and (g) PNIPAM-5% PFS after oxidation.

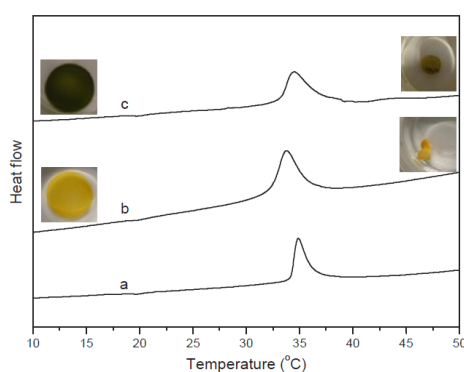


Figure 7.8 DSC traces of (a) PNIPAM hydrogel, (b) PNIPAM-2% PFS hydrogel and (c) PNIPAM-2% PFS hydrogel after oxidation, and images of the PNIPAM-2% PFS hydrogel in its neutral (yellow) and oxidized (dark blue) state. The insets on the right show the corresponding hydrogel samples to scale in their collapsed state.

7.2.2 *In-situ* formation of PNIPAM-PFS silver composites

The redox activity of the PFS chains in the hybrid hydrogels could be used to prepare PFS-PNIPAM-Ag composites in a facile *in-situ* process (Figure 7.9). Ag nanoparticles were formed *via* reduction of silver nitrate by PFS. This method led to uniformly distributed Ag nanoparticles within the networks, without using external reducing agents or organic solvents. PNIPAM-2% PFS hydrogel was chosen for the nanocomposite formation due to its suitable modulus and swelling properties. Gel-silver nanoparticle composites are raising much interest in the biomedical field.

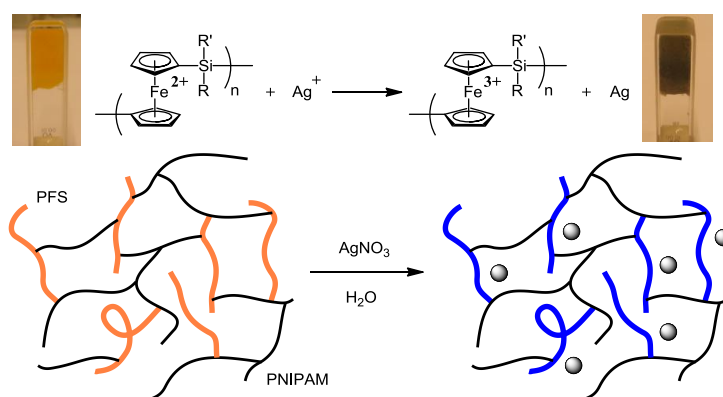


Figure 7.9 Schematic representation of the synthesis of a PNIPAM-PFS silver composite and photographs of its formation.

The formation of a silver nanoparticle composite was apparent from the bulk hydrogel, which turned from orange to brown after the addition of silver nitrate solution. It is hypothesized that the silver nanoparticles are immobilized throughout the hydrogel due to the homogeneously distributed PFS chains inside the network. This was confirmed by TEM measurements. The silver nanoparticles were uniformly deposited inside the hydrogel with particle sizes of around 10-50 nm. Energy Dispersive X-ray (EDX) was employed to further confirm the co-existence of silver and iron (Figure 7.10).

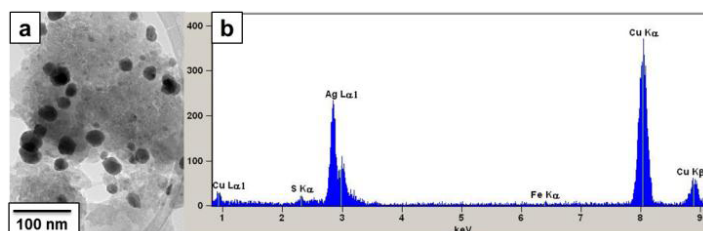


Figure 7.10 TEM image of silver nanoparticles inside the hydrogel and (b) EDX spectrum of the composite sample.

We studied the antibacterial activity of the formed hydrogel silver composites towards *E. coli*. A zone of inhibition (ZOI) test was performed to evaluate the efficacy of the developed hydrogels as smart coatings for biomedical applications. After 24 hours of incubation, a bacteria layer covered all the agar plates used for culture. Hydrogels with and without Ag nanoparticles were placed in contact with the *E. Coli* layer on top of the culture agar plates. A clearer area was visible around the silver containing sample (Figure 7.11b), while the area around the plain PFS-PNIPAM hydrogel remained opaque (Figure 7.11a) after 24 hours of contact. As metal nanoparticles and ions are known to interact with thiol groups (-SH), in our composite hydrogels silver nanoparticles may as well exert their activity by contact with the disulphide bonds of those proteins that in prokaryotic cells are exposed in the external part of the cellular membrane. Eventually, this interaction may be at the base of bacteria death.⁵⁶

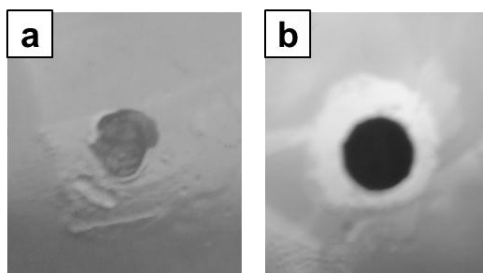


Figure 7.11 Antibacterial test on (a) PNIPAM hydrogel; (b) hydrogel silver composite after incubation for 24 h at 37 °C.

To further test the potential of the nanocomposites for biomedical applications, we evaluated their cytotoxicity with the murine fibroblastic cell line MC-3T3. The cell viability was tested on cells growing in contact with the gels and cells growing in the supernatant in which the gels were immersed. No significant influence was observed for cells growing in contact with the composites or in the supernatant (Figure 7.12). The selective antibacterial properties of the developed hydrogels might likely be due to the outer localization of the disulphide bonds in prokaryotic cells, whereas in eukaryotic cells these bonds are located in the inner side of the cellular membrane. These results suggest that the hybrid composites are biocompatible when used for cell cultures.

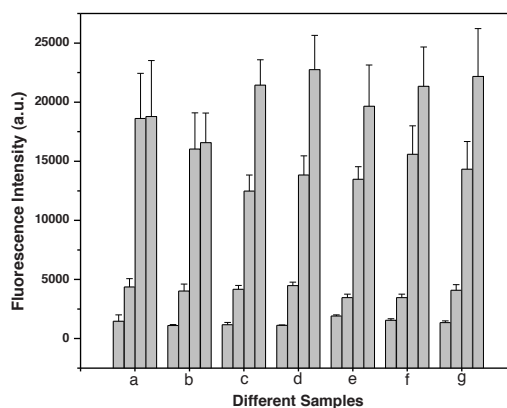


Figure 7.12 PrestoBlue™ graph showing cell metabolic activity increasing from day 1 to day 7 (from left to right, 1, 3, 5 and 7 days). (a) Cells only, (b) PNIPAM hydrogel in contact, (c) PNIPAM-2% PFS hydrogel in contact, (d) PNIPAM-2% PFS hydrogel silver composite in contact, (e) PNIPAM hydrogel supernatant, (f) PNIPAM-2% PFS hydrogel supernatant and (g) PNIPAM-2% PFS hydrogel silver composite supernatant. No significant differences can be seen among the samples taken over the days at the same time point (ANOVA test, $n=3$, $p \leq 0.05$).

7.3 Conclusions

A dual thermo- and redox-responsive PNIPAM-PFS-based hydrogel was synthesized under mild conditions. Photopolymerization of NIPAM and *N,N'*-methylenebisacrylamide with PFS chains featuring reactive acrylate side groups led to the PNIPAM-PFS gels. The equilibrium swelling ratio, dynamic mechanical properties and morphology of these hydrogels were studied. The PFS chains in the gel could be oxidized and reduced reversibly. DSC measurements showed that the LCST of PNIPAM was only slightly influenced by the incorporation of PFS. These hydrogels were used as precursor for the redox-induced formation of hydrogel silver composites. These composites showed a strong antimicrobial activity while maintaining a high biocompatibility with cells.

7.4 Experimental

Materials:

Poly(ferrocenyl[3-(acryloyloxy)propyl]methylsilane) (**2**) was prepared according to a previously published procedure (Chapter 6).²⁶ Tetrahydrofuran (THF) was obtained from Biosolve and purified by distillation from sodium-benzophenone under argon. *N*-isopropylacrylamide (NIPAM, Aldrich, 97%) was recrystallized twice from a toluene/hexane solution (50% v/v) and dried under vacuum (9 mbar) prior to use. 2,2-

Dimethoxy-2-phenylacetophenone (99%) (Irgacure 651), *N,N'*-methylenebisacrylamide (99%), silver nitrate ($\geq 99.0\%$) and iron(III) chloride (99%) were obtained from Aldrich and used without further purification. A high-power UV-LED (P8D236, Seoul Optodevice Co., South Korea) with a narrow emission spectrum (365 ± 5 nm) was mounted onto a printed circuit board (PCB) in series with a 4.7Ω power resistor and operated with a laboratory power supply.

Synthesis of PFS-PNIPAM hydrogels:

NIPAM (0.75 g, 6.63 mmol), PFS-acryl (24.6 mg, 1 mol% with respect to NIPAM) or (49.2 mg, 2 mol% with respect to NIPAM) or (123 mg, 5 mol% with respect to NIPAM), 2,2-dimethoxy-2-phenylacetophenone (photoinitiator, 9 mg, 0.035 mmol) and *N,N'*-methylenebisacrylamide (crosslinking agent, 18 mg, 0.117 mmol) were dissolved in THF (3.0 mL). The solution was purged with argon for 30 min prior to polymerization. The sample was placed at a distance of 20 mm from the LED. A voltage of 6.0 V was applied to the LED, resulting in a fixed forward current of 500 mA. Photopolymerization was conducted under UV-LED irradiation for 30 min at room temperature. After photopolymerization, the gel was washed with several portions of fresh THF to remove any unreacted monomer and photoinitiator, and the solvent was evaporated. Milli-Q water was subsequently added to form the hydrogel.

In-situ formation of silver composite hydrogels:

A solution of silver nitrate in water (5 mM) was added into the swollen PNIPAM-2% PFS hydrogel. The reaction was left to proceed overnight in the dark. The color of the hydrogel turned from orange to brown. To remove unreacted silver salts, the composite hydrogel was immersed in Milli-Q water, and this was changed at regular intervals over a period of 2 days.

Antimicrobial study:

A Lysogeny broth, LB-agar plate was prepared for each sample: tryptone (1 g), yeast extract (0.5 g), NaCl (1 g) and water (100 mL) were mixed together. The pH was adjusted to 7.0. Agar (1.75 g) was added to the solution before autoclave sterilization. *E. Coli* were seeded on the LB-agar plate and left to grow for 1 day in order to form a visible layer, on which 8 mm punched gels were placed. After 1 day, photographs of the zone of inhibition (ZOI)⁵⁴ were taken.

Cytotoxicity study:

MC-3T3 were seeded on a TC plate and, after 1 day of growth, were placed in contact with different samples. Cell metabolic activity was tested after 1, 3, 5 and 7 days of culture by the Presto blue assay. To prove the absence of release of cytotoxic compounds from the gels, a control experiment was run by immersing different

samples in cell culture medium. The supernatant in which the gels were immersed was used as a medium to culture the cells. A PrestoBlue™ assay⁵⁵ was carried out at different time points. Briefly, 10% Presto blue solution was prepared in culture media and placed on cells for 30 minutes. Fluorescence values were measured by a plate reader with an excitation wavelength of 560 nm and an emission wavelength of 590 nm. Optical microscopy images of the cells were also taken to check their viability under the gel to confirm the absence of cytotoxicity by contact with the samples.

Characterization:

Fourier transform infrared (FTIR) spectra were recorded using a Bruker ALPHA instrument.

The thermal stability of the samples was examined on a Perkin Elmer Thermo Gravimetric Analyzer (TGA 7, Waltham, MA, U.S.A.) in the temperature range of 50 – 600 °C (heating rate 20 °C/min) under a nitrogen atmosphere.

Swelling measurements were carried out by immersing dry gel samples in water. The hydrogels were allowed to equilibrate for 24 h until a constant weight was reached. The surface water was carefully wiped off before weighing. The swelling ratio (by weight), SW, was calculated as follows: $SW = (W_h - W_d)/W_d$, where W_h and W_d are the hydrated and dry sample weights, respectively.

Rheological experiments were carried out with a MCR 200 rheometer (Anton Paar) using a parallel plates (diameter 25 mm, gap 2 mm) configuration in the oscillatory mode at 25 °C. A frequency of 1 Hz and a strain of 1% were applied.

Differential scanning calorimetry (DSC) measurements were performed using a Perkin-Elmer Pyris 1 DSC (Waltham, MA, USA). Hydrogel samples (30 mg) were heated at a rate of 5.00 °C/min from 0 °C to 60 °C. After holding at 60 °C for 1 min, the samples were cooled from 60 °C to 0 °C at 5.00 °C/min.

Scanning Electron Microscopy (SEM) images of freeze-dried hydrogel samples were captured with a HR-LEO 1550 FEF SEM instrument. All hydrogels samples were first freeze-dried in liquid nitrogen and subsequent freeze-drying for a period of 24 h prior to imaging to preserve the microstructure of the original, swollen samples.

Transmission electron microscopic (TEM) measurements were performed with a FEI instrument and equipped with an EDX analyzer.

Cell attachment on hydrogels was assessed by light microscopy, employing a digital camera (Nikon Eclipse TE 300).

7.5 References

- 1 M. A. C. Stuart, W. T. S. Huck, J. Genzer, M. Müller, C. Ober, M. Stamm, G. B. Sukhorukov, I. Szleifer, V. V. Tsukruk, M. Urban, F. Winnik, S. Zauscher, I. Luzinov and S. Minko, *Nat. Mater.*, 2010, **9**, 101-113.
- 2 P. Calvert, *Adv. Mater.*, 2009, **21**, 743-756.
- 3 B. V. Slaughter, S. S. Khurshid, O. Z. Fisher, A. Khademhosseini and N. A. Peppas, *Adv. Mater.*, 2009, **21**, 3307-3329.
- 4 J. K. H. Hui, Z. Yu and M. J. MacLachlan, *Angew. Chem. -Int. Edit.*, 2007, **46**, 7980-7983.
- 5 M. A. Hempenius, C. Cirimi, F. Lo Savio, J. Song and G. J. Vancso, *Macromol. Rapid Commun.*, 2010, **31**, 772-783.
- 6 T. R. Hoare and D. S. Kohane, *Polymer*, 2008, **49**, 1993-2007.
- 7 J. Kopecek and J. Y. Yang, *Polym. Int.*, 2007, **56**, 1078-1098.
- 8 J. M. G. Swann and A. J. Ryan, *Polym. Int.*, 2009, **58**, 285-289.
- 9 K. Deligkaris, T. S. Tadele, W. Olthuis and A. van den Berg, *Sens. Actuator B-Chem.*, 2010, **147**, 765-774.
- 10 I. Tokarev and S. Minko, *Soft Matter*, 2009, **5**, 511-524.
- 11 K. T. Nguyen and J. L. West, *Biomaterials*, 2002, **23**, 4307-4314.
- 12 M. W. Tibbitt and K. S. Anseth, *Biotechnol. Bioeng.*, 2009, **103**, 655-663.
- 13 O. Franssen, L. Vandervennet, P. Roders and W. E. Hennink, *J. Control. Release*, 1999, **60**, 211-221.
- 14 J. Z. Hilt, A. K. Gupta, R. Bashir and N. A. Peppas, *Biomed. Microdevices*, 2003, **5**, 177-184.
- 15 M. Zrinyi, J. Feher and G. Filipcsei, *Macromolecules*, 2000, **33**, 5751-5753.
- 16 D. J. Beebe, J. S. Moore, J. M. Bauer, Q. Yu, R. H. Liu, C. Devadoss and B. H. Jo, *Nature*, 2000, **404**, 588-590.
- 17 L. Dong and H. Jiang, *Soft Matter*, 2007, **3**, 1223-1230.
- 18 O. Smidsrød and J. E. Guillet, *Macromolecules*, 1969, **2**, 272-277.
- 19 X. F. Sui, S. Zapotoczny, E. M. Benetti, M. Memesa, M. A. Hempenius and G. J. Vancso, *Polym. Chem.*, 2011, **2**, 879-884.
- 20 H. G. Schild, *Prog Polym Sci*, 1992, **17**, 163-249.
- 21 D. Kuckling, *Colloid Polym Sci*, 2009, **287**, 881-891.
- 22 P. M. Xulu, G. Filipcsei and M. Zrinyi, *Macromolecules*, 2000, **33**, 1716-1719.
- 23 M. Guenther, G. Gerlach, D. Kuckling, K. Kretschmer, C. Corten, J. Weber, J. Sorber, G. Suchanek, K. F. Arndt, *Smart Structures and Materials 2006: Smart Sensor Monitoring Systems and Applications 2006*, **6167**, T1670.
- 24 J. Zhang and N. A. Peppas, *Macromolecules*, 2000, **33**, 102-107.
- 25 X. Y. Du, J. B. Liu, J. P. Deng and W. T. Yang, *Polym. Chem.*, 2010, **1**, 1030-1038.
- 26 X. F. Sui, L. van Ingen, M. A. Hempenius and G. J. Vancso, *Macromol. Rapid Commun.*, 2010, **31**, 2059-2063.
- 27 G. R. Whittell and I. Manners, *Adv. Mater.*, 2007, **19**, 3439-3468.
- 28 V. Bellas and M. Rehahn, *Angew. Chem. -Int. Edit.*, 2007, **46**, 5082-5104.
- 29 R. Rulkens, A. J. Lough, I. Manners, S. R. Lovelace, C. Grant and W. E. Geiger, *J. Am. Chem. Soc.*, 1996, **118**, 12683-12695.
- 30 M. A. Hempenius, C. Cirimi, J. Song and G. J. Vancso, *Macromolecules*, 2009, **42**, 2324-2326.
- 31 N. S. Satarkar, D. Biswal and J. Z. Hilt, *Soft Matter*, 2010, **6**, 2364-2371.
- 32 E. M. Benetti, X. F. Sui, S. Zapotoczny and G. J. Vancso, *Adv. Funct. Mater.*, 2010, **20**, 939-944.

Chapter 7

- 33 H. Zhang, J. S. Han and B. Yang, *Adv. Funct. Mater.*, 2010, **20**, 1533-1550.
- 34 A. Kumar, P. K. Vemula, P. M. Ajayan and G. John, *Nat. Mater.*, 2008, **7**, 236-241.
- 35 V. Sambhy, M. M. MacBride, B. R. Peterson and A. Sen, *J. Am. Chem. Soc.*, 2006, **128**, 9798-9808.
- 36 M. Lv, S. Su, Y. He, Q. Huang, W. B. Hu, D. Li, C. H. Fan and S. T. Lee, *Adv. Mater.*, 2010, **22**, 5463-5467.
- 37 M. Uygun, M. U. Kahveci, D. Odaci, S. Timur and Y. Yagci, *Macromol. Chem. Phys.*, 2009, **210**, 1867-1875.
- 38 J. Garcia-Serrano, U. Pal, A. M. Herrera, P. Salas and C. Angeles-Chavez, *Chem. Mat.*, 2008, **20**, 5146-5153.
- 39 P. Raveendran, J. Fu and S. L. Wallen, *J. Am. Chem. Soc.*, 2003, **125**, 13940-13941.
- 40 X. S. Wang, H. Wang, N. Coombs, M. A. Winnik and I. Manners, *J. Am. Chem. Soc.*, 2005, **127**, 8924-8925.
- 41 H. Wang, X. S. Wang, M. A. Winnik and I. Manners, *J. Am. Chem. Soc.*, 2008, **130**, 12921-12930.
- 42 H. B. Eitouni and N. P. Balsara, *J. Am. Chem. Soc.*, 2004, **126**, 7446-7447.
- 43 J. S. Porterfield, *Bull. World Health Organ.*, 1960, **22**, 373-380.
- 44 S. A. Ahmed, R. M. Gogal, Jr. and J. E. Walsh, *J. Immunol. Methods*, 1994, **170**, 211-224.
- 45 T. Potta, C. Chun and S. C. Song, *Biomacromolecules*, 2010, **11**, 1741-1753.
- 46 R. Heeb, R. M. Bielecki, S. Lee and N. D. Spencer, *Macromolecules*, 2009, **42**, 9124-9132.
- 47 Y. Hara and R. Yoshida, *J. Phys. Chem. B*, 2005, **109**, 9451-9454.
- 48 N. Kuramoto, Y. Shishido and K. Nagai, *J. Polym. Sci. Pol. Chem.*, 1997, **35**, 1967-1972.
- 49 R. Yoshida, T. Sakai, S. Ito and T. Yamaguchi, *J. Am. Chem. Soc.*, 2002, **124**, 8095-8098.
- 50 T. Tatsuma, K. Takada, H. Matsui and N. Oyama, *Macromolecules*, 1994, **27**, 6687-6689.
- 51 N. Kuramoto and Y. Shishido, *Polymer*, 1998, **39**, 669-673.
- 52 S. T. Sun and P. Y. Wu, *J. Mater. Chem.*, 2011, **21**, 4095-4097.
- 53 S. T. Sun, J. Hu, H. Tang and P. Y. Wu, *J. Phys. Chem. B*, 2010, **114**, 9761-9770.
- 54 Y. Cui, C. Tao, S. P. Zheng, Q. He, S. F. Ai and J. B. Li, *Macromol. Rapid Commun.*, 2005, **26**, 1552-1556.
- 55 Y. W. Ding, X. D. Ye and G. Z. Zhang, *Macromolecules*, 2005, **38**, 904-908.
- 56 K. H. Cho, J. E. Park, T. Osaka and S. G. Park, *Electrochimica Acta*, 2005, **51**, 956-960.

Chapter 8

Poly(ferrocenylsilane)-based Redox-active Nanogels/Microgels

In this chapter, the synthesis of poly(ferrocenylsilane) PFS-based redox-active nanogels/microgels is reported. Besides PFS with acrylate side groups (PFS-acryl) (previously described in Chapter 6 and 7), another type of crosslinkable, water soluble PFS, PFS with vinyl imidazole groups (PFS polyionic liquids, PFS-PILs) is developed. PFS-PILs self-crosslink at low concentrations into nanogels or form macroscopic hydrogel networks at higher concentrations. PFS-PILs also prove to be an efficient dispersant in the microemulsion polymerization of methyl methacrylate, producing stable PFS-poly(methyl methacrylate) latex suspensions. Using PFS-PILs and PFS-acryl as precursors, uniform sized PFS microgels are obtained by using a microfluidic system coupled with UV photopolymerization. This novel, facile, flexible and straightforward microfluidic technique enables us to generate and precisely control the size of the redox responsive microspheres. These PFS nanogels/microgels produced show redox responsive properties and promising applications in catalysis and molecular release.

* Parts of this chapter have been published in: Sui, X.; Hempenius, M. A. and Vancso, G. J. *J. Am. Chem. Soc.*, **2012**, 134, 4023–4025.

8.1 Introduction

In this chapter, we first describe the synthesis of crosslinkable, redox-active poly(ferrocenylsilane)¹⁻⁵-poly(ionic liquid)s (PFS-PILs). The PFS-PILs could be converted into nanogels at low concentration. We then use these PFS-PILs together with another crosslinkable PFS, PFS with acrylate side groups (PFS-acryl),⁶ for the development of PFS microsphere particles.

Over the last decade, ionic liquids (ILs)⁷⁻⁹ have evolved from reaction media into highly tailorable, polymeric or polymer-supported materials in which the functionality of ILs is combined with the spatial control of IL moieties provided by polymer architectures.¹⁰ Responsive PILs constitute a novel, unexplored class of functional, addressable materials that may serve to create tailored, amendable interfaces between (bio)active species and their surroundings or act as responsive embedding media for such species. PILs have attracted much attention in recent years due to their unique properties and broad applicability as dispersants, solid-ion conductors, carbon precursors, etc.¹¹⁻¹⁶ In PILs, IL species, incorporating cationic groups such as pyridinium, imidazolium and alkylammonium moieties, are part of the repeat units of the polymer chain.¹⁴ Crosslinked, swellable PILs possess an even wider range of applications, and, although more rarely, some examples of gels and microgels based on PILs have been reported.¹⁷⁻¹⁹ The area of reactive and responsive PILs and PIL networks is still largely unexplored; however, a first example exhibiting reversible poration of a PIL gel in response to solvent variation²⁰ underscores the potential of responsive PIL structures as addressable, functional materials. Examples of organic solvent-swallowable, redox-active²¹ crosslinked networks/gels and nanogels from PFS homopolymers and block copolymers have been previously reported.²²

Here, we introduce a novel class of water-soluble PILs composed of PFS chains and polymerizable vinylimidazolium pendant groups. Alkyl-substituted imidazolium cations have attracted much interest as their delocalized charge and low symmetry led to ILs with low melting points. Due to the presence of polymerizable IL side groups, these organometallic polymers are easily transformed into redox-responsive PIL networks. A variety of water-swallowable redox-responsive structures, ranging from intermolecularly crosslinked macroscopic gel structures to intramolecularly crosslinked polymeric nanogels formed from a few polymer chains and tailored microgels generated by microfluidic methods are therefore within reach.

Microgels are spherical particles, consisting of chemically cross-linked, three-dimensional polymer networks, with dimensions ranging from the submicrometer to the micrometer size range. These gel objects have been used for preparing sensors, regulating cell culture, controlling drug release, and are applicable in many other

areas.²³⁻²⁵ It is evident that the precise engineering of gel particle size and morphology contributes strongly to their effectiveness in many of these applications. Microfluidic synthesis and assembly have offered a facile approach to the continuous production of microgels with precise control over their size, shape and morphology.^{24,26-28}

Capsules possessing a PFS shell showed a quick expansion accompanied by a drastic permeability change in response to a very small chemical oxidation trigger.³ PFS microspheres constitute a novel class of redox-responsive objects. Manners et al.^{29,30} used a precipitation polymerization method for the formation of hydrophobic PFS microspheres. Relatively well-defined microparticles with average diameters of 1–3 μm (PDI 1.1–1.5) were obtained by this method, and, depending on the composition of the reaction medium employed during polymerization, xylene-swelling microgel particles were formed. Chemical oxidation of the PFS microparticles allowed the Manners group to electrostatically bind negatively charged silica microspheres to the PFS microparticle surface.

In the second part of this Chapter, we describe a novel, versatile method for the fabrication of PFS-based microgels involving the use of a microfluidic device that allows UV-induced crosslinking of formed microgel precursor droplets. PFS-PIL and PFS-acryl are chosen as microgel precursors. The former are soluble in organic solvents such as toluene, while the latter are water-soluble PFS polycations constituting a new class of polyionic liquids. Microfluidic processing enables us to generate redox responsive microparticles with precisely controlled dimensions. We also demonstrate applications of these responsive microspheres as catalyst support and in molecular release.

8.2 Results and discussion

8.2.1 Preparation and characterization of PFS-PIL

The synthesis of PFS-PIL is depicted schematically in Figure 8.1. PFS-PIL chains bearing vinyl side groups were obtained by allowing poly(ferrocenyl(3-iodopropyl)methylsilane)³¹ to react with 1-vinylimidazole at 60 °C for 24 h. To increase the water solubility of the formed polycation, its iodide counterions were exchanged with chloride counterions by dialysis in 0.1 M aqueous sodium chloride. The counterion identity strongly influences PFS polyelectrolyte solubility and swellability.³¹⁻³³ The resulting PFS-PIL was characterized by means of ¹H and ¹³C NMR spectroscopy, gel permeation chromatography (GPC), FTIR (Figure 8.2), differential scanning calorimetry (DSC, Figure 8.3), thermogravimetric analysis (Figure 8.4) and X-ray photoelectron spectroscopy (XPS). NMR spectroscopy

indicated a quantitative conversion of PFS-I into PFS-PIL and showed that polymerization of the vinyl groups did not occur in this step. GPC showed PFS-PIL to be a high molar mass material with the same polydispersity as PFS-I, indicating that molar mass decline did not occur during interconversion. XPS results showed an almost complete counterion exchange from I^- to Cl^- . Importantly, a relatively low glass transition temperature of 48 °C was found for PFS-PIL by DSC. The presence of nonvolatile elements in PFS-PIL was confirmed by TGA analysis. PFS-PIL underwent thermal decomposition beyond 350 °C and left a high residual mass (40%). The chemical oxidation of the ferrocene units in PFS is accompanied by a very distinct color change from amber to blue/green.³⁴ To illustrate this, spots of PFS-PIL, deposited on a paper support, undergo a clear color change upon oxidation by *e.g.* hydrogen peroxide (Figure 8.1).

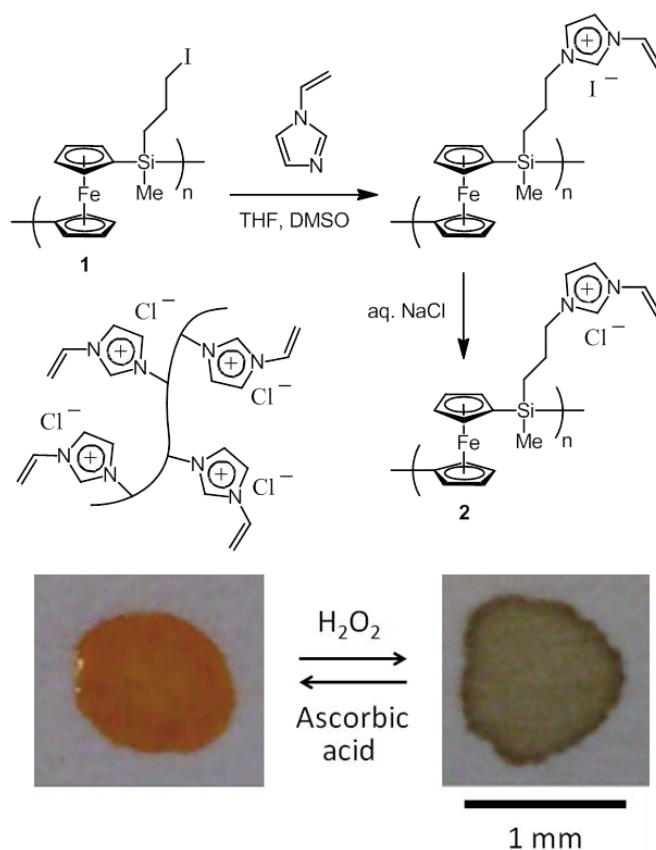


Figure 8.1 Synthesis of a crosslinkable PFS-PIL and color change of PFS-PIL associated with its reversible oxidation and reduction on a paper substrate.

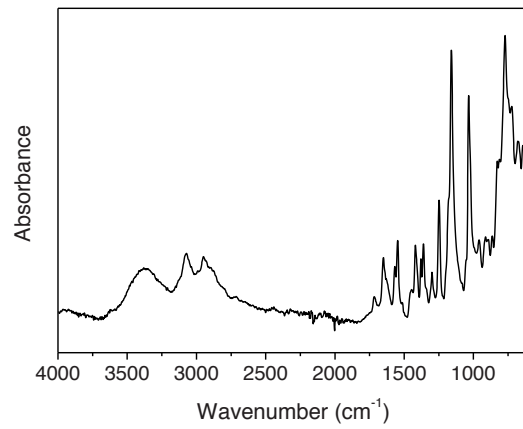


Figure 8.2 FTIR spectrum of PFS-PIL.

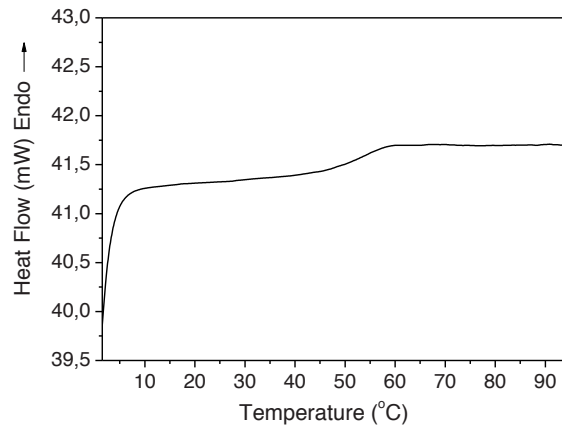


Figure 8.3 DSC trace of PFS-PIL, showing a glass transition at 48 °C (onset). The sample (3 mg) was heated from 0 °C to 100 °C at a rate of 30 °C/min.

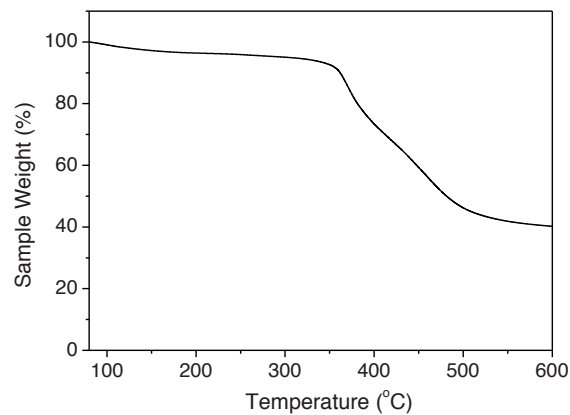


Figure 8.4 Thermogravimetric analysis trace of PFS-PIL.

8.2.2 PFS-PIL based nanogels

Crosslinking of PFS-PIL in water at high concentrations (60 mg/mL) led to the formation of transparent amber colored PFS hydrogels.^{4,6} Porous structures with pore diameters of approximately 15-20 μm were observed by SEM imaging (Figure 8.5).

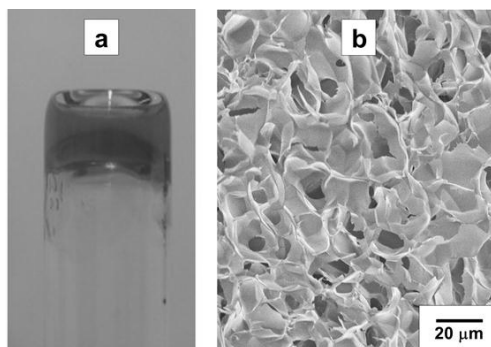


Figure 8.5 (a) Photograph of a PFS-PIL hydrogel and (b) SEM image of a PFS-PIL hydrogel after freeze drying.

The irradiation³⁵ of a dilute solution of PFS-PIL in water (0.5 mg/mL) with UV light ($\lambda = 365 \text{ nm}$) in the presence of a photoinitiator (Irgacure 2959) yielded a stable, translucent dispersion. TEM analysis (Figure 8.6b) showed the formation of crosslinked PFS-PIL nanogels³⁶⁻³⁸ with diameters in the range of 20-50 nm. Energy Dispersive X-ray (EDX) measurements obtained from these PFS-PIL nanogels demonstrated the presence of Fe (Figure 8.7). The excellent dispersibility of the formed nanoparticles in water is due to their small size and the electrostatic repulsion of the imidazolium moieties.¹⁷ The nature of the counterion significantly influenced the stability of the PFS-PIL nanogel dispersions. In solutions containing relatively hydrophobic PF_6^- anions,³⁹ the gel particles aggregated dramatically. In addition, PFS-PIL dispersions, aggregated in the presence of KPF_6 , underwent oxidation simply by being exposed to air which indicates that the PFS oxidation potential was significantly reduced by the PF_6^- counterions, likely due to ion-pairing effects.^{40,41} A cyclic voltammogram of the nanogel particles, recorded in aqueous NaNO_3 (Figure 8.8), shows the two oxidation and reduction waves typical of PFS.⁴²

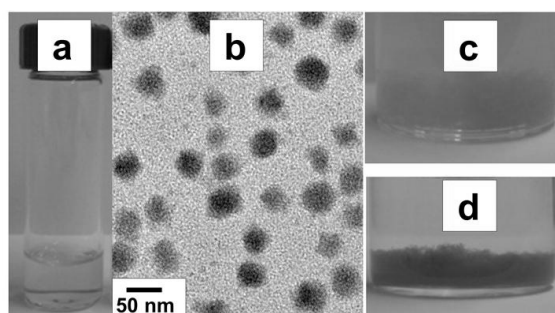


Figure 8.6 (a) PFS-PIL nanogels dispersed in water, (b) TEM image of PFS-PIL nanogels, (c) PFS-PIL nanogels dispersed in 0.1 M KPF₆ solution, and (d) PFS-PIL nanogels dispersed in 0.1 M aqueous KPF₆ after 12 hrs.

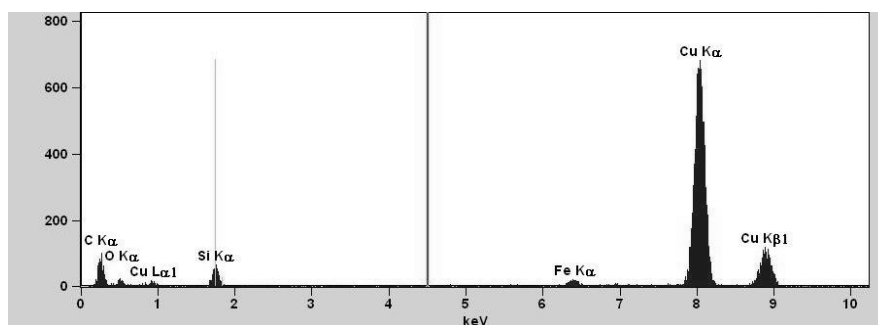


Figure 8.7 EDX spectrum obtained from the PFS-PIL nanogels.

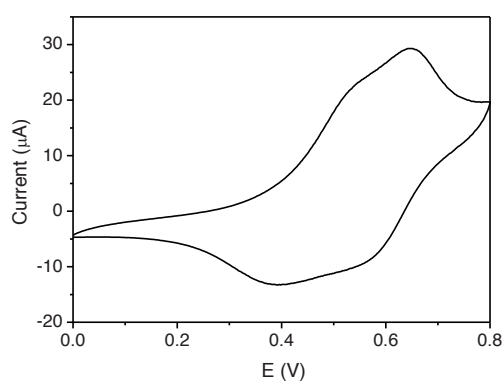


Figure 8.8 Cyclic voltammogram of PFS-PIL nanogel particles. Working electrode: Au, reference electrode: Ag/AgCl, counter electrode: Pt disk. Scan rate: 50 mV/s in 0.1 M NaNO₃.

Because PFS-PIL possesses charged, hydrophilic imidazolium chloride units and a hydrophobic main chain, it may potentially be useful as a stabilizer in microemulsion polymerizations in aqueous media.⁴³ To demonstrate this, PFS-PIL was added to stabilize methyl methacrylate (MMA) polymerization in water. By employing a ratio of PFS-PIL/MMA/H₂O = 1/100/1000, bulk photopolymerization resulted in stable polymer latex suspensions. The small particle size (45 ± 5 nm) obtained is evidence of the powerful stabilizing capability of the imidazolium-based PILs^{20,39,43} (Figure 8.9). Copolymerization between MMA and PFS-PIL was proved by recording FTIR and XPS spectra of the formed particles (Figure 8.10 and 8.11). The nanoparticles also aggregated strongly in KPF₆ solution as the surface of the PFS-PMMA latexes became more hydrophobic due to the anion exchange.⁴⁴

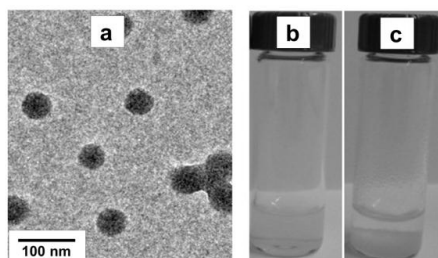


Figure 8.9 (a) TEM image of PFS-PMMA hybrid latexes from microemulsion polymerization, (b) hybrid latexes dispersed in water and (c) hybrid latexes dispersed in 0.1 M KPF₆ solution.

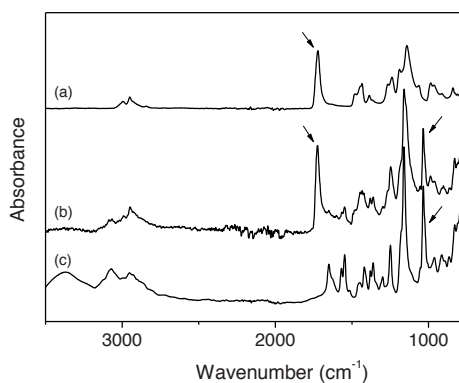


Figure 8.10 FTIR spectrum of PFS-PMMA latex obtained from microemulsion polymerization, (a) PMMA, (b) PFS-PIL/PMMA 50 wt% hybrid latex and (c) PFS-PIL (2). These hybrid latex samples were extensively washed with toluene, a selective solvent for PMMA. PMMA-specific absorption at 1725 cm^{-1} (C=O stretch), PFS-PIL absorption at 1035 cm^{-1} (asymmetric ring out-of-plane vibration for ferrocene).

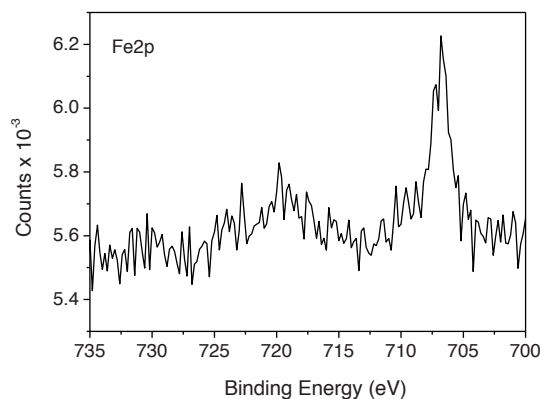


Figure 8.11 XPS element spectra scan of Fe in PFS-PIL/PMMA 1 wt% hybrid latex. The initial PFS-PIL/PMMA latex particles were washed with ethanol to remove unbound PFS-PIL.

8.2.3 PFS-PIL based microgels obtained by microfluidics

As demonstrated in Figure 8.12, PFS microgels were produced by the generation of monodisperse crosslinkable PFS droplets in a microfluidic device and subsequent solidification of these droplets by off-chip photopolymerization. The PFS microgel particles were then washed several times to remove any unreacted polymer and residual surfactant. By careful selection of chip devices, dispersed phase, continuous phase and surfactants,⁴⁵ monodisperse PFS microgels could be obtained.

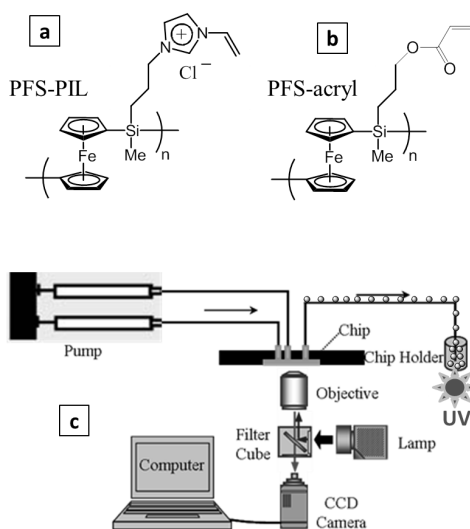


Figure 8.12 Schematic diagrams of the crosslinkable PFS chains and setup used for the formation of microgels. (a) PFS-PIL; (b) PFS-acryl and (c) schematic of the experimental setup.

For the formation of water soluble, crosslinkable PFS-PIL based microparticles, a flow-focusing⁴⁶ PDMS device was used. The employed immiscible streams in this case were an aqueous solution of PFS-PIL and a 1% Span 80 hexadecane solution as the dispersed and continuous phase, respectively. A representative image captured by a high speed camera during droplet formation is shown in Figure 8.13a. A highly periodic break-up of the thread of the dispersed phase yields droplets with a narrow size distribution. Subsequent UV-irradiation led to the formation of PFS-PIL microgels. Figure 8.13c shows SEM images of the microgel beads obtained, possessing a uniform size of about 20 μm . The PFS microgel particles displayed a rough surface morphology after drying (Figure 8.13d), likely resulting from aggregation of the hydrophobic PFS backbone chains at high concentrations.^{47,48}

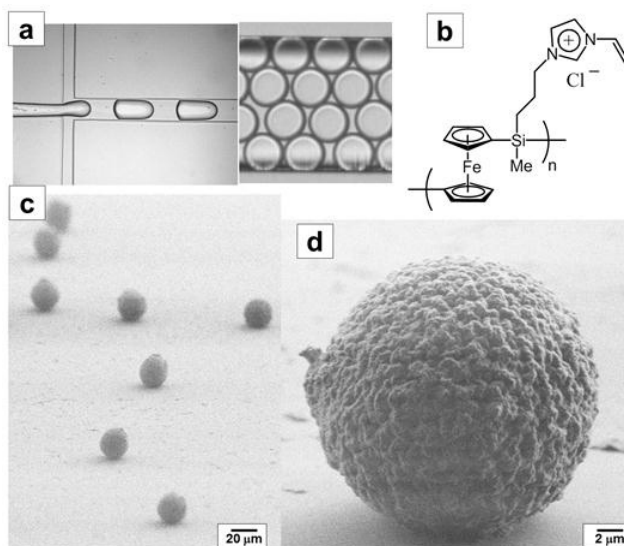


Figure 8.13 PFS microgels prepared from PFS-PIL. (a) High speed camera image of flow-focusing forming droplets, (b) PFS-PIL, (c) SEM images of PFS-PIL microgels and (d) SEM image of a single PFS-PIL microgel.

After generating the spherical particles, we incorporated a fluorescent dye (Rhodamine 6G, R6G) as molecular cargo into the polymer network. Cross-sectional confocal microscopy images taken at 2.6 μm depth steps through a single microsphere revealed that the dye molecules were uniformly distributed within the bead volume (Figure 8.14).

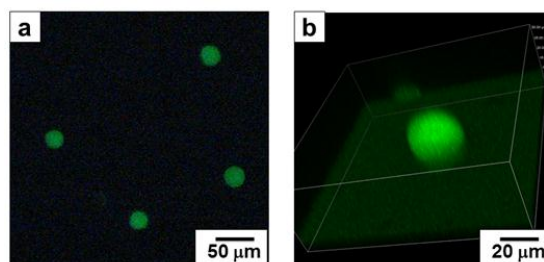


Figure 8.14 (a) Fluorescent images of Rhodamine 6G labeled PFS microspheres, (b) scanning confocal cross-sectional z-scan of a single PFS-PIL microsphere, the dye molecules are uniformly distributed within the bead volume.

In water, the microgel particles retained their cargo (Figure 8.15). Oxidation by ferric chloride (FeCl_3) has previously been shown to be an effective trigger for the release of cargo molecules from PFS capsules.³ Figure 8.16 demonstrates fluorescence microscopy images of PFS microgels before and after chemical oxidation. PFS microgels that originally showed no release of dye were treated with aqueous FeCl_3 solution (5 mg/mL) during *in-situ* imaging. As a result, the PFS microgels exhibited a continuous release of dye molecules accompanied by an increasing expansion (Figure 8.16). After oxidation, these PFS microgels remained intact due to their covalently crosslinked structure (Figure 8.17). Upon oxidation, the polarity of the PFS network chains increases as they become positively charged. Therefore, swelling of the gel particles in water increases, resulting in an enlarged average pore size and enhanced dye release. Moreover, R6G is a weakly basic dye with a pKa value of ~ 8.3 , making it positively charged at pH = 7.4.⁴⁹ Electrostatic repulsion between the positively charged R6G dye molecules and the positively charged microgel network chains is expected to accelerate dye release from the microgel particles.

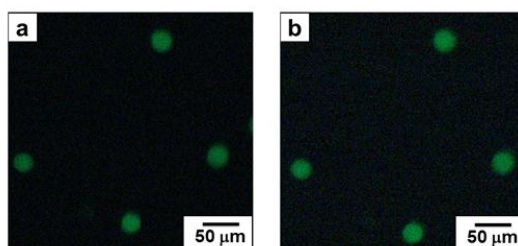


Figure 8.15 PFS-PIL microgels in water, (a) 0 minutes and (b) 30 minutes.

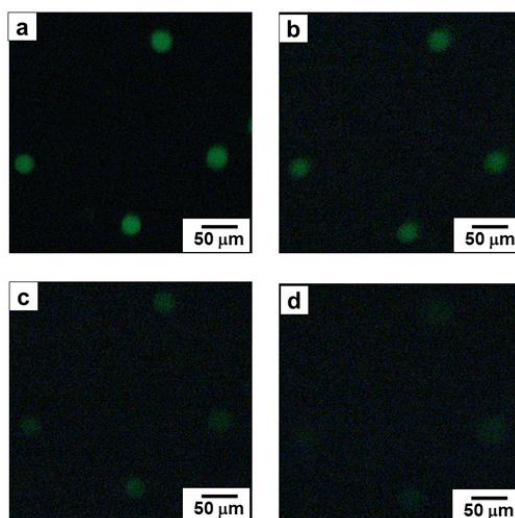


Figure 8.16 PFS-PIL microgels in FeCl_3 5 mg/mL, (a) 0 minutes, (b) 5 minutes, (c) 15 minutes and (d) 30 minutes.

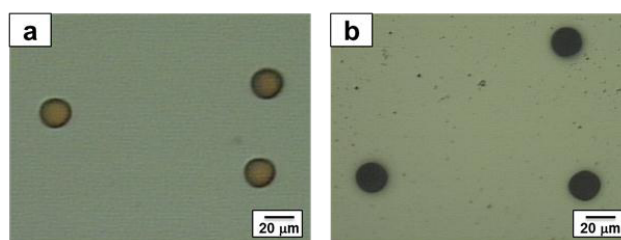


Figure 8.17 PFS-PIL microgels before and after oxidation with FeCl_3 .

8.2.4 PFS-acryl based microgels obtained by microfluidics

For PFS-acryl, a glass chip with T-junction^{28,50} was chosen to generate oil-in-water droplets, using toluene as the hydrophobic solvent. The two immiscible streams, in this case, were a solution of PFS-acryl in toluene and 1% Tween 20 in water as the dispersed and continuous phase, respectively. Figure 8.18a shows a representative image taken by a CCD camera (Orca ER) during droplet formation. Subsequent UV-irradiation led to the formation of PFS microgels. The microspheres can be produced with a range of desired diameters, depending on the fluid flow rates, and are near-monodisperse ($\text{PDI} < 1.1$). Figure 8.18c and 8.18d display SEM images of the monodisperse PFS microgels with different sizes and relatively smooth surfaces. We observed that microsphere size decreased monotonically with increasing water-to-oil flow rate ratios, as has also been shown in the literature.^{51,52} Particle diameters in the

range of 5–12 μm were obtained. We anticipated that this range can easily be extended through device design and flow rate ratio adjustments to produce spheres with submicrometer to hundred micrometer sizes. The highly monodisperse spheres assembled into 2D lattices on silicon substrates with a high degree of order and symmetry (Figure 8.18c).

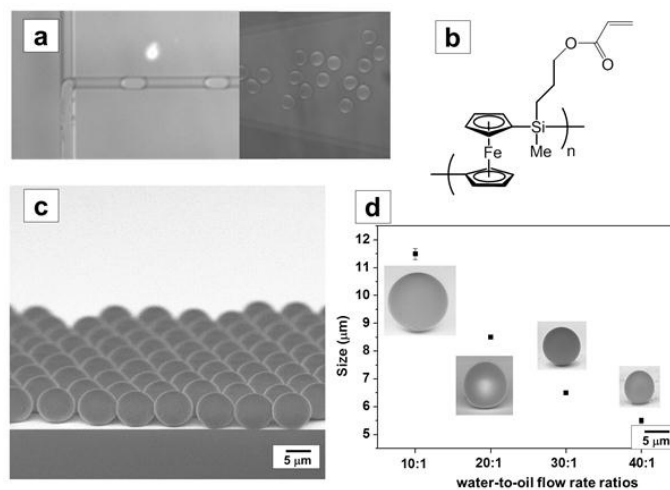


Figure 8.18 PFS microgels prepared from PFS-acryl. (a) High speed camera image of head-on forming droplets; (b) PFS-acryl; (c) SEM images of PFS-acryl microgels; (d) diameter of PFS-acryl microgels produced at increasing water-to-oil flow rate ratios, (10:1) $Q_w = 1 \mu\text{L}/\text{min}$, $Q_{PFS} = 0.1 \mu\text{L}/\text{min}$; (20:1) $Q_w = 2 \mu\text{L}/\text{min}$, $Q_{PFS} = 0.1 \mu\text{L}/\text{min}$; (30:1) $Q_w = 3 \mu\text{L}/\text{min}$, $Q_{PFS} = 0.1 \mu\text{L}/\text{min}$ and (40:1) $Q_w = 4 \mu\text{L}/\text{min}$, $Q_{PFS} = 0.1 \mu\text{L}/\text{min}$.

PFS chains have been shown to reduce silver ions to the corresponding metal (Chapter 7).⁵³⁻⁵⁵ In the case of cylindrical micelles possessing a PFS core,^{53,54} this redox reaction led to the formation of fascinating one-dimensional arrays of silver nanoparticles in the micellar core. When PFS-acryl based microspheres were immersed in a saturated solution of AgPF_6 in toluene, a color change from light yellow to black was observed. Silver nanostructures formed on the surface of the microspheres, covering the surface through a nucleation and growth process (Figure 8.19). The PFS microspheres not only acted as a reducing agent for the formation of metallic Ag but also served as templates that directed the growth of Ag structures.

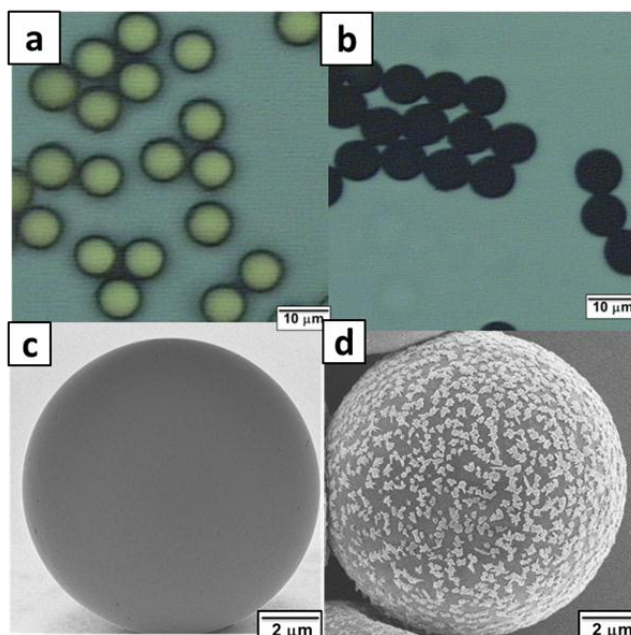


Figure 8.19 Redox induced formation of a PFS-acryl microgel-silver hybrid. (a) An optical microscopy image of the PFS-acryl microgels before adding AgPF_6 toluene solution, (b) An optical microscopy image of the PFS-acryl microgels after adding AgPF_6 toluene, (c) SEM image of a single PFS-acryl microgel before adding AgPF_6 toluene solution and (d) SEM image of a single PFS-acryl microgel after adding AgPF_6 toluene solution.

8.3 Conclusions

A new class of redox responsive organometallic polymers, PFS-PIL, composed of a redox-active PFS main chain and crosslinkable ionic liquid side groups, was synthesized. By tuning the concentration of crosslinkable PFS-PIL in water, nanogel and macroscopic hydrogel structures were successfully prepared. PFS microgels with uniform sizes based on PFS-PIL and PFS-acryl were prepared by microfluidic methods. Moreover, the redox-responsive behavior of the generated structures was demonstrated.

8.4 Experimental

Materials:

Poly(ferrocenyl(3-iodopropyl)methylsilane) (PFS-I) (M_w : 3.96×10^5 g/mol, M_n : 1.7×10^5 g/mol, M_w/M_n : 2.3) was prepared according to established procedures.³¹ The

detailed synthesis of the toluene-soluble crosslinkable PFS, PFS-acryl has been described elsewhere (Chapter 6).⁶ 1-Vinylimidazole (Aldrich 99%), dimethylsulfoxide (DMSO, Biosolve), tetrahydrofuran (THF, Biosolve), sodium chloride (Aldrich, 99.5%), toluene (AR), Rhodamine 6G (Aldrich 95%), Span 80, hexadecane (Aldrich 99%), Tween 20, Silver hexafluorophosphate (Aldrich 98%) and Iron(III) chloride (Aldrich 99%) were used without further purification. Methyl methacrylate (MMA, Aldrich, 99%) was purified by vacuum distillation. The photoinitiators, Irgacure 651 and Irgacure 2959, were obtained from Ciba Chemicals and used without further purification. Pre-polymerized Sylgard 184 Silicon Elastomer kit (polydimethylsiloxane, PDMS) was purchased from Dow Corning Corp. Water was purified with a Millipore desktop system.

Preparation of PFS-PIL:

To a solution of PFS-I (0.20 g, 0.5 mmol repeat units) in THF (6 mL), DMSO (3 mL) and 1-vinylimidazole (0.14 g, 1.5 mmol) were added and the reaction mixture was stirred at 60 °C for 24 hrs. The resulting mixture was transferred into a Spectra/Por 4 dialysis hose (MWCO 12-14000 g/mol) and dialyzed against 0.1 M NaCl (3×1L) and MilliQ water (3×1L). Concentration of the salt-free polyelectrolyte solution by a flow of N₂ produced PFS-PIL (2) as orange flakes. Yield: 0.15 g (80%). ¹H NMR (DMSO-*d*⁶): δ 0.41 (3H), 0.84 (2H), 1.84 (2H), 4.15 (2H), 3.99-4.13 (6H), 5.43 (1H), 5.93 (1H), 7.31(1H), 7.93 (1H), 8.21 (1H) and 9.52 (1H). ¹³C NMR (DMSO-*d*⁶): δ -3.6, 12.4, 23.3, 49.7, 69.7-73.2, 109.1, 119.2, 123.7, 129.2 and 136.8.

Preparation of PFS macroscopic hydrogels:

PFS-PIL (60 mg) and photoinitiator (Irgacure 2959, 2 mg) were dissolved in water (1 mL). The solution was purged with argon for 15 minutes and finally irradiated for 10 minutes by means of a UV lamp as described above, the sample-to-lamp distance was 1 cm. Following completion of the photopolymerization, the samples were extensively rinsed with water to remove low molar mass impurities such as initiator fragments.

Preparation of PFS nanogels:

PFS-PIL (5 mg) and photoinitiator (Irgacure 2959, 1 mg) were dissolved in water (10 mL). The solution was purged with argon for 15 minutes and finally irradiated for 30 minutes by means of a UV lamp ($\lambda=365$ nm). The sample-to-lamp distance was 2 cm. During the UV irradiation, the solution was stirred at ambient temperature.

Preparation of PFS-PMMA hybrid latexes:

In a typical emulsion polymerization, PFS-PIL (5 mg), photoinitiator (Irgacure 2959, 1 mg) and MMA (500 mg) were mixed in water (5 mL). The solution was purged with argon for 15 minutes, sonicated for 5 minutes and finally irradiated for 30 minutes by

means of a UV lamp as described earlier. The sample-to-lamp distance was 2 cm. During the UV irradiation, the solution was stirred at ambient temperature.

Microfluidic device fabrication and operation:

The microfluidic device for PFS-PIL was fabricated in PDMS elastomer using a standard soft-lithographic method.⁵⁶ Masters with microchannels were prepared with bas-relief features of SU-8 on silicon wafers by photolithography techniques. The PDMS elastomer was prepared by mixing prepolymer with the curing agent at the weight ratio of 4:1, respectively. Air bubbles were removed from the mixture under vacuum for 10 min for 3 times. The mixture of the prepolymer and curing agent was then poured onto the master, and cured in an oven at 60 °C overnight. After curing, the replica was carefully peeled off from master, and holes with a diameter of 2 mm were drilled at the designated positions using a needle. The patterned PDMS sheets and glass substrates were plasma treated for 45 seconds in a plasma cleaner chamber, and then brought to contact immediately. Finally, polyethylene tubing was placed into the holes. The dispersed phase included (150 mg PFS-PIL and 2 mg Irgacure 2959)/mL aqueous solution and the continuous phase consisted of Span 80 (1 wt%) hexadecane solution.

The microfluidic device for PFS-acryl was made of glass (Pyrex) wafers. Microchannels were fabricated in glass using standard photolithography procedures.²⁸ The interconnection holes were opened from the backside of the wafers by using powder-blasting techniques. Two wafers were then thermally bonded. The resulting bonded wafers were finally diced into 10 mm × 20 mm chips. Chips were fixed in a custom-built chip holder and connected to syringes via capillary tubing (OD 1/16 inch, ID 50 μm) and Nanoport connectors including a filter (INACOM INSTRUMENTS BV, Upchurch Scientific, The Netherlands). Connectors and chips were sonically cleaned in water for 15 min before use. Flow was controlled using a dual syringe pump (neMSYS syringe pump, Cetoni GmbH). The dispersed phase included (150 mg PFS-acryl and 2 mg Irgacure 651)/mL toluene and the continuous phase consisted of Tween 20 (1 wt%) aqueous solution.

Flow was controlled using a dual syringe pump (neMSYS syringe pump, Cetoni GmbH). The flow was visualized using an inverted microscope (Leica DMIRM) equipped with a mercury lamp and recorded by CCD cameras (Orca ER).

Characterization:

¹H and ¹³C NMR spectra were recorded using a Varian Unity Inova (300 MHz) instrument at 299.89 MHz and 75.52 MHz, respectively.

Fourier transform infrared (FTIR) spectra were acquired with a Bruker ALPHA instrument.

Gel permeation chromatography (GPC) on PFS-PIL was performed in DMSO containing LiCl (5.0 g/L) at 50 °C, using microstyragel columns (bead size 10 µm) with pore sizes of 10⁵, 10⁴, 10³ and 10⁶ Å (Waters) and a dual detection system consisting of a differential refractometer (Waters model 410) and a differential viscometer (Viscotek model H502). A flow rate of 0.8 mL/min was maintained.

Differential scanning calorimetry (DSC) measurements were performed using a Perkin-Elmer Pyris 1 DSC (Waltham, MA, USA). PFS-PIL samples (3 mg) were heated at a rate of 30 °C/min from 0 °C to 100 °C.

The thermal stability of samples was examined on a Perkin Elmer Thermo Gravimetric Analyzer (TGA 7, Waltham, MA, U.S.A.) with a heating rate of 20 °C/min from 50 to 600 °C under a nitrogen atmosphere. All samples were dried under vacuum for 24 h prior to TGA measurements.

Photochemical crosslinking was performed using a HAMAMATSU LC8 L9566-02 UV source.

Scanning Electron Microscopy (SEM) images were taken with a HR-LEO 1550 FEF SEM on hydrogel samples.

Transmission electron microscopy (TEM) was performed using a FEI Instrument. The TEM samples were prepared by placing one droplet of a diluted dispersion of PFS nanogels or PFS-PMMA hybrid latex on a 200 mesh carbon coated copper grid and left in air to dry.

XPS measurements were performed on a Quantera SXM (scanning XPS microprobe) from Physical Electronics, using a monochromatic Al K α X-ray source (1486.6 eV).

Electrochemical measurements were performed using an AUTOLAB PGSTAT302N instrument.

Pictures of microgels were taken using an Olympus BX60.

Fluorescent Pictures were taken using a Nikon fluorescent microscope Nikon Eclipse DS-Fi1c.

CLSM images were obtained with a Nikon A1, Scanner Selection: Galvano, Detector Selection: DU4, z step: 2.6 µm.

8.5 References

- 1 G. R. Whittell, M. D. Hager, U. S. Schubert and I. Manners, *Nat. Mater.*, 2011, **10**, 176-188.
- 2 V. Bellas and M. Rehahn, *Angew. Chem. -Int. Edit.*, 2007, **46**, 5082-5104.

Chapter 8

- 3 Y. J. Ma, W. F. Dong, M. A. Hempenius, H. Möhwald and G. J. Vancso, *Nat. Mater.*, 2006, **5**, 724-729.
- 4 M. A. Hempenius, C. Cirimi, F. Lo Savio, J. Song and G. J. Vancso, *Macromol. Rapid Commun.*, 2010, **31**, 772-783.
- 5 D. A. Foucher, B. Z. Tang and I. Manners, *J. Am. Chem. Soc.*, 1992, **114**, 6246-6248.
- 6 X. F. Sui, L. van Ingen, M. A. Hempenius and G. J. Vancso, *Macromol. Rapid Commun.*, 2010, **31**, 2059-2063.
- 7 J. P. Hallett and T. Welton, *Chem. Rev.*, 2011, **111**, 3508-3576.
- 8 T. Welton, *Chem. Rev.*, 1999, **99**, 2071-2083.
- 9 N. V. Plechkova and K. R. Seddon, *Chem. Soc. Rev.*, 2008, **37**, 123-150.
- 10 T. Ueki and M. Watanabe, *Macromolecules*, 2008, **41**, 3739-3749.
- 11 D. Mecerreyes, *Prog. Poly. Sci.*, 2011, **36**, 1629-1648.
- 12 J. M. Lu, F. Yan and J. Texter, *Prog. Polym. Sci.*, 2009, **34**, 431-448.
- 13 O. Green, S. Grubjesic, S. W. Lee and M. A. Firestone, *Polym. Rev.*, 2009, **49**, 339-360.
- 14 J. Y. Yuan and M. Antonietti, *Polymer*, 2011, **52**, 1469-1482.
- 15 J. Y. Yuan, S. Soll, M. Drechsler, A. H. E. Muller and M. Antonietti, *J. Am. Chem. Soc.*, 2011, **133**, 17556-17559.
- 16 E. B. Anderson and T. E. Long, *Polymer*, 2010, **51**, 2447-2454.
- 17 J. Y. Yuan and M. Antonietti, *Macromolecules*, 2011, **44**, 744-750.
- 18 C. Thiot, M. Schmutz, A. Wagner and C. Mioskowski, *Angew. Chem. -Int. Edit.*, 2006, **45**, 2868-2871.
- 19 R. Marcilla, M. Sanchez-Paniagua, B. Lopez-Ruiz, E. Lopez-Cabarcos, E. Ochoteco, H. Grande and D. Mecerreyes, *J. Polym. Sci. Pol. Chem.*, 2006, **44**, 3958-3965.
- 20 F. Yan and J. Texter, *Angew. Chem. -Int. Edit.*, 2007, **46**, 2440-2443.
- 21 M. Péter, R. G. Lammertink, M. A. Hempenius and G. J. Vancso, *Langmuir*, 2005, **21**, 5115-5123.
- 22 X. S. Wang, K. Liu, A. C. Arsenault, D. A. Rider, G. A. Ozin, M. A. Winnik and I. Manners, *J. Am. Chem. Soc.*, 2007, **129**, 5630-5639.
- 23 L. A. Lyon, Z. Y. Meng, N. Singh, C. D. Sorrell and A. S. John, *Chem Soc Rev*, 2009, **38**, 865-874.
- 24 R. K. Shah, J. W. Kim, J. J. Agresti, D. A. Weitz and L. Y. Chu, *Soft Matter*, 2008, **4**, 2303-2309.
- 25 S. Q. Xu, Z. H. Nie, M. Seo, P. Lewis, E. Kumacheva, H. A. Stone, P. Garstecki, D. B. Weibel, I. Gitlin and G. M. Whitesides, *Angew. Chem. -Int. Edit.*, 2005, **44**, 724-728.
- 26 S. Seiffert and D. A. Weitz, *Polymer*, 2010, **51**, 5883-5889.
- 27 E. Tumarkin and E. Kumacheva, *Chem. Soc. Rev.*, 2009, **38**, 2161-2168.
- 28 L. L. Shui, F. Mugele, A. van den Berg and J. C. T. Eijkel, *Appl. Phys. Lett.*, 2008, **93**, 153113.
- 29 K. Kulbaba, A. Cheng, A. Bartole, S. Greenberg, R. Resendes, N. Coombs, A. Safa-Sefat, J. E. Greedan, H. D. H. Stover, G. A. Ozin and I. Manners, *J. Am. Chem. Soc.*, 2002, **124**, 12522-12534.
- 30 K. Kulbaba, R. Resendes, A. Cheng, A. Bartole, A. Safa-Sefat, N. Coombs, H. D. H. Stover, J. E. Greedan, G. A. Ozin and I. Manners, *Adv. Mater.*, 2001, **13**, 732-736.
- 31 M. A. Hempenius, F. F. Brito and G. J. Vancso, *Macromolecules*, 2003, **36**, 6683-6688.
- 32 J. B. Schlenoff and L. J. Wang, *Macromolecules*, 1991, **24**, 6653-6659.
- 33 M. A. Hempenius, C. Cirimi, J. Song and G. J. Vancso, *Macromolecules*, 2009, **42**, 2324-2326.
- 34 M. T. Nguyen, A. F. Diaz, V. V. Dementev and K. H. Pannell, *Chem. Mat.*, 1994, **6**, 952-954.
- 35 X. F. Hu, J. Y. Zhang and W. T. Yang, *Polymer*, 2009, **50**, 141-147.
- 36 E. J. Foster, E. B. Berda and E. W. Meijer, *J. Am. Chem. Soc.*, 2009, **131**, 6964-6966.
- 37 A. E. Cherian, F. C. Sun, S. S. Sheiko and G. W. Coates, *J. Am. Chem. Soc.*, 2007, **129**, 11350-11351.

- 38 M. E. Mackay, T. T. Dao, A. Tuteja, D. L. Ho, B. Van Horn, H. C. Kim and C. J. Hawker, *Nat. Mater.*, 2003, **2**, 762-766.
- 39 F. Yan and J. Texter, *Chem. Commun.*, 2006, 2696-2698.
- 40 G. A. Planes, M. C. Miras and C. Barbero, *Polym. Int.*, 2002, **51**, 429-433.
- 41 G. K. Rowe and S. E. Creager, *Langmuir*, 1991, **7**, 2307-2312.
- 42 R. Rulkens, A. J. Lough, I. Manners, S. R. Lovelace, C. Grant and W. E. Geiger, *J. Am. Chem. Soc.*, 1996, **118**, 12683-12695.
- 43 J. Y. Yuan, N. ten Brummelhuis, M. Junginger, Z. L. Xie, Y. Lu, A. Taubert and H. Schlaad, *Macromol. Rapid Commun.*, 2011, **32**, 1157-1162.
- 44 H. Itoh, K. Naka and Y. Chujo, *J. Am. Chem. Soc.*, 2004, **126**, 3026-3027.
- 45 L. L. Shui, A. van den Berg and J. C. T. Eijkel, *Lab Chip*, 2009, **9**, 795-801.
- 46 S. L. Anna, N. Bontoux and H. A. Stone, *Appl. Phys. Lett.*, 2003, **82**, 364-366.
- 47 R. A. McAloney, V. Dudnik and M. C. Goh, *Langmuir*, 2003, **19**, 3947-3952.
- 48 R. A. McAloney, M. Sinyor, V. Dudnik and M. C. Goh, *Langmuir*, 2001, **17**, 6655-6663.
- 49 M. Das, S. Mardiyani, W. C. W. Chan and E. Kumacheva, *Adv. Mater.*, 2006, **18**, 80-83.
- 50 T. Thorsen, R. W. Roberts, F. H. Arnold and S. R. Quake, *Phys. Rev. Lett.*, 2001, **86**, 4163-4166.
- 51 L. L. Shui, A. van den Berg and J. C. T. Eijkel, *J. Appl. Phys.*, 2009, **106**, 124305.
- 52 D. N. Breslauer, S. J. Muller and L. P. Lee, *Biomacromolecules*, 2010, **11**, 643-647.
- 53 X. S. Wang, H. Wang, N. Coombs, M. A. Winnik and I. Manners, *J. Am. Chem. Soc.*, 2005, **127**, 8924-8925.
- 54 H. Wang, X. S. Wang, M. A. Winnik and I. Manners, *J. Am. Chem. Soc.*, 2008, **130**, 12921-12930.
- 55 H. B. Eitouni and N. P. Balsara, *J. Am. Chem. Soc.*, 2004, **126**, 7446-7447.
- 56 Y. N. Xia and G. M. Whitesides, *Angew. Chem. -Int. Edit.*, 1998, **37**, 551-575.

Outlook

This Thesis describes our work on preparing various responsive polymer architectures such as polymer grafts on surfaces and polymer networks in bulk systems. The length scales cover a range from tens of nanometers to a few centimeters. Below, we discuss a few follow-up directions for further explorations.

Nanostructured polymer grafts have attracted a growing interest to different fields like lubrication, antifouling and biomedical devices.¹⁻³ With their macroscopic sizes and molecular scale thickness, they combine the properties of macroscopic materials and colloids along with those of individual molecules.^{4,5} Poly(*N*-isopropylacrylamide) - PNIPAM grafts (Chapter 3), PNIPAM and poly(methacrylic acid) - PMAA mixed grafts (Chapter 4) and poly(ferrocenylsilane) - PFS grafts (Chapter 5) have been successfully developed *via* “grafting from” or “grafting to” approaches. A combination of different approaches and various responsive polymers in one system can be the next step. For example, pH and temperature responsive poly(*N,N*-dimethylamino-2-ethyl methacrylate),⁶ PDMAEMA grafts can be grown on surfaces by “grafting from” - surface-initiated atom transfer radical polymerization (SI-ATRP). Poly(ferrocenyl(3-iodopropyl)methylsilane), PFS-I can then be attached to the PDMAEMA grafts *via* a “grafting to” – quaternization reaction.⁷ A ultrathin redox responsive brush-gel structure can be obtained. The storage function of these brush-gel films (their ability to accommodate various nanoparticles, dyes, enzymes, etc.) can be explored for a substantial increase in the range of functional properties. In addition, these thin films can also be detached and transferred to the surface of another material or directly used as a free-standing film.

For polymer network studies, we have introduced two kinds of crosslinkable PFSs, PFS bearing acrylate side groups (PFS-acryl) and PFS with vinyl imidazole groups (PFS polyionic liquids, PFS-PIL). These synthetic approaches are versatile for the post-functionalization of polymers⁸ with halogen side groups. In the Thesis, various PFS based macroscopic hydrogels, microgels and nanogels have been prepared using these crosslinkable PFS chains. In the Manners group, PFS gels have been examined as pyrolytic precursors to iron-containing magnetic ceramics due to the presence of skeletal transition metal atoms.^{9,10} Moreover, recent studies showed that ionic liquid monomers and polymers can be used as precursors of highly conductive, mesoporous, graphitic carbon nanostructures.¹¹ Pyrolysis of freeze-dried PFS-PIL hydrogels may lead to porous, magnetic, carbon nanostructures which can find applications in separation, or catalyst areas.

The use of a designed microfluidic reactor to produce PFS microgels provides us with a unique opportunity to generate particles with precise control over their size and size distribution, shape, composition and morphology in a continuous and highly tailorable

process.¹²⁻¹⁴ Shell-crosslinked PFS capsules, porous PFS microgels and PFS particles with different shapes can be fabricated. Based on the experiences with electrochemical sensing (Chapter 5) and the distinct color change of PFS between oxidized and reduced states (Chapter 6 and Chapter 8), these tailored PFS particles can be attractive for applications in *e.g.* benefits biosensors.

Besides the 2D and 3D structures discussed in the Thesis, nowadays, 1D nanostructures also become the focus of intensive research owing to their unique applications in mesoscopic physics and fabrication of nanoscale devices.^{15,16} Electrospinning is an effective method to prepare 1D polymer, composite and inorganic submicro- or nano-materials.¹⁷⁻¹⁹ For instance, using the crosslinkable PFS-acryl as precursor, crosslinked PFS nanofibers can be produced *via* electrospinning coupled with UV irradiation. Further modifications could be *in-situ* formation of silver nanocomposite and pyrolysis for magnetic hybrid materials.

References

- 1 M. A. C. Stuart, W. T. S. Huck, J. Genzer, M. Müller, C. Ober, M. Stamm, G. B. Sukhorukov, I. Szleifer, V. V. Tsukruk, M. Urban, F. Winnik, S. Zauscher, I. Luzinov and S. Minko, *Nat. Mater.*, 2010, **9**, 101-113.
- 2 V. Kozlovskaya, E. Kharlampieva, I. Erel and S. A. Sukhishvili, *Soft Matter*, 2009, **5**, 4077-4087.
- 3 I. Tokarev and S. Minko, *Soft Matter*, 2009, **5**, 511-524.
- 4 R. Vendamme, S. Y. Onoue, A. Nakao and T. Kunitake, *Nat. Mater.*, 2006, **5**, 494-501.
- 5 A. D. Stroock, R. S. Kane, M. Weck, S. J. Metallo and G. M. Whitesides, *Langmuir*, 2003, **19**, 2466-2472.
- 6 X. F. Sui, J. Y. Yuan, M. Zhou, J. Zhang, H. J. Yang, W. Z. Yuan, Y. Wei and C. Y. Pan, *Biomacromolecules*, 2008, **9**, 2615-2620.
- 7 M. A. Hempenius, C. Cirmi, J. Song and G. J. Vancso, *Macromolecules*, 2009, **42**, 2324-2326.
- 8 M. A. Gauthier, M. I. Gibson and H. A. Klok, *Angew. Chem. -Int. Edit.*, 2009, **48**, 48-58.
- 9 M. J. MacLachlan, M. Ginzburg, N. Coombs, T. W. Coyle, N. P. Raju, J. E. Greedan, G. A. Ozin and I. Manners, *Science*, 2000, **287**, 1460-1463.
- 10 K. Liu, S. Fournier-Bidoz, G. A. Ozin and I. Manners, *Chem. Mat.*, 2009, **21**, 1781-1783.
- 11 J. Y. Yuan, C. Giordano and M. Antonietti, *Chem. Mat.*, 2010, **22**, 5003-5012.
- 12 E. Tumarkin and E. Kumacheva, *Chem. Soc. Rev.*, 2009, **38**, 2161-2168.
- 13 H. Zhang, E. Tumarkin, R. M. A. Sullan, G. C. Walker and E. Kumacheva, *Macromol. Rapid Commun.*, 2007, **28**, 527-538.
- 14 D. Dendukuri, D. C. Pregibon, J. Collins, T. A. Hatton and P. S. Doyle, *Nat. Mater.*, 2006, **5**, 365-369.
- 15 Y. N. Xia, P. D. Yang, Y. G. Sun, Y. Y. Wu, B. Mayers, B. Gates, Y. D. Yin, F. Kim and Y. Q. Yan, *Adv. Mater.*, 2003, **15**, 353-389.
- 16 X. S. Wang, K. Liu, A. C. Arsenault, D. A. Rider, G. A. Ozin, M. A. Winnik and I. Manners, *J. Am. Chem. Soc.*, 2007, **129**, 5630-5639.
- 17 X. F. Lu, C. Wang and Y. Wei, *Small*, 2009, **5**, 2349-2370.
- 18 Z. Y. Hou, G. G. Li, H. Z. Lian and J. Lin, *J. Mater. Chem.*, 2012, **22**, 5254-5276.
- 19 J. J. McDowell, N. S. Zacharia, D. Puzzo, I. Manners and G. A. Ozin, *J. Am. Chem. Soc.*, 2010, **132**, 3236-3237.

Summary

This Thesis describes the preparation and characterization of addressable responsive polymer structures and their versatile applications. Stimuli responsive polymer chains including temperature responsive poly(*N*-isopropylacrylamide), PNIPAM, pH responsive poly(methacrylic acid), PMAA and redox responsive poly(ferrocenylsilane) PFS can be assembled into various functional polymer architectures such as polymer grafts on surfaces by “grafting to” and “grafting from” approaches and polymer networks in bulk including macroscopic hydrogels and microgels/nanogels systems.

A short introduction to the topics related to this Thesis and the motivation of the research are presented in *Chapter 1*.

In *Chapter 2* a literature overview is provided, covering polymer grafts, macroscopic hydrogels and microgels/nanogels. The general background of stimuli-responsive polymer materials is highlighted. The approaches used to obtain the various structures are also introduced.

In *Chapter 3*, the behavior of PNIPAM grafts with three different grafting densities under varied solvent and temperature conditions is described. The grafts are prepared by a “grafting from” approach, using surface-initiated atom transfer radical polymerization (SI-ATRP) from substrate-immobilized monochlorosilane- or trimethoxysilane-functional ATRP initiators. *In-situ* spectroscopic ellipsometry is used to study the temperature-induced collapse of PNIPAM grafts as a function of phase state across the lower critical solution temperature (LCST) in real time. A model involving a bi-layer with a gradually changing density profile is presented, which adequately fitted the data therewith enabling a quantitative discussion of the reversible thickness change.

The effect of co-nonsolvency, as well as grafting density on the mechanical properties, more specifically the *apparent* Young’s moduli of these PNIPAM grafts are studied using an AFM based colloidal probe nano-indentation method. The collapse dynamics of the PNIPAM grafts is investigated by monitoring the change of adherence between the grafted surface and the colloidal probe. AFM based friction force microscopy, utilized to investigate the stimulus-induced tribological behavior, shows that the friction coefficient of PNIPAM grafts in water and in the co-nonsolvent differs.

The trimethoxysilane-anchored PNIPAM grafts are found to be much more stable than the monochlorosilane ones under cell-culture medium conditions. The trimethoxysilane-anchored polymer grafts are evaluated as supporting substrates for MC-3T3 cell cultures. At 37 °C ($T > \text{LCST}$), the seeded cells adhere, spread, and proliferate, whereas at 25 °C ($T < \text{LCST}$), the cells detach from the surface. The low

density polymer grafts show the highest cell adhesion, featuring adhering cells with an elongated morphology.

Chapter 4 describes the preparation and characterization of mixed polymer grafts consisting of PNIPAM and PMAA. The mixed grafts are also prepared by “grafting from” approaches, a sequential combination of SI-ATRP and iniferter-mediated photopolymerization (SI-IMP). The responsive behavior as a function of pH is investigated. Reversible structural reorganization, variation of grafts thickness and of wetting characteristics are monitored.

Utilizing a "grafting to" approach - amine alkylation reaction, PFS chains (poly(ferrocenyl(3-iodopropyl)methylsilane), PFS-I) are tethered onto silicon or gold substrates. Robust, relatively dense redox-active films with a height of around 10 nm are successfully formed by reaction of PFS-I with amine-terminated monolayers on silicon or gold surfaces. In **Chapter 5**, the electrochemical properties of these PFS grafts are studied both in water and organic media. Information on the properties of these films as a function of redox state is gained using quantitative adherence measurements between the films and AFM tips. An ascorbic acid electrochemical sensor based on these surface-anchored PFS chains, exhibiting a high sensitivity and stability, is also fabricated.

As mentioned in Chapter 5, the iodo groups of PFS-I could be easily replaced by a variety of nucleophiles under mild conditions, thus forming highly tailorable redox-active derivatives. The weak nucleophile sodium acrylate could be attached in the presence of the crown ether 15-crown-5 with quantitative conversion, giving a crosslinkable PFS bearing acrylate side groups (PFS-acryl). In **Chapter 6**, by using PFS-acryl as precursor, a rapidly forming redox responsive PFS-poly(ethylene glycol) (PFS-PEG)-based macroscopic hydrogel is generated *via* thiol-Michael addition click reaction. The equilibrium swelling ratio, morphology, dynamic mechanical properties and redox responsive properties of the hydrogel are studied.

PFS-acryl could also copolymerize with other monomers with different ratios to form various networks. In **Chapter 7**, multi-responsive macroscopic hydrogels composed of PNIPAM and PFS are formed by photopolymerization of NIPAM and PFS-acryl. Crosslinking occurs under mild conditions, providing homogeneous hydrogels. The thermo-responsive properties of the hydrogels are studied as a function of the PFS oxidation state. The *in-situ* fabrication of silver nanoparticles inside the hydrogel network *via* reduction of silver nitrate is also described. These composites show strong antimicrobial activity while maintaining a high biocompatibility with cells.

In **Chapter 8**, the preparation of PFS microgels/nanogels is described. Besides the PFS-acryl studied in Chapter 6 and Chapter 7, a new type of crosslinkable, water soluble PFS, PFS with vinyl imidazole groups (PFS polyionic liquids, PFS-PILs) is

developed. PFS-PIL is also derived from PFS-I, by reacting with 1-vinylimidazole at 60 °C for 24 h. To increase the water solubility of the formed polycation, its iodide counterions are exchanged with chloride counterions by dialysis in 0.1 M aqueous sodium chloride. PFS-PIL self-crosslinks at low concentrations into nanogels or forms macroscopic hydrogel networks at higher concentrations. PFS-PIL also proves to be an efficient dispersant in the microemulsion polymerization of methyl methacrylate, producing stable PFS-poly(methyl methacrylate) latex suspensions. Using PFS-PIL and PFS-acryl as precursors, uniform sized PFS microgels are obtained by using a microfluidic system coupled with UV photopolymerization. This novel, facile, flexible and straightforward microfluidic technique enables us to generate and precisely control the size of these redox responsive microspheres. These PFS nanogels/microgels produced show redox responsive properties and promising applications in catalysis and molecular release.

Summary

Samenvatting

Dit proefschrift beschrijft de synthese en karakterisering van responsieve polymeerstructuren en hun veelzijdige toepassingsmogelijkheden. Op stimuli reagerende polymeerketens, waaronder poly(*N*-isopropylacrylamide), PNIPAM, pH-responsief poly(methacrylzuur), PMAA en redox-responsief poly(ferrocenylsilaan) PFS kunnen worden geassembleerd in verschillende functionele polymeerarchitecturen zoals polymeer "grafts" op oppervlakken via "grafting to" en "grafting from" methoden en polymeernetwerken in bulk inclusief macroscopische hydrogels en microgels/nanogels systemen.

Een korte inleiding van de onderwerpen gerelateerd aan dit Proefschrift en de motivatie van het onderzoek worden gepresenteerd in *Hoofdstuk 1*.

In *Hoofdstuk 2* wordt een literatuuroverzicht gegeven, waarin polymeer "grafts", macroscopische hydrogels en micro/nanogels worden behandeld. De achtergrond van stimuli-responsieve polymere materialen wordt besproken. De methoden om de diverse polymeerstructuren te verkrijgen worden eveneens geïntroduceerd.

In *Hoofdstuk 3* wordt het gedrag van PNIPAM "grafts" met drie verschillende "grafting" dichtheden onder verschillende oplosmiddel- en temperaturomstandigheden beschreven. De "grafts" worden gefabriceerd door middel van een "grafting from" methode, via oppervlakte-geïnitieerde atom transfer radicaalpolymerisatie (SI-ATRP) vanaf substraat-geïmmobiliseerde monochloor- of trimethoxysilaan-gefunctionaliseerde ATRP initiators. *In-situ* spectroscopische ellipsometrie wordt gebruikt om de temperatuur-geïnduceerde contractie van PNIPAM "grafts" als functie van hun fasetoestand rond de "lower critical solution temperature" (LCST) direct te bestuderen. Een model gebaseerd op een dubbellaag met een geleidelijk veranderend dichtheidsprofiel, waarmee de data goed konden worden gefit, wordt gepresenteerd. Hierdoor wordt een kwantitatieve behandeling van de reversibele filmdikteverandering mogelijk gemaakt.

De invloed van "co-nonsolvency" en van "grafting" dichtheid op de mechanische eigenschappen, meer specifiek de *schijnbare* Young's moduli van deze PNIPAM "grafts", worden bestudeerd door middel van een op AFM gebaseerde colloïdale "probe" nano-indentatiemethode. De contractiedynamica van de PNIPAM "grafts" wordt bestudeerd door de adhesieverandering tussen het "grafted" oppervlak en de colloïdale "probe" te volgen. Op AFM gebaseerde wrijvingskrachtmicroscopie, gebruikt om het stimulus-geïnduceerde tribologische gedrag te onderzoeken, toont aan dat de wrijvingscoëfficiënt van de PNIPAM "grafts" in water en in het "co-nonsolvent" verschilt.

De trimethoxysilaan-verankerde PNIPAM "grafts" blijken veel stabiel te zijn dan de via monochloorsilaangroepen geïmmobiliseerde "grafts" onder celcultuur medium omstandigheden. De trimethoxysilaan-verankerde polymeer "grafts" worden geëvalueerd als onderliggende substraten voor MC-3T3 celculturen. Bij 37 °C ($T > LCST$) hechten de cellen, spreiden zich over het oppervlak en groeit hun populatie, terwijl de cellen bij 25 °C ($T < LCST$) zich losmaken van het oppervlak. De laagdiktheid polymeer "grafts" vertonen de hoogste celadhesie en laten cellen zien met een uitgestrekte morfologie.

Hoofdstuk 4 beschrijft de fabricage en karakterisering van gemengde polymeer "grafts" bestaande uit PNIPAM en PMAA. De gemengde "grafts" worden ook gemaakt door "grafting from" methoden, een opeenvolgende combinatie van SI-ATRP en iniferter-gestuurde fotopolymerisatie (SI-IMP). Het responsieve gedrag als functie van pH wordt onderzocht. Reversibele structurele reorganisatie, verandering van "graft"-laagdikte en van bevochtigingseigenschappen worden bestudeerd.

Gebruikmakend van een "grafting to" methode, een amine alkyleringsreactie, worden PFS ketens (poly(ferrocenyl(3-iodopropyl)methylsilaan), PFS-I) gehecht aan silicium- of goudsubstraten. Robuuste, relatief dichte redox-actieve films met een hoogte van ongeveer 10 nm worden succesvol gevormd door reactie van PFS-I met amine-geïmmobiliseerde monolagen op silicium- of goudoppervlakken. In **Hoofdstuk 5** worden de electrochemische eigenschappen van PFS "grafts" zowel in water als in organische media bestudeerd. Informatie over de eigenschappen van deze films als functie van hun redoxtoestand wordt verkregen door middel van kwantitatieve adhesiemetingen tussen de films en AFM tips. Een electrochemische ascorbinezuur sensor gebaseerd op deze oppervlakte-geïmmobiliseerde PFS ketens, die een hoge gevoeligheid en stabiliteit bezit, wordt tevens gefabriceerd.

Zoals genoemd in Hoofdstuk 5 kan de iodogroep van PFS-I gemakkelijk worden vervangen door een reeks van nucleofielen onder milde omstandigheden waardoor veel redox-actieve PFS derivaten bereikbaar zijn. Het zwakke nucleofiel natrium methacrylaat kon met 100% conversie worden gehecht aan PFS-I in aanwezigheid van de kroonether 15-crown-5, waardoor een crosslinkbaar PFS met acrylaat zijgroepen (PFS-acryl) werd verkregen. In **Hoofdstuk 6**, door PFS-acryl te gebruiken als uitgangsmateriaal, werd een snel vormende redox-responsieve PFS-poly(ethyleen glycol) (PFS-PEG) macroscopische hydrogel gegenereerd via een thiol-Michael additiereactie. De evenwichtszwelling, morfologie, dynamisch mechanische eigenschappen en redox-responsieve eigenschappen van de hydrogel werden bestudeerd.

PFS-acryl kon ook copolymeriseren met andere monomeren in verschillende verhoudingen zodat diverse netwerken konden worden gevormd. In **Hoofdstuk 7** worden multi-responsieve macroscopische hydrogels, bestaand uit PNIPAM en PFS,

gevormd door fotopolymerisatie van NIPAM en PFS-acryl. Crosslinking geschiedt onder milde omstandigheden en leidt tot homogene hydrogels. De thermo-responsieve eigenschappen van de hydrogels worden bestudeerd als functie van de PFS oxidatietoestand. De *in-situ* fabricage van zilver nanodeeltjes in het hydrogel netwerk via reductie van zilvernitraat wordt ook beschreven. Deze composieten bezitten een hoge antimicrobiële activiteit maar behouden tegelijkertijd een hoge biocompatibiliteit met cellen.

In **Hoofdstuk 8** wordt de bereiding van PFS microgels/nanogels beschreven. Naast de PFS-acryl beschreven in Hoofdstuk 6 en Hoofdstuk 7 werd een nieuw soort crosslinkbaar, wateroplosbaar PFS, PFS met vinylimidazoolgroepen (PFS polyionic liquids, PFS-PILs) ontwikkeld. Ook PFS-PIL werd gevormd vanuit PFS-I door reactie met 1-vinylimidazool bij 60 °C voor 24 h. Om de wateroplosbaarheid van het gevormde polykation te verhogen werden de iodide tegenionen uitgewisseld met chloride tegenionen door dialyse in 0.1 M natriumchloride. PFS-PIL crosslinkt intramoleculair bij lage concentraties tot nanogels en vormt macroscopische hydrogel netwerken bij hogere PFS-PIL concentraties.

PFS-PIL bleek ook een efficiënt disperseermiddel in de microemulsie polymerisatie van methyl methacrylaat te zijn, wat leidde tot stabiele PFS-poly(methyl methacrylaat) latex suspensies. Met PFS-PIL en PFS-acryl als precursors werden uniforme PFS microgel deeltjes verkregen door middel van een microfluidisch systeem in combinatie met UV fotopolymerisatie. Deze nieuwe, eenvoudige, flexibele microfluidische techniek maakte het mogelijk om uniforme, redox-actieve microdeeltjes met nauwkeurig bepaalde afmetingen te produceren. Deze PFS nanogels/microgels bezitten redox-responsieve eigenschappen en veelbelovende toepassingsmogelijkheden in catalyse en in moleculaire opslag en afgifte.

Samenvatting

Acknowledgements

Summer, Autumn, Winter, Spring ~~~~again Summer, It has been already 4 years since I live in this small but lovely city - Enschede. Now sitting under the tree in the garden, I am reading this Thesis, while Yuying and Runxi are playing on the grass just 10 meters away. White clouds in the blue sky, birds are singing, vegetables and flowers I planted in Spring are now full of vigor. At this enjoyable moment, looking back to my PhD life, many thanks come into my mind.

The first person I would like to thank is my promoter, Prof. Julius Vancso, for offering me the opportunity to pursue my PhD study in MTP group. Julius, the first time I met you was during Xiangshan Science Conference in October 2007, at Tsinghua University. We were talking about this fascinating TOP Grant project at the hotel lobby while the Nobel Prize winner Jean-Marie Lehn was playing piano there. During the PhD study, you gave me the freedom and the trust to carry out research and collaborations. I learned a lot from the discussions with you. Your broad knowledge, attitude towards research, insight of science, set up a nice example for me to follow. I also treasure the talks we had about my personal future careers, they helped me to know myself and make the choice.

I sincerely thank my assistant promoter, Dr. Mark Hempenius. Mark, to work with you is a great fortune for me. Whenever I need help: doing experiments, shaping research routes, correcting papers, your supports were always there. I saw from you how to be a real good Chemist. I enjoyed all the working time with you, your highly skilled experimental techniques, your working spirits and your humor time by time.

I am grateful to Clemens Padberg and Geneviève Rietveld. Clemens, you are a wonderful lab manager! Thanks for teaching me the use of all the necessary equipments and the help of many beautiful measurements. Geneviève, thank you so much for helping for all the documents and the design of this splendid Thesis cover.

Many results described in this Thesis came from successful collaborations. Grateful acknowledgements to all of them, Dr. Edmondo M. Benetti, Dr. Canet Acikgöz, Dr. Szczepan Zapotoczny, Dr. Qi Chen, Dr. Joost Duvigneau, Dr. E. Stefan Kooij, Michel Klein Gunnewiek, Andrea Di Luca, Edit Kutnyanszky, Dr. Peter Schön, Jin Cui, Dr. Lingling Shui, Dr. Jing Song and Xueling Feng.

Eddy, you introduced me into the surface modification field, your passion on experiments, your knowledge with polymers inspired me a lot. Together with Janet, nanopatterned grafts were successfully prepared. Szczepan, we worked on the mixed polymer grafts project, your input was invaluable. Thanks for the invitation to YES workshop in Krakow, it was a wonderful time. Qi, your work with *in-situ* AFM opened a new window on these polymer grafts. Joost, we enjoyed on the preparation

Acknowledgements

of confined grafts by photopolymerization during my first year. Also thanks for all the help and support. Stefan, an expert on ellipsometry, the work solved the problem of understanding the mechanism of swelling behavior of these polymer grafts. Andrea, the cell culture and antimicrobial work showed nice potential applications of the grafts and hydrogels. Michel, your work on polymer grafts with varied grafting densities was really helpful. Edit, it is my pleasure to work with you on the same project, you are always helpful, for discussions and measurements. Also, thanks a lot for all the detailed corrections on this Thesis. Peter, thanks a lot for the calibration of the cantilever, it worked. Jin, you carried out the microgel project quite well with your hard work and creative thinking. Lingling, our collaboration on microfluidics resulted in a huge success, the results were amazing. Jing, you showed the way to electrochemistry study of PFS, thanks a lot for the warm host in Singapore. Xueling, you are growing up to be an excellent expert on electrochemistry.

I wish to express my special thanks to my paranimfen, Bart Kieviet and Xueling Feng. Bart, you are a good neighbor in both office and home. Xueling, you are not only a good coworker in the lab, you are also a good friend of our family, thanks a lot for all the help you gave to us.

I am thankful to all the past and present MTP members during my stay.

I truly appreciate the support and company of many friends, you make my life here easier and happier: Lixian and Hongping, Shumin and Yan, Weihua and Qiwei, Jumeng and Haiyan, Chunlin and Huaqiong, Jie and Yali, Ran and Juan, Qi and Yujie, Haifeng and Wenxin, Tian and Xin, Hao and Lingling, Hao and Lanti, Wei and Yumei, Xiangqiong and Li, Mingliang and Lingling, Shanglong and Wei, Yanbo, Haishan, Haining, Qi An, Yu He, Wei Cheng. Thank you so much for the wonderful times we had together.

Finally and most importantly, I owe my family my deepest gratitude for giving me their unconditional support all through these years. Papa (隋金承), Mama (王翠珍), My brother (隋晓军), thanks for all the love you gave to me to pursue my dream. I regret for not spending enough time with you over the past years. Yuying (玉英), you are always there to help me. You give me the opportunity to find out my real passion. I could not say more words about you. Runxi 润晞 (Tsingsing), you are so lovely. You make the home full of joy every day.

Xiaofeng Sui
隋晓锋
Enschede 2012

List of Publications, Ph.D. Thesis

1. **X. Sui**, X. Feng (co-first author), J. Song, M. A. Hempenius and G. J. Vancso.
Electrochemical Sensing by Surface-immobilized Poly(ferrocenylsilane) Grafts.
Journal of Materials Chemistry, 2012, 22, 11261-11267.
2. **X. Sui**, M. A. Hempenius, and G. J. Vancso.
Redox-active Crosslinkable Poly(ionic liquid)s.
Journal of the American Chemical Society, 2012, 134, 4023–4025.
3. M. Klein Gunnewiek, A. Di Luca, **X. Sui**, C. A. van Blitterswijk, L. Moroni, and G. J. Vancso.
Controlled Surface Initiated Polymerization of *N*-isopropylacrylamide from Polycaprolactone Substrates for Regulating Cell Attachment and Detachment.
Israel Journal of Chemistry, 2012, 52, 339-346.
4. **X. Sui**, A. Di Luca, M. Klein Gunnewiek, E. S. Kooij, C. A. van Blitterswijk, L. Moroni, M. A. Hempenius, and G. J. Vancso.
Stability and Cell Adhesion Properties of Poly(*N*-isopropylacrylamide) Brushes with Variable Grafting Densities.
Australian Journal of Chemistry, 2011, 64, 1261-1268.
5. E. M. Benetti, C. Acikgöz, **X. Sui**, B. Vratzov, M. A. Hempenius, J. Huskens, and G. J. Vancso.
Nanostructured Polymer Brushes by UV-Assisted Imprint Lithography and Surface-Initiated Polymerization for Biological Functions.
Advanced Functional Materials, 2011, 21, 2088–2095.
6. **X. Sui**, Q. Chen (co-first author), M. A. Hempenius and G. J. Vancso.
Probing Collapse Dynamics of Poly(*N*-isopropylacrylamide) Brushes by AFM: Effects of Co-Nonsolvency and Grafting Densities.
Small, 2011, 7, 1440–1447.
7. **X. Sui**, S. Zapotoczny, E. M. Benetti, M. Memesa, M. A. Hempenius and G. J. Vancso.
Grafting Mixed Responsive Brushes of Poly(*N*-isopropylacrylamide) and Poly(methacrylic acid) from Gold by Selective Initiation.
Polymer Chemistry, 2011, 2, 879-884.
8. **X. Sui**, S. Zapotoczny, E. M. Benetti, P. Schön and G. J. Vancso.
Characterization and Molecular Engineering of Surface-Grafted Polymer Brushes Across the Length Scales by Atomic Force Microscopy.
Journal of Materials Chemistry, 2010, 20, 4981-4993.

List of Publications

9. E. M. Benetti, **X. Sui**, S. Zapotoczny and G. J. Vancso.
Surface-Grafted Gel-Brush/Metal Nanoparticle Hybrids.
Advanced Functional Materials, 2010, 20, 939–944.
10. **X. Sui**, L. van Ingen, M. A. Hempenius and G. J. Vancso.
Preparation of a Rapidly Forming Poly(ferrocenylsilane)- Poly(ethylene glycol)-based Hydrogel by a Thiol-Michael Addition Click Reaction.
Macromolecular Rapid Communications, 2010, 31, 2059–2063.

Manuscripts

11. **X. Sui**, X. Feng, A. Di Luca, C. A. van Blitterswijk, L. Moroni, M. A. Hempenius, and G. J. Vancso.
Poly(*N*-isopropylacrylamide)-Poly(ferrocenylsilane) Dual-Responsive Hydrogels: Synthesis, Characterization and Antimicrobial Applications. *Submitted*.
12. **X. Sui**, L. Shui, J. Cui, J. Song, A. van den Berg, M. A. Hempenius and G. J. Vancso.
Poly(ferrocenylsilane) Based Redox Responsive Microgel Particles Obtained by Microfluidics. *In preparation*.
13. **X. Sui**, X. Feng, J. Cui, M. A. Hempenius and G. J. Vancso.
Redox Active Gels: Synthesis, Structures and Applications. *In preparation*.
14. E. S. Kooij, **X. Sui**, M. A. Hempenius, H. J. W. Zandvliet and G. J. Vancso.
Probing the Thermal Collapse of Poly(*N*-isopropylacrylamide) Grafts by Quantitative *in-situ* Ellipsometry. *Submitted*.
15. Qi Chen, **X. Sui** (co-first author), E. S. Kooij, P. M. Schön, M. A. Hempenius and G. J. Vancso.
Effects of Solvent Quality and Grafting Density on the Swelling, Collapse and Friction Properties of Poly(*N*-isopropylacrylamide) Grafts. *Submitted*.

Other Publications

16. H. Qi, **X. Sui**, J. Yuan, Y. Wei and L. Zhang.
Electrospinning of Cellulose-Based Fibers From NaOH/Urea Aqueous System.
Macromolecular Materials and Engineering, 2010, 295, 695–700.
17. **X. Sui**, J. Yuan, M. Zhou, J. Zhang, H. Yang, W. Yuan, Y. Wei and C. Pan.
Synthesis of Cellulose-graft-Poly(*N,N*-dimethylamino-2-ethyl methacrylate) Copolymers *via* Homogeneous ATRP and Their Aggregates in Aqueous Media.
Biomacromolecules, 2008, 9, 2615–2620.

18. **X. Sui**, J. Yuan, W. Yuan and M. Zhou.
Preparation of Cellulose Nanofibers/nanoparticles *via* Electrospray.
Chemistry Letters, 2008, 1, 114-115.
19. **X. Sui**, J. Yuan, W. Yuan and M. Zhou.
Recent Progress in the Surface-Initiated Living Radical Polymerization from
Inorganics Nanomaterials.
Progress in Chemistry, 2008, 20, 1122-1127.
20. Q. Yan, **X. Sui**, J. Yuan.
Living/Controlled Polymerization in the Synthesis of Star Polymer.
Progress in Chemistry, 2008, 20, 1562-1571.
21. J. Yuan, **X. Sui** and M. Zhou.
An Easy Way to Prepare Cellulose Nanomaterials *via* Electrospray.
Chinese Patent, ZL 2007 1 0120293.7.
22. **X. Sui**, J. Yuan, M. Zhou and Y. He.
Recent Progress in the Application of *N*-Bromosuccinimide to Organic Chemical
Reactions.
Chinese Journal of Organic Chemistry, 2006, 26, 1518-1524.

List of Publications

Curriculum Vitae

Xiaofeng Sui was born on November 19th, 1983 in Shandong, China. After graduating from No.9 Middle School in Laiyang, he entered Tsinghua University in Beijing without taking the National exams due to his outstanding performance in Chemistry Olympiad (2002) of high school students all over China. In 2006, he obtained his Bachelor's degree in Chemistry. Then, he started his master's studies at the same university under the supervision of Prof. Dr. Jinying Yuan, graduating in 2008 with an Master degree in Polymer Chemistry and Physics. Thereafter, he joined Materials Science and Technology of Polymers group in University of Twente, the Netherlands, as a Ph.D. student under the supervision of Prof. Dr. G. Julius Vancso. His research subjects is centered around preparing responsive polymer materials as building blocks for addressable structures, their characterization, and their applications. Stimuli responsive polymer chains can be assembled into various functional polymer architectures such as polymer grafts on surfaces and polymer networks in bulk. The results of this four year research are presented in this Thesis. In 2010, he received the Chinese Government Award for Outstanding Self-Financed Students Abroad.

